

Role of Dissipation in Resonance: A Variational Principle approach

by

Arindam Phani

A thesis submitted in partial fulfillment of the requirements for the degree
of

Doctor of Philosophy

in Materials Engineering

Department of Chemical and Materials Engineering
University of Alberta

Abstract

Resonance is at the heart of sensing and characterization tools in all fields of science. A nanoresonator has achieved the remarkable resolution of a proton mass. The coupling of a micromechanical oscillator to an optical field in a high finesse cavity has allowed sensitive probing even in the quantum regime. Such techniques rely on the frequency shift and/or amplitude change of a very narrow-band resonator. The key to obtaining a narrow bandwidth of response lies in overcoming the damping effects, considered detrimental in the context. The primary aim in the design of resonators has been to minimize all dissipative effects thus. Unavoidably, dissipation is always introduced both from viscous friction with the fluid media and internal losses of the material, and is maximized at resonance. We take an alternative view of the role of dissipation in resonance and the information it conveys pertaining to a system. We explain the condition of maximization of dissipation at resonance as a variational problem dependent on phase, the phase appearing from an arbitrary path. We look at both mechanical and electrical resonance platforms and try to study the importance of dissipation in such systems in defining resonance altogether.

The underlying phenomenon of standing waves is re-explored to explain the elusive resonance amplification from a radically alternate perspective using a path integral approach similar in form to Feynman's quantum theory. Standing wave definition from the aspect of phase ϕ in time and space is considered. We comment on resonance amplification factor from a hypothesis-formulated in terms of measured ϕ in space. This time-phase evolution in space is explained as a continuous accumulated phase within the physical bounds of a resonator. The importance of the evolution of phase ϕ and its role in the origin of standing waves at resonance is highlighted. Comparison of theoretical results

and experimental data show an excellent match. In addition, the fundamental treatment makes the formulation applicable to all resonating systems in a general way.

We study a nanostructured mechanical resonator and show that when multiple coupled oscillators are involved, in the limits of continuum breakdown, inherent randomness in interactions with the media molecules can no longer be neglected leading to an additional non-continuum energy scale. The two energy scales compete in bringing long-range order over an inherent randomness and we show that such interplay can be explained by generalized Gibbs measure. The implication of such competing dynamic scales in the limits of continuum breakdown is profound revealing an extraordinary exponential amplification phenomenon. The work tries to highlight this in the context of an apparent dynamic range magnification of gas kinematic viscosity, making it a suitable parameter for gas characterization even in normal atmospheric conditions.

We introduce photothermal electrical resonance spectroscopy of physisorbed molecules on a semiconductor nanowire resonator combined with infrared (IR) for molecular recognition of femtograms of adsorbed molecules exploiting dissipation signature at electrical resonance. The technique exploits the combination of very low thermal mass of the nanowire and high number of surfaces states on the nanowire for detection. We highlight that dissipation driven transition at play a crucial role in surface state population and de-population.

We show that dissipation itself can be used as a measuring tool in the resonator-based devices. The new paradigm of dissipation-based sensing introduced in this work can be utilized in a broad range of fast, inexpensive, hand-held measuring devices.

Preface

The thesis is paper based with an Introductory and Conclusion chapter binding the results.

It is organized into five sections as follows –

Section I. is the introductory chapter. It reviews the concept of resonance in the light of complex response function. The importance of the imaginary part of the response function as a measure of the dissipated energy is explained. A variational principle approach to understanding dissipation as a functional of phase ϕ , dependent on arbitrary paths in a system is also introduced.

Section II. is a monograph communicated for publication as **Arindam Phani**, C. W. Van Neste and Thomas Thundat, “*Standing wave revisited: accumulated phase and resonance amplification*”. It reviews resonance in the light of standing waves.

Contribution to the paper: A.P designed, characterized and performed all experiments. C.V.N was involved in experimental design. A.P and T.T were involved in study design, data interpretation and theoretical analysis, and wrote the manuscript. All authors discussed results and commented on the manuscript.

Section III. has been published as **Arindam Phani**, Vakhtang Putkaradze, John E. Hawk, Kovur Prashanthi and Thomas Thundat, “*A nanostructured surface increases friction exponentially at the solid-gas interface*” in *Scientific Reports* 6, Article number: 32996 (2016). It addresses a surprising effect brought about by nanostructuring a surface of a macro resonating system.

Contribution to the paper: A.P synthesized, characterized, designed and performed all experiments. J.E.H wrote machine interface codes in LabVIEW and K.P was involved in study design. A.P, V.P, and T.T were involved in study design, data interpretation and

theoretical analysis, and wrote the manuscript. All authors discussed results and commented on the manuscript.

Section IV. is published as Kovur Prashanthi, **Arindam Phani**, and Thomas Thundat, “*Photothermal electrical resonance spectroscopy of physisorbed molecules on a nanowire resonator*” in *Nano Lett.*, 2015, *15* (8), pp 5658–5663. It introduces a new platform of using a semiconductor nanowire combined with infrared (IR) for molecular recognition of femtograms of adsorbed molecules exploiting dissipation signature at electrical resonance.

Contribution to the paper: Authors have equal contribution. K.P and A.P. were involved in study design and data interpretation. Experiments were conceived by T.T. All authors were involved in study design, data interpretation and theoretical analysis, and wrote the manuscript. All authors discussed results and commented on the manuscript.

Section V. concludes and summarizes the overall thesis and also gives a brief account on the future aspects of the present work.

Bibliography presents a comprehensive list of literature relevant to the work presented

Dedicated to

Family

*"My heart sings at the wonder of my place
In this world of light and life;
At the feel in my pulse of the rhythm of creation
Cadenced by the swing of the endless time.
I feel the tenderness of the grass in my forest walk,
The wayside flowers startle me:
That the gifts of the infinite are strewn in the dust
Wakens my song in wonder.
I have seen, have heard, have lived;
In the depth of the known have felt
The truth that exceeds all knowledge
Which fills my heart with wonder and I sing."*

----- Rabindranath Tagore

*"If you want to find the secrets of the universe,
think in terms of energy, frequency and vibration."*

----- Nikola Tesla

Acknowledgement

It gives me immense pleasure to get an opportunity to thank all those people without whom this thesis would not have been possible. However, writing an acknowledgement section such as this seemed to be the most difficult part, not only for the fear of overlooking contributions of people who deserve due acknowledgement but also a sense of apprehension concerning the fact that it happens to be the most neglected section of any literature or book. I shall try to keep it short and more general in terms of names for the sake of reducing error in judgement and oversight.

First and foremost, the valuable guidance from my supervisor and Guru, *Dr. Thomas Thundat* has encouraged me and in fact strengthened my desire to eventually become a leader in my field of research in whatever small way it can be. His supervision at various stages of this work has helped in giving a true shape to this thesis.

I hereby take this opportunity to express my sincere gratitude to Chemical and materials Engineering Department at University of Alberta for giving me the opportunity to pursue my PhD. The beautiful and truly academic environment setting have thoroughly enriched me in my endeavors so far. The *Canada Excellence Research Chair in Oil Sands and Molecular Engineering* funding of Dr. Thomas Thundat funded the entire work.

The work discussed in **Section III** of the thesis is part of collaboration work done with Dr. Vakhtang Putkaradze of Mathematical and Statistical Sciences Department at UofA. I sincerely thank him for his efforts and his guidance on mathematical formulations that allowed giving a proper shape to the research findings. Our association would go a long way in further collaborative works in the future.

I am thankful to my fellow lab mates of NIME group, especially Dr. Charles Van Neste and fellow graduate student, Mr. John Hawk for creating a youthful, enjoyable yet constant learning environment. Discussions, arguments and months of closed room board-

work at various stages of the work have been quite illuminating and is an inherent part of this thesis.

Sincere thanks to my well-wishers whose encouragement and love have helped me in finishing this endeavor successfully in a joyful mood. I am specifically resisting myself in mentioning names here because I believe that their contribution to this thesis goes much beyond just simple names. In no way they are lesser than the others mentioned. I intend to cherish their due acknowledgement individually in my own heart.

Last but most importantly, this thesis would not have been possible without the constant motivation of my beloved wife. Her sacrifice of the time, which I spent on my research and her effort in tolerating my technical jargons without losing temper, has been the constant inspiration to bring this endeavor to a successful and fruitful end.

Finally I must acknowledge my Parents, my In-Laws, my Sister and her family and my Sister-in-Law, for their constant support and encouragement. Their instilled moral strength to pursue this endeavor with my heart's content, has been and will always be unmatched. This thesis is dedicated to all of them.

Arindam Phani

TABLE OF CONTENTS

I. Role of dissipation in resonance: A variational principle approach ...	1
1.1 Understanding Resonance -----	2
1.2 Forces in classical dynamics and response function -----	5
1.3 Causality -----	9
1.4 Kramers-Kronig relations and resonance -----	9
1.5 Resonance and dissipation -----	14
1.6 Dissipation maximization and its relation to $Im \chi$ -----	18
1.7 A variational principle approach of dissipation -----	20
1.8 Application of the variational principle approach in practical dissipation studies at resonance -----	27
II. Standing wave revisited: accumulated phase and resonance amplification	31
2.1 Introduction -----	32
2.2 Waves in isotropic space and phase of a wave -----	35
2.3 Phase from the consideration of non-isotropic space -----	37
2.4 Phase at resonance -----	39
2.5 The condition of accumulated phase and physical significance -----	42
2.6 The standing wave function in terms of accumulated phase -----	44
2.7 Significance of accumulated phase in resonance amplification factor α -----	46
2.8 Physical analogy of accumulated phase in a wire-----	50
2.9 Conclusion and Discussions-----	52
2.10 Dicussion on single wire electrical power transfer using resonance -----	52
References -----	55
III. A nanotructures surface increases friction exponentially at the solid-gas interface	58
3.1 Introduction -----	59
3.2 Objectives and key result of the work -----	62
3.3 Experimental design -----	63

3.4	Measured quantitites and presentation of results -----	64
3.5	Experimental results of dissipation enhancement for nanostructures interface -----	65
3.6	Limiting sensitivity: Relevance to sensing applications -----	68
3.7	Theoretical analysis of results -----	71
3.8	Key result on the theoretical analysis and relevance to experimental data -----	75
3.9	Discussion on time and length scales -----	79
3.10	Conclusions -----	80
3.11	Materials and Method	
3.11.1	Surface Nanostructuring -----	80
3.11.2	Flow system for analyte introduction -----	81
3.11.3	Impedence measurement -----	82
	References -----	83
	Supplementary Materials	
S1.	FE-SEM of nanostructured surface -----	88
S2.	XRD analysis of nanostructured surface -----	88
S3.	Measured data accuracy analysis and estimation -----	89
S4.	Dissipation response for different gas media -----	91
S5.	Estimation of gas mixture viscosities -----	92
S6.	Estimation of gas viscosity at different temperatures -----	93
S7.	Estimation of vibration amplitude at 5mV drive from impedance measurement -----	93
S8.	Explanation of exponential amplitude dependence -----	94
	Reference -----	95

IV.	<i>Photothermal electrical resonance spectroscopy of physisorbed molecules on a nanowire resonator</i>	97
4.1	Introduction -----	98
4.2	Experimental technique -----	101
4.3	Analysis of results -----	101
4.4	Surface state density and significance in dissipation response -----	103
4.5	Significance of low thermal mass -----	104
4.6	Demonstration of IR dissipation IR spectroscopy -----	106
4.7	Conclusion -----	110

4.8 Materials and Methods	
4.8.1 Preparation of BFO nanowire resonator -----	111
4.8.2 Chemicals -----	111
4.8.3 Dynamic impedance IR spectroscopy setup -----	111
4.8.4 FTIR spectroscopy -----	112
References -----	114
Supplementary Materials	
S1. Equivalent circuit model for nanowire resonator -----	116
S2. Electrical resonance of nanowire resonators -----	119
S3. Dissipation response due to the adsorption of molecules -----	120
S4. The variation of dissipation due to IR absorption by molecules -----	123
Reference -----	123
V Conclusions and Future prospects of the work	
5.1 Conclusions -----	124
5.2 Future prospects -----	130
List of Publications -----	131
Bibliography -----	133
Appendix I : MATLAB codes for diffraction pattern simulation -----	158
Appendix II :MATLAB codes for filtering of obtained image -----	161

List of Symbols

x	Displacement, dynamical degree of freedom
\dot{x}, v, \mathbf{v}	Velocity
\ddot{x}	Acceleration
$A, \mathbf{a}, \mathbf{X}_0$	Amplitude
t	Time
m	Mass
m_{eff}	Effective mass
γ	Damping coefficient
ϕ, ϕ'	Phase
$\phi_{\Delta x}$	Phase function dependent on arbitrary path
ϕ_r	Phase function in r
ϕ_s	Spatial phase
ϕ_t	Temporal/Time phase
$\Delta\phi_r$	Accumulated phase
ω, ω', Ω	Angular frequency
ω_0	Fundamental frequency
ω_i	Eigen frequency
ω_*	Poles in the complex plane
f	Frequency
$f(), g()$	Function
$\chi()$	Response function
$[]'$	Real part of a complex quantity
$[]''$	Imaginary part of a complex quantity
$[]^*$	Complex conjugate
Re	Real
Im	Imaginary
h	Plank's constant

π	Pi
Q	Q-factor
E	Energy
T	Kinetic energy
V	Potential energy
\mathcal{H}, H	Hamiltonian
S	Classical action
L , L	Lagrangian
F	External drive force
R	Random external force
ε	Small shift or change of a variable
\mathcal{P}	Principal value of integral
$\delta(t)$	Delta function
W	Work
∇^2, Δ	Laplacian
r	Space coordinate
ψ	Wave function
$()_x$	First order partial derivative in x
$()_{xx}$	Second order partial derivative in x
$\xi(\), \eta(\)$	Characteristics – constants
ξ_r, η_r	Deformed/warped characteristics
λ	Wavelength of wave or light, Arbitrary deformation constant
$\lambda(r)$	Deformation factor in r
β	Wavenumber
Ψ_r	Standing wave function
T	Time period
V	Potential
V'	Imaginary potential
$q(\), \dot{q}(\)$	Generalized coordinate and velocity
α	Amplification factor
u , U	Fluid/gas velocity

ν	Kinematic viscosity
η	Dynamic viscosity
ρ	Density
Re	Reynolds number
p	Pressure
D	Dissipation, Damping rate
D-factor	Dissipation factor
L	Length of nanorods
d	Diameter of nanorods
w	Width between nanorods
${}^i P$	Probability of event i
τ	Timescale, relation time
N_i	Total number
δ	Dynamic viscous length
w	Width between nanorods
S_{\perp}	Cross-section normal to a surface
$S_{ }$	Cross-section parallel to a surface
l_*	Mean free path of gas molecules
$\Psi(\phi)$	State function, Potential function
ζ	Noise autocorrelation function
ΔW	Work of fluid friction (Stokes energy scale)
τ_m	Molecular motion time scale
τ_n	Nanorod motion time scale
D_{ij}	Diffusion coefficient of component i into j
σ_i	Average collision diameter of molecular species i
Ω_c	Temperature dependent collision integral
R_S, \wp_s	Series resistance
c_s, C, C_S	Series capacitance
L_S	Series Inductance

X_L	Inductive reactance
X_C	Capacitive reactance
i	Current
T	Temperature
Q	Heat
C_p	Thermal heat capacity

List of Abbreviations

SW	Standing Wave
QC	Quartz Crystal
mfp	Mean Free Path
SR	Stochastic Resonance
BFO	Bismuth Ferrite (BiFeO_3)
fg	femtogram
IR	Infrared
FTIR	Fourier Transform Infrared
SEM	Scanning Electron Microscopy
PERS	Photothermal Electrical Resonance Spectrum
QCL	Quantum Cascade Laser
RDX	Cyclotrimethylene Trinitramine
SRF	Self-resonating frequency

List of Figures

Fig 1.1| Resonance and wavefunctions in a potential well; the classical case being the quantum case limit of $\hbar \rightarrow 0$.

Fig 1.2| Contour integral giving $f(\omega)$ in the upper-half plane.

Fig 1.3| The real part of function (9) representing $\chi'(\omega)$.

Fig 1.4| The imaginary part of function (9) representing $\chi''(\omega)$.

Fig 1.5| The real, reactive part of response function for underdamped case of a harmonic oscillator, plotted with $\omega_0 = 4$ and $\gamma = 0.2$

Fig 1.6| The imaginary, dissipative part of response function for underdamped case of a harmonic oscillator, plotted with $\omega_0 = 4$ and $\gamma = 0.2$

Fig 1.7| The Real and Complex part of response function and Energy.

Fig 1.8| The amplitude and phase response at resonance.

Fig 1.9| Comparison of the imaginary and widely used amplitude response.

Fig 1.10| Approximation graphs of series expansion of $\tan(\phi)$ in orders of ϕ .

Fig 1.11| The evolution of \dot{x} or $\phi_{\Delta x}$ in the real and complex plane as a function of path Δx_i .

Fig 2.1| Schematic representing isotropic space.

Fig 2.2| Schematic representing non-isotropic space.

Fig 2.3| Relation of time phase ϕ' and phase front ϕ .

Fig 2.4| Standing wave schematic assuming non-isotropicity describing the accumulated phase.

Fig 2.5| Implications of accumulated phase and the resulting standing wave description: **A.** The case of a travelling wave in isotropic space, where β and \mathbf{v} , both are constants giving $\beta \cdot \mathbf{v} = \omega$, a constant for a general propagating wave. **B.** The accumulated phase renders the medium non-isotropic in space, signifying that the perturbation would take a longer time to traverse

in space (time dilation), which in other words would mean that the perturbation was slowing down in space. Relativistically, to the wave its velocity remains constant, while the effective path length Δl contracts (length contraction) because of the accumulated phase $\Delta\phi_r$. From an inertial frame however, Δl appears expanded. It thus enforces the condition that β and \mathbf{v} both become functions of $\Delta\phi_r$ from an observers frame of reference outside, and should be related hyperbolically to satisfy the condition $\beta_r \cdot \mathbf{v}_r = \omega$, the resonance frequency or the eigensolution defining the SW case. **C.** Under the conditions of accumulated phase, the familiar wavenumber $\beta = 2\pi/\lambda$ in a propagating wave reduces to a propagation factor $\beta_i = \Delta\phi_r/\Delta l = 2\pi/\lambda_i$, with $\sum_{\text{all paths}} \Delta l = \lambda/4$ in case of a quarter

SW with λ_i analogous to the compressional or deformation factor $\lambda(\mathbf{r})$ in our generalized definition. Since λ_i compresses in \mathbf{r} , β_i gradually increases with $\Delta\phi_r$ giving the very essence of a wave having to go through more number of cycles to travel the same physical length space Δl losing its propagation quality and transforming to a standing or stationary state. Alternatively, the perturbation seems to slow down in space with a gradual reduction in phase velocity \mathbf{v}_r . This fundamental change in the wave description on consideration of the accumulated phase $\Delta\phi_r$ at sub-wavelength scales implying the SW function (4), has profound implications in general.

Fig 2.6| At the fundamental mode resonance in a straight wire, $\Delta\phi_r$ as measured is not a constant agreeing to our hypothesis of accumulated phase. This is in contrary to usual belief. As is clear, the theoretical solutions of (5) for \mathbf{V}_r (blue dashed-dotted lines) with boundary conditions obtained from measured $\Delta\phi_r$ in experiments (red dashed line fits) matches the experimentally measured potentials with an accuracy $\approx 98\%$.

Fig 2.7| A. The match of experimental measured data to theoretical fit obtained from equation (6). The standard wave reflection amplification factor $\alpha = 2$ obtained with the condition of $\Delta\phi_r = 0$ as in a standard definition of wave is highlighted. The background color inlay represents the complex wave field in 2D as a function of accumulated phase $\Delta\phi_r$. **B.** Simulated plots of the complex potential vs the real potential as a function of $\Delta\phi_r$. The generic higher amplification character with higher accumulated phase is evident.

Fig 2.8| Resonance breaks the electron cloud symmetry at the SW frequency creating a nonlinear dependence of the potential explainable through the condition (4) and the phase dependent solution

of (5), the deformation being dependent on the accumulated phase. The condition $\int_r \partial\phi_r \rightarrow \pi/2$

makes the electron cloud deformation extreme. The higher asymmetric electron cloud takes a higher finite time to make its effect felt as a function of space in the metal lattice, hence the accumulated phase. The greater overlap of electron cloud changes the charge distribution in space making them static charges rather than moving charges as in the usual case of $\Delta\phi_r = 0$. The medium thus appears non-isotropic to the perturbation or wave, with the functional form of $\Delta\phi_r$ being a measure of the non-isotropicity. The distributed charges leads to more storage of energy and lesser dissipation for reduction in charge flow. The stored energy corresponds to the imaginary part of the solution of (5) which when plotted in phase space makes evident the accumulated phase that diverges out in spirals rather than collapsing onto the real axis forming a circle or an ellipse.

Fig 3.1| Experimental Schematic with key result. (a) A typical measured graph of dissipation (top) and an artist's impression of a nanostructured resonator surface interacting with gas molecules (bottom). (b) Amplitude response graphs for a nanostructured surface for three measurements of increasing viscosity of ambient gas (black, red, green) showing the exponential variation of the dissipation D on viscosity (inset). (c) Amplitude response graphs for a bare surface for similar three measurements of increasing viscosity of ambient gas (black, red, green) showing the linear variation of D on viscosity (inset). The blue dotted lines joining the amplitude peaks in (b) and (c) represent the same relative change in amplitudes in both cases.

Fig 3.2| Damping with varying media conditions. (a) Results of experiments for a wide range of viscosities for different gases at a fixed temperature, and also temperature dependence for a single gas. 2 orders of magnitude deviation from Stokes' theory shown with a Red arrow. Panels (b) and (c) show the effective magnification of dynamic range of V as a measurement parameter, where 3 orders of dissipation enhancement as compared to a bare surface are highlighted.

Fig 3.3| Observed absolute relative frequency changes $|\Delta f/f|$. Resonance frequency f measured in dry air at normal temperature and pressure conditions for the lowest drive input. All variations in frequency correspond to the expected values with orders of magnitude of 10^{-6} .

Fig 3.4| Damping for a single vapor concentration vs normalized changes resonance amplitude. (a) Shows high sensitivity of the dissipation for a nanostructured resonator vs an equivalent resonator with a non-structured surface. Dashed blue line shows exponential fit

corroborating to our theory. As a representative for detailed analysis check Fig 3.S3 for data points (i) and (ii). **(b)** The corresponding frequency variations, commonly used as a measuring parameter, shows substantial enhancement for nanostructured case, and remains in the order of ppm. **(c)** The variations of velocity are linearly proportional to the change in amplitude, with the slope being very close to 1, as expected.

Fig 3.5| Illustration of the mechanism for spontaneous out-of-phase rod dynamics enhancing dissipation. **(a)** Illustrating in-phase motion of the rods, only the friction of the motion parallel to the resonator contributes to dissipation. **(b)** Two incidents of out-of-phase motion of the rods create a strong motion transversal to the resonator, enhancing the dissipation. The potential function $\Psi(\phi)$ defining the energy of a given state, having the minima at $\phi = 0$ and $\phi = \pi$ with the potential barrier separating the two states (the in-phase and out-of-phase) being ΔE . **(c)** Compiled graphical comparison of experiment and theoretical analysis.

Fig 3.6| Experimental Schematic.

Fig 3.S1| FE-SEM image of nanostructured QC with embedded scale-bars.

Fig 3.S2| XRD-analysis of nanostructured QC.

Fig 3.S3| Conductance vs Frequency response of the Nanostructured QC resonator for small changes in input drive energy.

Fig 3.S4| Accuracy analysis of measured data.

Fig 3.S5| A representative set of dissipation measurements for different gas media as done in sequence. Note that each graph is obtained as a concatenated fit of multiple readings similar to that presented in Fig 3.S3 above.

Fig 4.1| (a) Schematic representation nanowire resonator with equivalent electrical circuit model (please refer to section 1b, Supplementary Information) and the concept of coupling electrical resonances of the nanowire with optical excitation for high selectivity and high sensitivity chemical sensing, (b) SEM images of BFO nanowire, (c) dissipation (D) IR spectrum of adsorbed molecules. Electrical resonance frequency of the nanowire changes due to molecular adsorption, enabling detection of f_g levels of adsorbed mass. Resonant IR excitation of adsorbed molecules produce

large changes in the dissipation of nanowire resonator due to population-depopulation of surface states by thermally generated carriers.

Fig 4.2| (a) Typical time response curve for low thermal mass and high thermal mass systems. (b) Thermal response sensitivity of nanowire resonator with low thermal mass analyzed at SRF as a function of external drive. Inset shows normalized changes in dissipation (D/D_0) as a function of relative changes above room temperature. (c) Time response (τ) variations as a function of heat energy (Q) floor corresponding to external drive; subsequent variations in normalized dissipation (D/D_0) of the nanowire resonator for the same energy fluctuations. Electronic state distribution in a material typically follows Boltzmann distribution and hence their variations as a function of energy all follow logarithmic trends, evident from thermal responses.

Fig 4.3| Electrical resonance of the nanowire resonator without and with adsorbed RDX molecules. The dissipation of the nanowire resonator also changes as a function of molecular adsorption. Inset of Figure 3 show higher magnification in the region of interest. Dissipation change proportional to adsorbed mass.

Fig 4.4| (a) Dynamic dissipation of the nanowire resonator with RDX molecules adsorbed on its surface and irradiated by IR. (b) Normalized dissipation (D/D_0) response of the nanowire resonator as a function of its response time. The selectivity in detection is through to the unique spectral absorption characteristics of the adsorbates in the mid-IR region. A variation in internal dissipation of the nanowire resonator is reflected by its dynamic dissipation in proportion to the small temperature changes due to IR absorption by adsorbates. The dynamic dissipation of the nanowire resonator with adsorbed molecules (without IR irradiation) served as the reference signal.

Fig 4.5| (a) PERS of RDX molecules adsorbed on nanowire (b) comparison PERS and FTIR spectroscopy of RDX molecules. The peaks on the measured PERS matches very well with the FTIR spectra of the analyte molecules. The observed high spectral resolution (linewidth) in PERS of the nanowire resonator is due to its extremely low thermal mass and fast response time ns significantly reducing thermal broadening compared to FTIR. FTIR absorbance \approx photon count; Dissipation from IR absorption is a complementary response in terms of phonon induced heat.

Scheme 4.1| Equivalent RLC circuit model for nanowire resonator (with typical RLC values; $R \sim \Omega$, $L \sim 10^{-7} H$ and $C \sim nF$)

Fig 4.S1| Variation of electrical series inductance (a) and series capacitance (b) of the nanowire resonator as a function of frequency. Variation in inductance is insignificant at resonance whereas, a clear capacitance variation is seen at resonance.

Fig 4.S2| (a) Electrical resonance response of nanowire resonators with various lengths of nanowires. (b) Dissipation and resonance frequency response of nanowire resonators obtained for various nanowire lengths.

Fig 4.S3| Variation in dissipation (a) & capacitance (b) obtained for the nanowire resonator without and with RDX molecules. The order of shift is in KHz to even minute quantities of adsorbates of the order of fg.

Fig 4.S4| Variation in dissipation (a), series capacitance (b) obtained for the nanowire resonator with RDX irradiated at different IR wavelengths.

Fig 5.1| Eigenstate response at a shallow potential of an energy well.

Fig 5.2| Eigenstate response at a deep potential of an energy well.

Forward

The subject of resonance originates from the study of oscillating systems in classical mechanics, philosophically describing dynamics in a potential well, like in a gravitational or a harmonic field binding a particle elastically to origin. It is central to many physical theories in electromagnetism, optics, acoustics, and quantum mechanics, among others. Resonance pertains to motion in a general sense, as in physical displacement in a mechanical system or distribution of charge in an electrical case. Resonance amplifies a small external action by orders of magnitude, while matching the frequency of the external action to a characteristic frequency of the system. This amplification character is exploited in multitude of ideas both in the classical and quantum regime. Resonance has been the key to high sensitive and high accuracy sensing in the past few decades. At its heart is a mechanical resonator, which is driven with the characteristic resonance frequency in order to sustain the motion with the least amount of driving force. The natural goal in such a design is the generation of stable, large amplitude, narrow band oscillations closely approaching the linear (harmonic, or single frequency) regime. The forcing is usually provided through a feedback mechanism, ensuring compensation of energy losses every cycle in order to maintain the constant amplitude. Evidently, the energy losses are deleterious, as higher dissipation leads to broadening of resonance and lowering of amplitude, increasing the need for a higher compensating force, thus decreasing the overall efficiency of the device. Such losses must be accounted for in designing a sensitive sensor platform. Thus, it becomes imperative to understand the nature and origin of this loss. From the aspect of sensor design, dissipation has always been looked upon as something unwanted and thus a primary strategy is to get rid of dissipation effects altogether.

The general equation of motion of a driven resonator expressed in a conventional force balance form (inertial, elastic/compliance, friction/damping and drive) is

$$\ddot{x} + \gamma \dot{x} + \omega_0^2 x = A \cos(\omega t)$$

where the overdots denote derivatives with respect to time, γ the dissipation coefficient related to the Q-factor and ω_0 the resonant frequency given by $\omega_0 = \sqrt{\frac{k}{m}}$ relating the compliance/stiffness to the mass of the resonator. The above equation is the most favourite for people working with resonator based sensing. However, there is more to resonance beyond this equation. In the most general form for the sake of analysis, the drive component is considered a real quantity that has an amplitude A and a frequency chosen to be close to the resonance frequency ω_0 . Systems with feedback adjust A and ω in time by maintaining the amplitude of oscillation x constant. Scaling down to the micron scale typically increases ω_0 to order of hundreds of kHz or even to tens of MHz. More so, it is important to note that the dissipation coefficient γ typically increases slower than ω_0 when the scale of the system is brought down. Recent trend has been to miniaturize the resonators to increase the sensitivity. Also, focus on design and operation of such devices has been on obtaining minimum possible dissipation achievable at that scale. Generally, one attempts to eliminate friction with ambient gas by conducting experiments in high vacuum and low temperatures. While that seems to be an accepted method, the need for high vacuum has been questioned. Theory predicts that at ultra-thin scales, where the mean-free path of the ambient gas molecule is greater than the characteristic length of the resonator, the continuum assumptions breakdown. At such scales, random molecular interactions take effect. As an example, the gain in Q-factor by going from moderate to high vacuum is little, as has been further confirmed by experiments too. That brings us

back to the fundamental question of the undergoing physical phenomenon that causes dissipation.

Dissipation is central to every motion, since there is always an inherent randomness between events at the molecular scale. As a child, we have all at some point of time played with rubber strings in the form of mechanical resonators stretched between two fingers. We may recall that when plucked, the string vibrates with maximum amplitude fixed by the displacement produced by the act of plucking and a frequency essentially depending on the length and stiffness of the string. The more we keep it stretched higher is the frequency. The other fundamental observation in such a playful resonator is the gradual diminishing of the amplitude of vibration in time, which is attributed to mechanical damping. Now what happens if we keep on reducing the size of the string? It is a common observation that the time it takes to stop vibrating goes down and thus must be related to change in damping losses. It becomes customary to understand why the system should damp at all. It turns out to be due to the volume of the fluid in contact with the surface of the string, which it displaces and drags along while in motion. The molecular motion in the fluid is central to the cause of damping. It was Einstein's celebrated work on Brownian motion in 1905, that introduced the concept of molecular motion as heat. His relation, $\mathcal{D} = \mu K T$, relating diffusion coefficient \mathcal{D} of a Brownian particle to its mobility μ , provided a very good basis for experimentally verifying that Brownian motion is in fact related to the thermal motion of molecules. It turns out that this relation is obtained from the equation of motion by equating the energy dissipated by a particle in motion under Stokes drag - $6\pi d\eta v$ to the thermal energy $K T$. Dissipation in a general sense thus originates from time dependent random collision events at the molecular scale. In fluids, it is from the momentum transfer between molecules on collision, viscosity being a measure of the momentum transfer. In electrical system, it is from scattering of free electrons at the

lattice centers, the damping coefficient being the resistance. In all cases, the loss of energy from the aspect of a source is a gain or absorption of energy from the point of view of the system. This has another significance in terms of information content. Since any random event is not invariant under a time reversal $t \rightarrow -t$, information related to the random time events or collisions is inherently encoded in the dissipation. Dissipation is thus a gold mine of information on random events involved in any motion and remains unutilized or overlooked.

Scope and Objective of Thesis

In this work, we show that studying dissipation at resonance, is a way to tap to the dissipation-encoded information, since the resonance condition of motion is a unique state where dissipation is maximized. The goal of this work is to understand the role of dissipation in resonance more fundamentally. We highlight the fact that resonance is not possible without dissipation. In our study, we try to demonstrate that it is possible to use the dissipation as a signature for sensing. This is, to our knowledge, the first time that sensing with dissipation has been demonstrated.

We introduce a variational principle approach in interpreting dissipation by considering any small displacement Δx in the complex plane as,

$$\Delta x(t) = \Delta x'(t) + i\Delta x''(t)$$

with $\Delta x'$ and $\Delta x''$ as the real and imaginary parts of an absolute displacement. The slope of Δx in time, giving the velocity \dot{x} is given by $\tan(\phi) = \Delta x''/\Delta x'$, where ϕ is the phase. The evolution of \dot{x} in motion corresponds to changes in $\tan(\phi)$. A large change in slope corresponds to a rapid change in effective \dot{x} , which means $\Delta x''$ changes more rapidly

compared to $\Delta x'$, leading to higher dissipation in the system. With this consideration, a measure of the dissipated energy or the work done on the system for a displacement Δx ,

translates to

$$I = \int_{path} \dot{x} \Delta x'' = \int_{path} \phi_{\Delta x_j} \Delta x''$$

over any arbitrary path j in which the motion takes place and where $\phi_{\Delta x_i} = \dot{x}$ is the phase functional corresponding to a path j . Dissipation is thus introduced as a variational problem where the integral I , representing accumulative action of dissipative forces, is maximized at the condition of resonance.

The inherent maximization property of dissipation at resonance has a profound significance in terms of understanding the nature of dynamics in a generic potential well. Physically it means that a particle undergoing a motion in a potential well is drawn to the potential well minima at resonance. Dissipation promotes this transition. Resonance frequencies or Eigen solutions in general thus define the potential minima's allowable in a system and dissipation corresponds to the cumulative sum of energy lost by a particle undergoing motion to attain that potential minima.

Organization of thesis

Section I. *Role of Dissipation in Resonance: A Variational Principle Approach* – is the introductory chapter. It reviews the concept of resonance in the light of complex response function. The importance of the imaginary part of the response function as a measure of the dissipated energy is explained. A variational principle approach to understanding dissipation as a functional of phase ϕ , dependent on arbitrary paths in a system is also introduced.

Section II. *Standing wave revisited: accumulated phase and resonance amplification* - reviews resonance in the light of standing waves. The underlying phenomenon of standing waves is re-explored to explain the elusive resonance amplification from a radically alternate perspective using a path integral approach similar in form to Feynman's quantum theory. The monograph carefully reconsiders standing wave definition from the aspect of phase ϕ in time and space, and comments on resonance amplification factor from a hypothesis-formulated in terms of measured ϕ in space. This time-phase evolution in space is explained as a continuous accumulated phase within the physical bounds of a resonator. The importance of the evolution of phase ϕ and its role in the origin of standing waves at resonance is highlighted. Comparison of theoretical results and experimental data show an excellent match. In addition, the fundamental treatment makes the formulation applicable to all resonating systems in a general way. More specifically, the fundamental question concerning resonance - *How does the amplification come about and what determines the amplification factor of a resonant system in the light of dissipation* is addressed. An in-depth discussion of the argument of dissipation driven transition of a particle to a potential

well minima is presented in the light of the amplification factor or the efficiency of the transition as the ratio of the stored to the dissipated energy.

Section III. A nanostructured surface increases friction exponentially at the solid-gas interface - addresses a surprising effect brought about by nanostructuring a surface of a macro resonating system. The key observation points of the research are the following:

- A drastic deviation from the age-old Stokes linearity law of friction drag with respect to media viscosity change.
- A dense array of nanostructures on a surface with spacing comparable to mean free path of air molecules, can bring about such deviation, greatly enhancing frictional drag by orders of magnitude.
- The deviation in particular follows an exponential law with respect to changes in the kinematic viscosity.
- The profound amplification effect can be utilized in designing new age sensors and can also be the basis of further fundamental studies of nanoscale flows at solid-gas interfaces.

The Stokesian regime of very low Reynolds number typically deals with a continuum energy scale governed by the long range viscous interactions. The work in this monograph shows that, when multiple coupled oscillators are involved, in the limits of continuum breakdown, inherent randomness in interactions with the media molecules can no longer be neglected leading to an additional non-continuum energy scale. These two scales compete in bringing long range order over an inherent randomness and we show that such interplay of energy scales can be explained by generalized Gibbs measure. The implication of such competing dynamic scales in the limits of continuum breakdown is profound revealing an extraordinary amplification phenomenon. The work tries to highlight this in the context of an apparent dynamic range magnification of gas kinematic viscosity, making it a suitable parameter for gas characterization even in normal atmospheric conditions. The results obtained from this work can be extended to other physical systems where such

competing scales can be in play in *Nature*. One such example can be the hierarchical micro-nanostructures on wing-cuticles of insects, where the role of many such structures is still not known.

Section IV. Photothermal electrical resonance spectroscopy of physisorbed molecules on a nanowire resonator - introduces a new platform of using a semiconductor nanowire combined with infrared (IR) for molecular recognition of femtograms of adsorbed molecules exploiting dissipation signature at electrical resonance. The technique exploits the combination of very low thermal mass of the nanowire and high number of surface states on the nanowire for detection. Researchers always try to avoid surface states as they cause noises in the system during normal working of a semiconductor. Most of the surface states effects are very small for bulk systems. Because of the large surface-to-volume ratio of a nanowire, they play a significant role in nanowire electrical properties. Dissipation driven transition at play is studied here in the light of surface state population and de-population. The results obtained from this work can be extended in determining the density of surface states in a semiconductor material resonantly from dissipation signature.

Section V. Conclusion and Discussions - summarizes the overall thesis and research progress done so far and also gives a brief account on the future aspects of the present work.

Bibliography presents a comprehensive list of literature relevant to the work presented.

I. Role of Dissipation in Resonance: A Variational Principle Approach

1.1 Understanding Resonance

The concept of resonance originates from the study of oscillating systems in classical mechanics. Philosophically, it caters to dynamics in a potential well, like in a gravitational or a harmonic field binding a particle elastically to origin. Resonance is central to many physical theories in electromagnetism, optics, acoustics, and quantum mechanics, among others. Resonance amplifies a small external action by orders of magnitude, while matching the frequency of the external action to a characteristic frequency of the system. This amplification character is exploited in multitude of ideas both in the classical and quantum regime, mostly in sensing and characterization. Standing waves are at the heart of explaining the phenomenon with resonance treated as eigenvalue solutions (standing waves) of an eigenfunction (wavefunction or quantized energy state of a potential well) in the quantum analogue. The classical eigenstate becomes a function of the external force (repulsive action) that balances the attractive potential forces towards the center of the well.

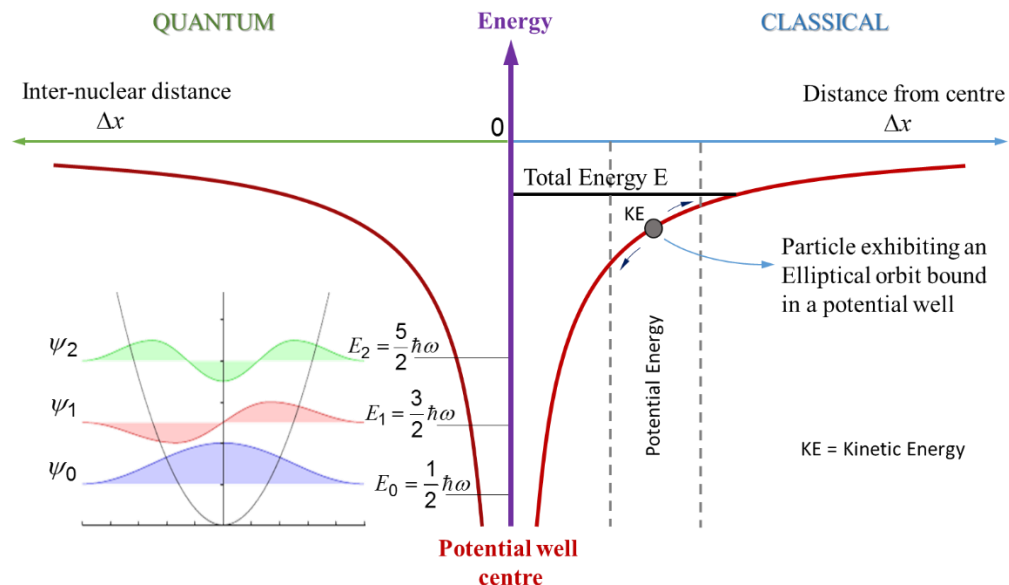


Fig 1.1| Resonance and wavefunctions in a potential well;
the classical case being in the limit $n \rightarrow \infty$.

At the turn of the 20th century, understanding particle dynamics from the aspect of a wave description became central in linking two seemingly scale-disjoint classical and quantum fields with a broad applicability from atomic to cosmological scale in a general sense. The phenomenon of resonance was the backbone. Historically, formulations starting from Plank's work on energy of resonators and Bohr's description of an atom to Heisenberg's idea of quantization map bear justice to this. Schrödinger's description of quantum numbers as eigenvalues of the wavefunction is the forerunner in the field. Interestingly, the time dependent form of Schrödinger's wavefunction, similar in form to a non-linear wave equation, yields from the classical à la the Hamilton-Jacobi equation. In another historic work, de Broglie introduced the concept of electrons having the wave property though being a fundamental particle of matter. A little later, Feynman introduced a path integral approach connecting quantum mechanical behavior with such classical ideas as the Lagrangian or in particular, the indefinite integral of the Lagrangian in describing general Hamilton's principle. All such seminal ideas bear testimony to some quantum phenomenon or measurements, though was argued against by Lamb. Incidentally, the classical regime was explained as a special case of quantum in the limit of $n \rightarrow \infty$, where n is the number of energy levels or eigenstates. Some recent expositions rekindle interests in reconsidering the fundamentals in the context of classical resonance description. Here in the introduction chapter of this thesis we will expound a mathematical framework discussing properties of response function that describes classical resonance and simultaneously highlights the importance of dissipation in a general sense. Understanding the origin and role of dissipation will be our guide in binding the results obtained for different resonating

systems, crucial in understanding the resonance process in general. An exhaustive bibliography at the end of the thesis follows, citing relevant research work.

Resonance amplification has always been studied in the light of improving quality factor (Q-factor) of response in order to achieve higher frequency sensitivity crucial in sensor or filter designs. The Q-factor is defined as the ratio of the stored to dissipated energy per cycle of motion at resonance. Resonance pertains to motion in a general sense, as in physical displacement (mechanical) or distribution of charge (electrical), and hence in order to understand resonance it is required to understand general motion itself from the aspect of response theory. The goal of response theory is to understand the reaction of a system to outside influences like an applied force, electric and magnetic fields, or an applied pressure. A brief mathematical primer on response function is necessary to form a better understanding of complex dynamics involved in resonance conditions.

We start by explaining, what is meant by an outside influence on a system. E.g., if a shearing force is applied to a fluid, its response is to move; the viscosity determines how much it moves. If a temperature gradient is applied, the response is for heat to flow; the amount of heat is determined by the thermal conductivity. If a potential gradient is applied across a wire, the response is a flow of current; the resistance determining the magnitude of current. Such flow problems in physics are generally studied in terms of a time independent constant external influence. Resonance on the other hand occur from time dependent external influences and hence we will restrict our discussions to time dependent oscillating actions. As we will see, by studying the response of the system at different frequencies, we learn important information about what is going on inside the system itself.

1.2 Forces in Classical Dynamics and Response Function

Consider a simple dynamical system with some generalized coordinates $x_i(t)$ that depend on time. When left alone, these coordinates obey Newton's laws giving equations of motion for unit mass of the form,

$$\ddot{x}_i + g_i(\dot{x}, x) = 0.$$

where $g(\dot{x}, x)$ is a function dependent on the displacement and the rate of displacement defining the system. The dynamics described by the above equation in general need not always be Hamiltonian i.e., where the sum of the kinetic and potential energies $T + V = \text{constant}$, T being the kinetic energy and V the potential energy in usual notations of classical mechanics. Indeed, often, or in almost all cases, frictional forces need to be accounted for, since in all dynamics, there are inherent losses involved. The deviation from a Hamiltonian thus stems from the non-conservative frictional forces inherent in any motion. The outside influence arise from perturbing the system by the addition of some driving forces $F_i(t)$, where the equations of motion become,

$$\ddot{x}_i + g_i(\dot{x}, x) = F_i(t) \quad (1)$$

In the expressions above $x_i(t)$ are dynamical degrees of freedom exhibited by the motion. This is what we solve for in general in understanding the dynamics of the system. In contrast, $F_i(t)$ are not dynamical since they are forces that are under our control, like someone pulling on the end of a spring or an external potential source connected to an electrical line. In many cases, the outside influence can be a random force $\xi_i(t)$ leading to stochastic dynamics. The random force in general is a stochastic process randomly changing in time. Such random external forces $\xi_i(t)$ cause random physical processes and

can be independent of $F_i(t)$, like in Brownian dynamics, and the problem reduces to solving a Langevin type equation for $x_i(t)$ and $\dot{x}_i(t)$ that are stochastic. Here in our discussions, we will focus on classical non-stochastic equations only. Implications of stochastic interactions and its relation to general dynamics at resonance will be elucidated in the conclusion chapter (section *V*), with reference to results that are presented in sections *III and IV* of this thesis. First, let us discuss the dynamics that is dependent on $F_i(t)$ where the time dependence can be decided or is known.

It would be useful to have a concrete example at the back of our mind in understanding dynamics at resonance from the general equation of motion (1). For this, we take the case of a simple harmonic oscillator with sinusoidal forcing $F(t) = F_0 e^{i\omega t}$. We also include a friction term, proportional to damping coefficient γ , with which the kernel $g_i(\dot{x}, x)$ in (1) can be expanded in terms of dissipation and harmonic components giving,

$$\ddot{x} + \gamma \dot{x} + \omega_0^2 x = F(t), \quad (2)$$

ω_0 being the characteristic undamped fundamental harmonic frequency of the system. We will discuss this model in detail and comment on the evolution of the dissipation term $\gamma \dot{x}$.

It is necessary to determine the response function or Green's function, $\chi(t - t')$ of this system at an elapsed time t' , which effectively solves for the dynamics of the system. It follows that if the form of $F(t)$ is known, then the motion is given by

$$x(t) = \int_{-\infty}^{+\infty} F(t') \chi(t - t') dt' \quad (3)$$

The standard method to determine $\chi(t)$ is through an inverse Fourier transform in ω

$$\chi(t) = \int \frac{d\omega}{2\pi} e^{-i\omega t} \chi(\omega)$$

where, the Fourier transform is obtained in terms of ω , the external influence or drive frequencies giving the spectral density of response $\chi(\omega)$. Using the above form of $\chi(t)$, the equation of motion (2) reduces to,

$$\int_{-\infty}^{+\infty} \frac{d\omega}{2\pi} \int_{-\infty}^{+\infty} dt' [-\omega^2 - i\gamma\omega + \omega_0^2] e^{-i\omega(t-t')} \chi(\omega) F(t') = F(t) \quad (4)$$

This has a solution if $\int d\omega$ gives a delta function of the form $\delta(t) = \frac{1}{2\pi} \int e^{-i\omega t} d\omega$, obtained

when $\chi(\omega) = \frac{1}{-\omega^2 + i\gamma\omega + \omega_0^2}$. (5)

This is independently deducible for a drive function in a general complex form $F(t) = e^{i\omega t}$ in ω . It is interesting to note that the generalized response function is complex in natural form and not a real quantity. There is a whole lot of simple physics in the complex response function in ω given by equation (5) which we will explain below and that can be carried over to more complicated systems in a general sense. It is useful to express the response function $\chi(\omega) = Re \chi(\omega) + i Im \chi(\omega)$ as

$$\chi(\omega) \equiv \chi'(\omega) + i\chi''(\omega)$$

where the real and imaginary parts have different interpretations and physical significances in terms of the dynamical information. Let's look at these in turn.

- **Imaginary Part:** The imaginary part of $\chi(\omega)$ can be expressed as

$$\begin{aligned} \chi''(\omega) &= -\frac{i}{2} [\chi(\omega) - \chi^*(\omega)] \\ &= -\frac{i}{2} \int_{-\infty}^{+\infty} dt \chi(t) [e^{i\omega t} - e^{-i\omega t}] \end{aligned}$$

$$= -\frac{i}{2} \int_{-\infty}^{+\infty} dt e^{i\omega t} [\chi(t) - \chi(-t)],$$

where $\chi^*(\omega)$ is the complex conjugate of $\chi(\omega)$. It is evident that the imaginary part of $\chi(\omega)$ is a component of the response function that is not invariant under a time reversal $t \rightarrow -t$. The physical significance being that the imaginary $\chi''(\omega)$ encodes dynamical information of time dependent interactions during motion. In other words, $\chi''(\omega)$ knows the arrow of time. The forces involved in bringing about the imaginary part of the response function are non-conservative and thus typically originate from processes that result in energy dissipation in a system. Dissipation thus plays a key role in the response dynamics and we will discuss in detail the origin of dissipation in a forthcoming section.

- **Real Part:** Similar analysis as above also deduces to

$$\chi'(\omega) = \frac{1}{2} \int_{-\infty}^{+\infty} dt e^{i\omega t} [\chi(t) + \chi(-t)],$$

as a time invariant part, that does not care about the arrow of time. It is the reactive part of the response function and corresponds to the storage components in the system and is an even function since $\chi'(-\omega) = +\chi'(\omega)$. It is called the reactive part since it represents the reaction to external action. The physical significance is that the reactive/stored energy part corresponding to any motion encodes the total energy or the Hamiltonian of the system at any moment in time.

The fact that the imaginary part knows the arrow of time is crucial in understanding the importance of dissipation in any motion that directly follows from the mathematical properties of the response function. So, first let us discuss in detail the mathematical properties of the relations expressed above in relation to motion.

1.3 Causality

One of the biding laws of all motion is that it cannot affect the past. This statement of causality demands that any response function must satisfy

$$\chi(t) = 0 \quad \text{for all } t < 0.$$

For this reason, the response function χ is often referred to as the causal Green's function or retarded Green's function. The causality requirement has the following property for the

Fourier expansion $\chi(t) = \int_{-\infty}^{+\infty} \frac{d\omega}{2\pi} e^{-i\omega t} \chi(\omega)$: for $t < 0$, the integral can only be enforced

by completing the contour in the upper-half plane, the exponent becoming $-i\omega \times (-i|t|) \rightarrow -\infty$ leading to the result $\chi(t) = 0$. Of course, the integral is given by the sum of the residues inside the contour. So for the response function to vanish for all $t < 0$, the response function $\chi(\omega)$ should have no poles in the upper-half plane. In other words, causality demands that $\chi(\omega)$ is analytic for all $\text{Im } \omega > 0$. From the physics aspect, it means that the response function should not have any singularity i.e., an unbounded response.

The fact that χ is analytic in the upper half plane means that the real and imaginary parts, χ' and χ'' are related, and are given by the Kramers-Kronig relations. We derive the relations below to understand the nature of the response function in general, crucial in understanding resonance.

1.4 Kramers-Kronig relations and Resonance

To gauge the dynamics in ω or in Fourier space, it is required to understand the behavior of the response function χ at all points in the upper-half plane or in a general sense in the

interval $\omega \in [-\infty, \infty]$. Invoking analyticity of χ in the upper-half plane following the condition of causality, it is required to compute the integral

$$f(\omega) = \frac{1}{i\pi} \oint_C d\omega' \frac{\chi(\omega')}{\omega' - \omega} \quad \omega \in [-\infty, \infty] \quad (6)$$

Here, the contour C skims over the real axis, with bounds at infinity. The function $f(\omega)$ in essence gives the relation between χ' and χ'' of a general response function in (5).

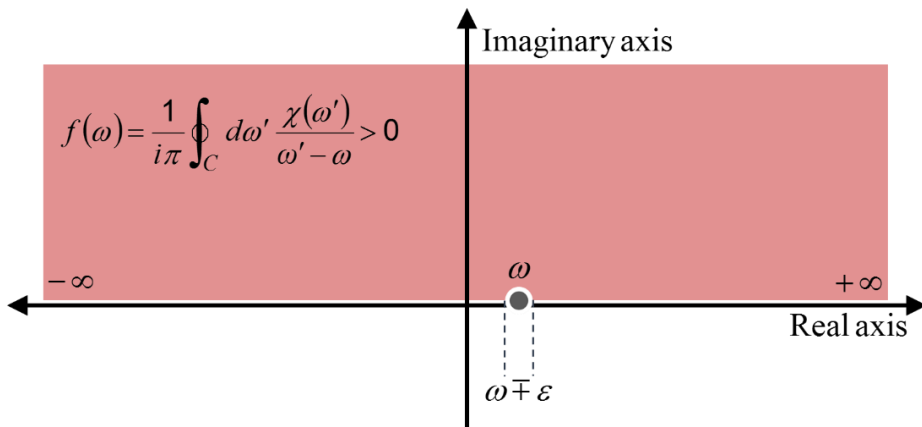


Fig 1.2| Contour integral giving $f(\omega)$ in the upper-half plane.

It is clear from (6) that the integral diverges at $\omega' = \omega$, denoting the resonance frequency for a harmonic oscillator in general. So in order to avoid the singularity, the contour of the integral running into the complex plane needs to be deformed, either just above the singularity along $\omega' + i\varepsilon$ or just below the singularity along $\omega' - i\varepsilon$. This is equivalent to shifting the position of the singularity to $\omega \rightarrow \omega \mp \varepsilon$ on the real axis, represented in the figure above by the white annular area around the singularity point ω . Invariably, the shifted positions $\omega \mp \varepsilon$ give different results for the integral in (6). Invoking Cauchy's residue theorem, the effective response function can be determined using,

$$\frac{1}{2} [f(\omega + i\varepsilon) - f(\omega - i\varepsilon)] = \chi(\omega) \quad (7)$$

as the difference of the results about the singularity ω , while the principal or the average value of the two functions, either side of the discontinuity, deducing to,

$$\frac{1}{2}[f(\omega+i\varepsilon)+f(\omega-i\varepsilon)] = \frac{1}{i\pi} \mathcal{P} \int_{-\infty}^{+\infty} \frac{\chi(\omega')}{\omega'-\omega} d\omega' \quad (8)$$

Here \mathcal{P} denotes the principal value of the integral. The physical meaning of the principal part is revealed from the real and imaginary parts of the denominator in the integrant $1/[\omega' - (\omega \pm i\varepsilon)]$,

$$\frac{1}{\omega' - (\omega \pm i\varepsilon)} = \frac{\omega' - \omega}{(\omega' - \omega)^2 + \varepsilon^2} \pm i \frac{\varepsilon}{(\omega' - \omega)^2 + \varepsilon^2} \quad (9)$$

As evident, the sum of $f(\omega+i\varepsilon)$ and $f(\omega-i\varepsilon)$ in (8) isolates the real part in (9) above. In essence, the real part $\chi'(\omega)$ represents a smooth function going through zero that has been obtained by suitably truncating a small segment of $1/(\omega' - \omega)$, symmetric about the divergent point ω , plotted below for $\omega' = 1$ (the point of singularity) and different ε 's.

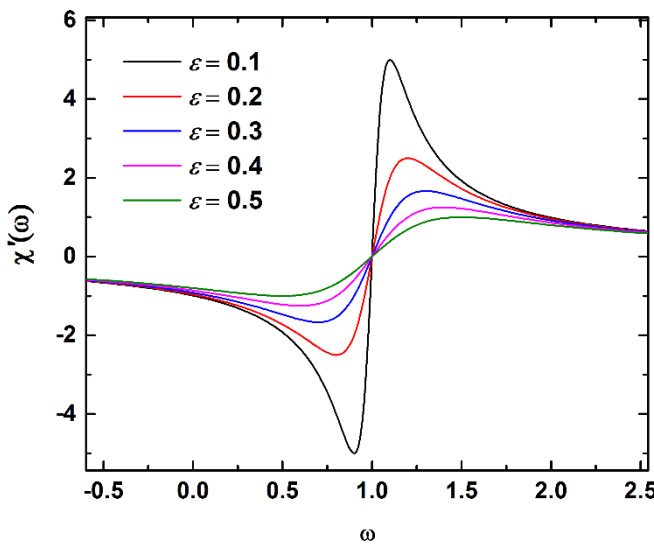


Fig 1.3| The real part of function (9) representing $\chi'(\omega)$.

As $\varepsilon \rightarrow 0$, $\chi'(\omega)$ becomes a rapidly varying function in ω at the 0 crossing. We can also see the meaning of the imaginary part of (9) when plotted for $\omega' = 1$ and different ε 's.

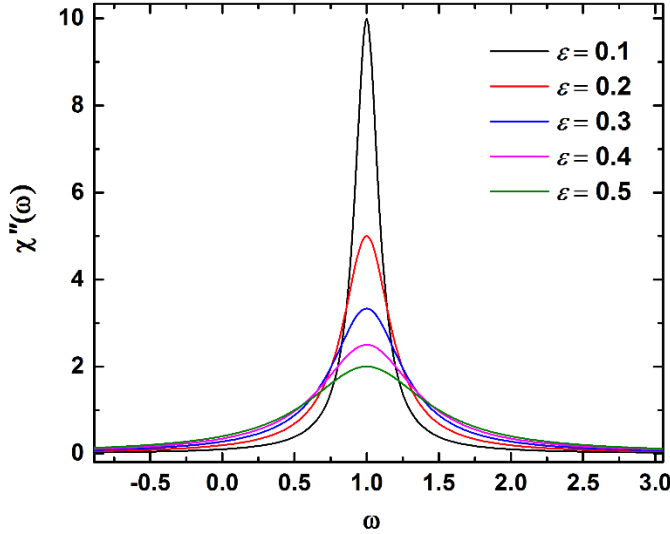


Fig 1.4| The imaginary part of function (9) representing $\chi''(\omega)$.

As $\varepsilon \rightarrow 0$, $\chi''(\omega)$ tends towards a delta function as expected from (5) and (7). For a finite ε , $\chi''(\omega)$ is a regularized version of the delta function. Using equations (7) and (8)

$$f(\omega - i\varepsilon) = \frac{1}{i\pi} \mathcal{P} \left[\int_{-\infty}^{+\infty} \frac{\chi(\omega')}{\omega' - \omega} d\omega' \right] - \chi(\omega) \quad (10)$$

From the condition of causality, the integral in (6) has to be zero since $\chi(\omega)$ has no poles in the upper-half plane, and is also equivalent to $f(\omega - i\varepsilon)$. This means that $f(\omega - i\varepsilon) = 0$, or from (10)

$$\chi(\omega) = \frac{1}{i\pi} \mathcal{P} \int_{-\infty}^{+\infty} \frac{\chi(\omega')}{\omega' - \omega} d\omega' \quad (11)$$

Of importance is the factor of “ i ” in the denominator giving the complex form of response function as in (9), the real and imaginary parts of which has been plotted above. Obtaining the real and imaginary parts gives,

$$Re \chi(\omega) = \chi'(\omega) = \frac{1}{\pi} \mathcal{P} \int_{-\infty}^{+\infty} \frac{Im \chi(\omega')}{\omega' - \omega} d\omega' \quad (12)$$

and

$$Im \chi(\omega) = \chi''(\omega) = -\frac{1}{\pi} \mathcal{P} \int_{-\infty}^{+\infty} \frac{Re \chi(\omega')}{\omega' - \omega} d\omega' \quad (13)$$

These are the Kramers-Kronig relations and they follow from the condition of causality.

The importance of the relations is that the dissipative imaginary part of the response function $\chi''(\omega)$ is determined in terms of the real part $\chi'(\omega)$, and vice-versa, though the relationship is non-local in frequency space. That is, either has to be known for all frequencies to reconstruct the other.

Another way of writing these relations to reconstruct $\chi(\omega)$ directly from (5) is to consider the integral

$$\int_{-\infty}^{+\infty} \frac{1}{i\pi} \frac{Im \chi(\omega')}{\omega' - \omega - i\varepsilon} d\omega' \quad (14)$$

where the “ $-i\varepsilon$ ” in the denominator considers integration just below the real axis. Here ε takes the meaning of the dissipation constant γ in (2) and (5) describing motion. Using equation (7) and (8) once again,

$$\begin{aligned} \int_{-\infty}^{+\infty} \frac{1}{i\pi} \frac{Im \chi(\omega')}{\omega' - \omega - i\varepsilon} d\omega' &= Im \chi(\omega) + \mathcal{P} \int_{-\infty}^{+\infty} \frac{1}{i\pi} \frac{Im \chi(\omega')}{\omega' - \omega - i\varepsilon} d\omega' \\ &= Im \chi(\omega) - i Re \chi(\omega) \end{aligned} \quad (15)$$

Thus, knowing the dissipative part of the response function, the entire response function $\chi(\omega)$ can be reconstructed.

This singular mathematical property of the imaginary or the dissipative term is actively considered in resonance analysis. The imaginary $\chi''(\omega)$ is called the dissipative or absorptive part of the response function, with ε being the coefficient of absorption. From the aspect of the source or external action, ε represents the damping coefficient. $\chi''(\omega)$ is also known as spectral function containing information about the density of states in the system that take part in absorptive processes. These will be further discussed later.

1.5 Resonance and Dissipation

Now that a mathematical primer on the complex response function and its properties has been discussed, let us rewrite (15) in the form of $\chi(\omega) = \operatorname{Re} \chi(\omega) + i \operatorname{Im} \chi(\omega)$ giving the *main result* describing resonance response from equation of motion (2) as,

$$\chi(\omega) = \int_{-\infty}^{+\infty} \frac{1}{\pi} \frac{\operatorname{Im} \chi(\omega')}{\omega' - \omega - i\gamma} d\omega' \quad (16)$$

The above result represents the spectral response or the Fourier space response of a general motion described by equation (2) with $\gamma \propto \varepsilon$ denoting the damping or the annular area of the contour deformation satisfying the condition of causality. The entire point of avoiding the point of singularity in the contour integral is to get a real function continuous through 0 giving a measure of the stored energy component that is tangible. The singularity makes the response function complex, the imaginary part giving a measure of the lost energy that is not perceivable. It is only at resonance, that the imaginary part is reflected as a spectral peak denoting the absorption density. As pointed before, the entire response of the system can be reconstructed if the imaginary part of the response function is known. Thus obtaining the Fourier space response of a system for harmonic analysis in essence

investigates equation (16) in a physical experiment involving a resonator. The magnitude of ε is dependent on the random processes as an inherent part of the motion. This would be elucidated more in the conclusion section, once we discuss in detail experimental findings involving random effects in sections *III and IV*.

As has been established before, (16) can be solved if $\int d\omega'$ is a delta function and since it can be represented in the form of $2\pi\delta(t) = \int e^{-i\omega't} d\omega'$, (16) reduces to,

$$\chi(\omega) = \frac{1}{-\omega^2 + i\gamma\omega + \omega_0^2} \quad (17)$$

Let us understand the physics involved in the above result. Firstly, the equation above can be analyzed from the point of view of susceptibility of motion, i.e., $\chi(\omega=0)$ giving

$$\chi(\omega=0) = \frac{1}{\omega_0^2} \quad (18)$$

Evidently, the observable change by a *time independent* perturbation of the system, i.e., a static force would give

$$x = \frac{F}{\omega_0^2} \quad (19)$$

or the spring deformation for an external force F as expected, following the equation of motion (2).

For *time dependent* perturbations the structure of the response function needs to be analyzed in the complex ω -plane vide discussions in Sections 1.2 and 1.3 above. The poles are at the solution points of $\omega_*^2 + i\gamma\omega_* - \omega_0^2 = 0$. Solving the quadratic using Sridhacharya's formula gives,

$$\omega_* = -\frac{i\gamma}{2} \pm \sqrt{\omega_0^2 - \gamma^2/4} \quad (20)$$

Note: ω_* can be both positive and negative. The positive and negative frequencies are the result of properties of the Fourier transform that refer to the clockwise (-ve) and anti-clockwise (+ve) sense of rotations of the complex exponentials in the imaginary plane.

There are three different regimes that we can consider separately,

- **Underdamped:** $\omega_0^2 > \gamma^2/4$. In this case, the poles have both a real and imaginary part and they both are on the lower half plane. This agrees to the general discussion on causality before – Section 1.2, signifying that the response function remains analytic in the upper-half plane.
- **Overdamped:** $\omega_0^2 < \gamma^2/4$. Here, the poles lie on the negative imaginary axis and neither are on the upper-half plane. This condition is also consistent with causality.
- **Critically damped:** $\omega_0^2 = \gamma^2/4$. The single pole in this case is on the negative imaginary axis, also consistent with the condition of causality.

Further, a few mathematical steps gives the real and the imaginary parts of the response function, which when plotted, physically represent the energy associated with the motion, and allows us to gain some intuition about the response at resonance. From (17) it follows,

$$\operatorname{Re} \chi(\omega) = \frac{\omega_0^2 - \omega^2}{(\omega_0^2 - \omega^2)^2 + \gamma^2 \omega^2} \quad (20)$$

This represents the real or the stored component of the system corresponding to the potential function or the potential well of the system in which the oscillations take place.

Parallel can be drawn in terms of Hamiltonian analysis where this real part corresponds to the total energy of the system at any point in time. Physically, the higher the functional value of $\text{Re } \chi(\omega)$, more the system responds to a frequency. As discussed before, the real part being time invariant, the function is even or mirror symmetric about $\omega=0$ in frequency space as revealed in the figure plotted.

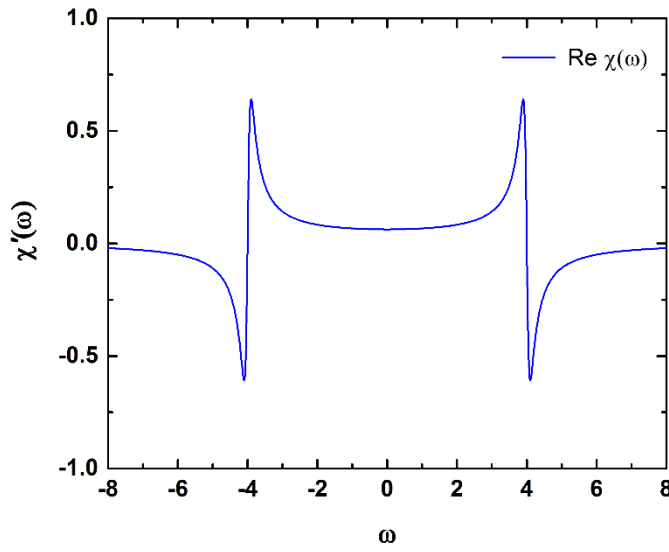


Fig 1.5| The real, reactive part of response function for underdamped case of a harmonic oscillator, plotted with $\omega_0 = 4$ and $\gamma = 0.2$

Similarly, the imaginary part from (17) reduces to

$$\text{Im } \chi(\omega) = \frac{\gamma\omega}{(\omega_0^2 - \omega^2)^2 + \gamma^2\omega^2} \quad (21)$$

The imaginary part is most interesting, representing the dissipative part of the response function. As clear from the plot of the underdamped case above, it is an odd function that peaks at $\omega \rightarrow \pm\omega_0$, the frequencies where the system vibrates naturally. Unlike the real part that crosses through 0 at the natural frequencies, the imaginary part peaks. This character makes the imaginary part most interesting in terms of the dissipation in the system, signifying that the system is most efficient in absorbing energy at the peak

frequency. It must be noted here that $\text{Im } \chi$ is proportional to γ , the frictional coefficient. However, as $\gamma \rightarrow 0$, $\text{Im } \chi$ does not become 0; instead it tends towards two delta functions at $\omega \rightarrow \pm\omega_0$.

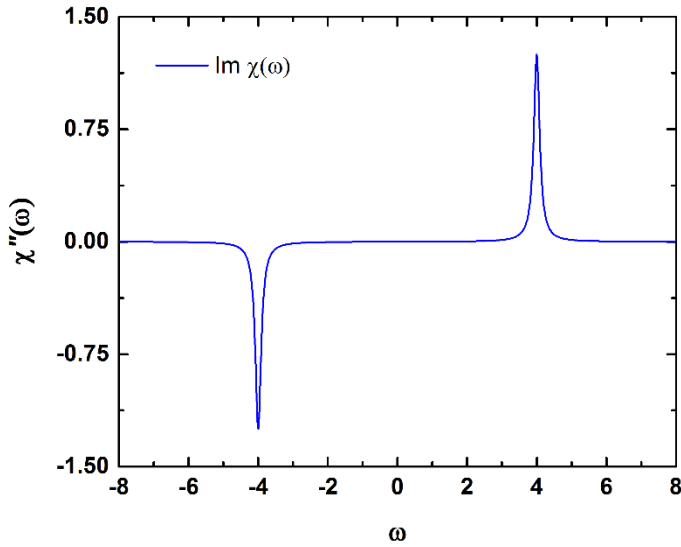


Fig 1.6 The imaginary, dissipative part of response function for underdamped case of a harmonic oscillator, plotted with $\omega_0 = 4$ and $\gamma = 0.2$

1.6 Dissipation maximization and its relation to $\text{Im } \chi$

Dissipation can be understood by computing the energy absorbed by the system and its rate is given by $\frac{dW}{dt} = F(t) \dot{x}(t)$. In a true sense, the vector product of the force and the velocity gives the rate of work done. Here let us assume for the time being that they are vector-collinear. Non-collinearity would only add a pre-factor in the result depending on the vector angle between the two. Expanding it in terms of the response function, we get,

$$\frac{dW}{dt} = F(t) \frac{d}{dt} \int_{-\infty}^{+\infty} \chi(t-t') F(t') dt'$$

$$\begin{aligned}
&= F(t) \int_{-\infty}^{+\infty} dt' \int_{-\infty}^{+\infty} \frac{d\omega}{2\pi} (-i\omega) e^{-i\omega(t-t')} \chi(\omega) F(t') \\
&= \int_{-\infty}^{+\infty} \frac{d\omega}{2\pi} \frac{d\omega'}{2\pi} [-i\omega \chi(\omega)] e^{-i(\omega+\omega')t} F(\omega) F(\omega') \quad (22)
\end{aligned}$$

Let us now drive the system with a force of a specific frequency Ω , as usually done in experiments, so that

$$F(t) = F_0 \cos \Omega t = F_0 \operatorname{Re}(e^{-i\Omega t}) \quad (23)$$

It is crucial that we make the force real here at this stage of formulation following the reality of force (or source) to abide by the analytic properties of response function as discussed in Sections 1.2 and 1.3 before. A more detailed formulation dependent on complex forcing can be developed, that essentially would give non-linear response functions. Here, we restrict ourselves to linear responses only for simplicity of presentation and for making a fundamental point on the nature of dissipation. Taking the Fourier transform, the driving force is

$$F(\omega) = 2\pi F_0 [\delta(\omega - \Omega) + \delta(\omega + \Omega)] \quad (24)$$

Using (24) in equation (22) we get,

$$\frac{dW}{dt} = -i F_0 \Omega [\chi(\Omega) e^{-i\Omega t} - \chi(-\Omega) e^{i\Omega t}] [e^{-i\Omega t} + e^{i\Omega t}] \quad (25)$$

This is an oscillating function in time and it is more useful to take an average over a cycle,

$$\overline{\frac{dW}{dt}} \equiv \frac{\Omega}{2\pi} \int_0^{2\pi/\Omega} dt \frac{dW}{dt} = -i F_0^2 \Omega [\chi(\Omega) - \chi(-\Omega)] \quad (26)$$

The over-bar represents the average. Now from discussions in sections above, $\operatorname{Re} \chi(\omega)$ is an even function while $\operatorname{Im} \chi(\omega)$ is odd. Using this property, from (26) we can write

$$\overline{\frac{dW}{dt}} = 2F_0^2\Omega \operatorname{Im} \chi(\omega) \quad (27)$$

i.e., the work done is proportional to $\operatorname{Im} \chi(\omega)$. We have derived this result on general grounds only from the even/odd property of the real/imaginary parts and not the exact form of the response function.

For a damped harmonic oscillator we can use the explicit form (21) and the result above in (27) to derive the *important result*

$$\overline{\frac{dW}{dt}} = 2F_0^2 \frac{\gamma \Omega^2}{(\omega_0^2 - \Omega^2)^2 + (\gamma \Omega)^2} \quad (28)$$

This is maximum when the harmonic oscillator is driven at its natural frequency, $\Omega = \omega_0$. As the treatment above illustrates, the imaginary part of the response function gives us the frequencies at which the system naturally vibrates. In essence, the system absorbs energy most efficiently at these frequencies.

1.7 A variational principle approach of Dissipation

It is interesting that dissipation maximizes at the condition of resonance and not elsewhere i.e, for driving frequencies Ω way off from ω_0 . For such off-frequencies, dissipation is much less compared to the real or the stored energy in the system. This is the physical significance of general Lagrangian and Hamiltonian analysis with the assumption that dissipation is negligible. The physics behind it being the assumption that the generalized motion $x_i(t)$ with an external influence following equation (2) is typically small, making the $\dot{x}_i(t)$ also small to an extent that the dissipation force $\gamma \dot{x}_i$ and its variation with motion can be neglected.

For considering the stored or the real component of the energy, the real part of the response function $\chi'(\omega)$ is crucial, obtained as a contour integral over the real axis as in equation (7) with the points of singularity truncated. It is analogous to computing the Hamiltonian $H = T + V$ of a system, where T is the kinetic energy and V is the potential energy in usual notations. H gives a measure of the energy of the system that is responsible for giving the real response. As has been discussed before, higher the real part of the response function, more the system responds to an external action. This fact can be reflected upon from the mathematical properties of $\chi'(\omega) = \text{Re } \chi(\omega)$, that is continuous and

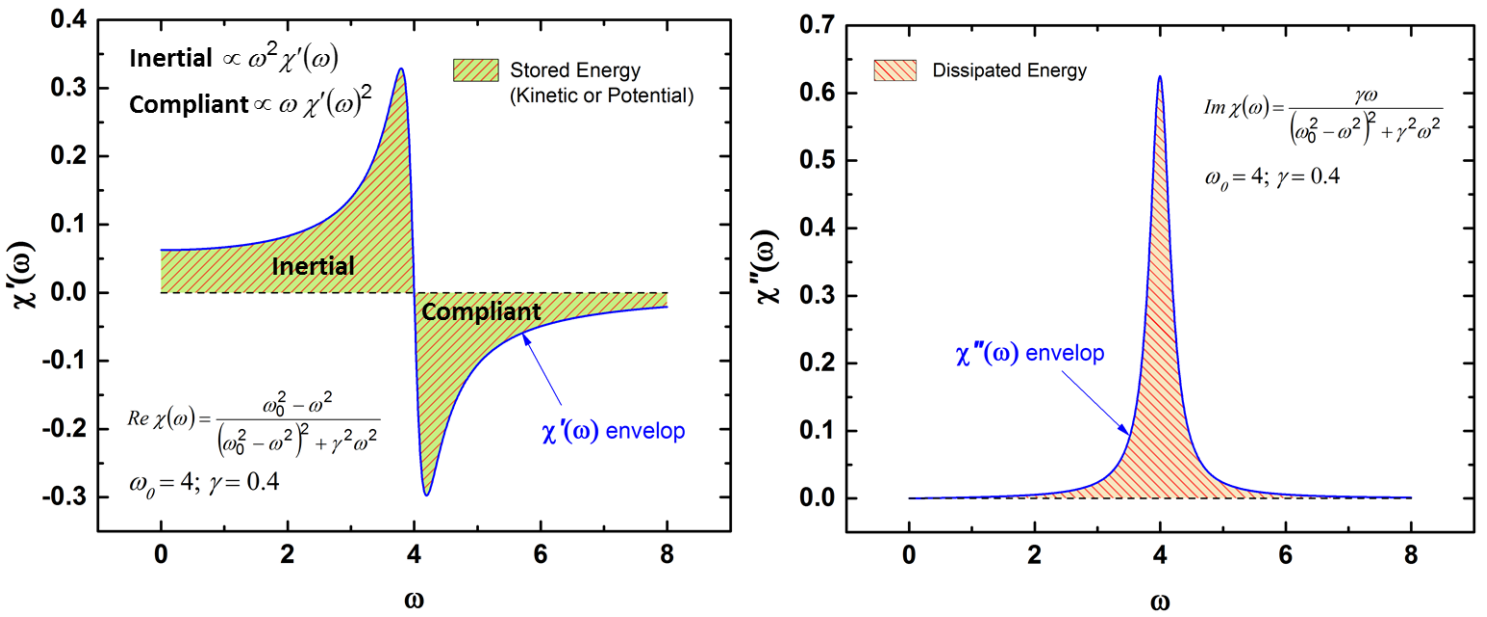


Fig 1.7| The Real and Complex part of response function and Energy

mirror symmetric and has a 0 crossing about the center or resonance frequency. At resonance, the real energy is either kinetic $T \propto \frac{1}{2} \dot{x}^2$ or potential $V \propto \frac{1}{2} x^2$ every half cycle, the other being equal to 0 in that half cycle. This is the physical significance of zero crossing of $\chi'(\omega)$. On the other hand, $\chi''(\omega)$ is not mirror symmetric and does not have a

0 crossing. In fact the imaginary part is never 0. It peaks at the resonance frequency, the function approaching the nature of a delta function in the limit $\gamma \rightarrow 0$.

In all experiments, resonance is analyzed in terms of a measurable amplitude and phase as

$A = |\chi'(\omega) + i\chi''(\omega)|$ and $\phi = \tan^{-1} [\chi''(\omega)/\chi'(\omega)]$ respectively as plotted below.

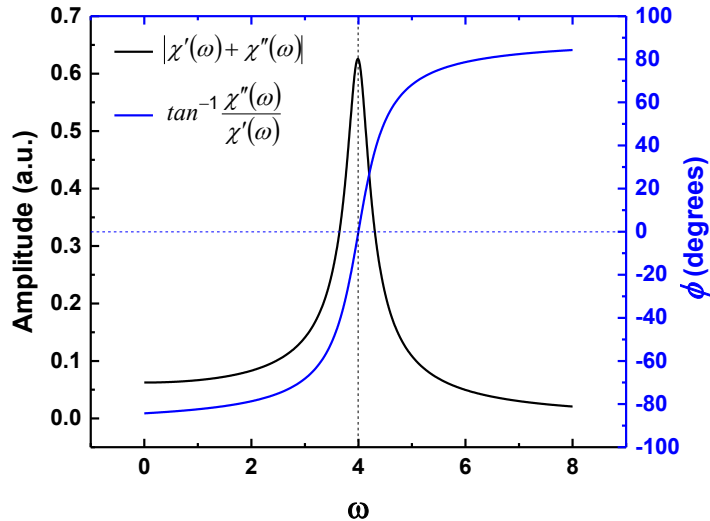


Fig 1.8| The amplitude and phase response at resonance.

The amplitude response resembles the complex part of the response function. Close to the resonant frequency, they overlap, signifying that response goes more in-phase near the peak. Indeed, the phase has a zero crossover at resonance. The net dissipated energy from the imaginary part of the response is obtainable as the area under the $\chi''(\omega)$ curve.

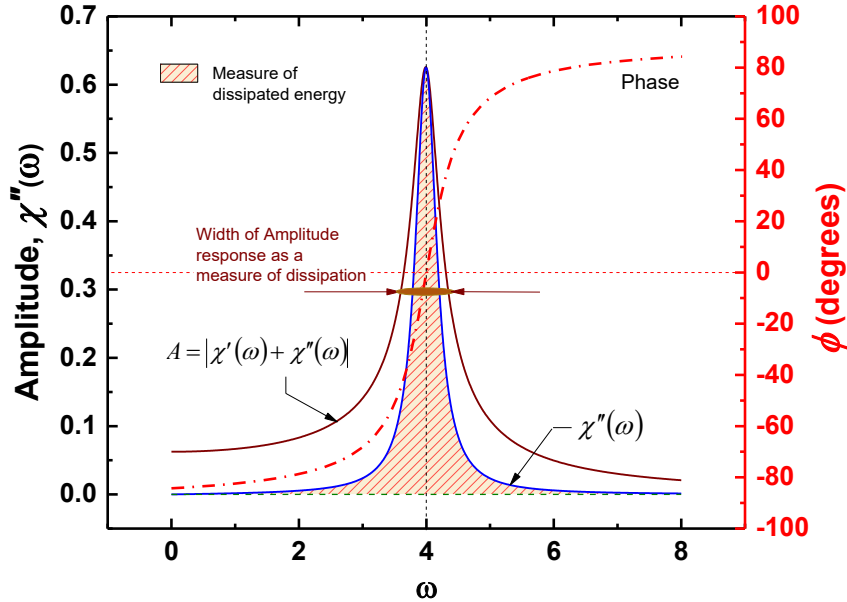


Fig 1.9| Comparison of the imaginary and widely used amplitude response.

The condition of maximization of dissipation at resonance could be explained by analyzing general motion in terms of the evolution of velocity \dot{x} , dissipation being proportional to it. In a general sense, \dot{x} is the slope of the displacement Δx vs time at every point on the displacement curve. When Δx is relatively small, the slope $\dot{x} = dx/dt = \tan(\phi)$ is equal to the angle ϕ . The evolution of the slope as a function of drive frequency ω needs consideration in resonance analysis.

The condition of linearity holds in the small angle approximation only. Another way to look at this is considering the series expansion form of the slope function,

$$f(\phi) = \tan(\phi) = \phi + \frac{\phi^3}{3} + \frac{2\phi^5}{15} + \frac{17\phi^7}{315} + \frac{62\phi^9}{2835} + \dots \quad \text{for } |\phi| < \frac{\pi}{2} \quad (29)$$

where ϕ is in radian measure. For values close to $\pi/2$, approximation even with 5th term (9th power in ϕ) of the expansion series, deviates off from the actual slope $-\tan(\phi)$ as

shown. Higher order power terms are necessary to follow the slope close to $\phi = \pi/2$, which is the phase condition of the output response with respect to the driving force at resonance.

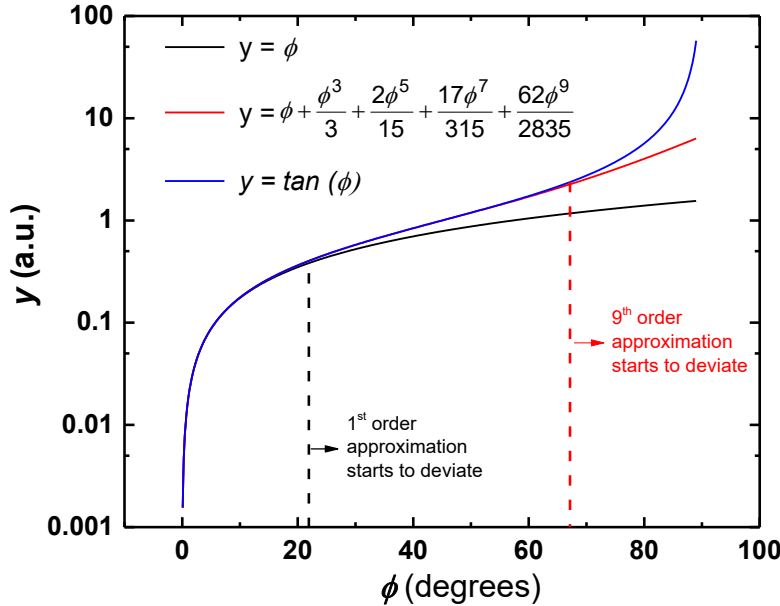


Fig 1.10| Approximation graphs of series expansion of $\tan(\phi)$ in orders of ϕ .

The key to understanding this deviation is noticing how ϕ varies with motion in a system. For small relative displacements Δx with respect to external action, the variation in ϕ is also negligible as clear from the phase response in Figure 1.8. This is true for drive frequencies way off from the resonance frequency. However, near resonance, as the phase $\phi \rightarrow \pi/2$, $\tan(\phi)$ is a rapidly changing function tending to $\rightarrow \infty$. In effect, $\chi''(\omega)$ also changes sharply for added dissipative effects. The amplitude change on the other hand, is a relatively slow varying function in ω in comparison (Fig. 1.9), and follows the peak of $\chi''(\omega)$, while the real part $\chi'(\omega)$ approaches zero. One way to interpret the complex response function is considering the small displacement Δx in the complex plane as,

$$\Delta x(t) = \Delta x'(t) + i \Delta x''(t) \quad (30)$$

with $\Delta x'$ and $\Delta x''$ as the real and imaginary parts of the absolute displacement Δx . The slope of Δx in time \dot{x} thus becomes $\tan(\phi) = \Delta x''/\Delta x'$. The evolution of \dot{x} corresponds to changes in $\tan(\phi)$. A large change in slope corresponds to a rapid change in effective \dot{x} , which means $\Delta x''$ changes more rapidly compared to $\Delta x'$, leading to higher dissipation in the system. With this consideration, a measure of the dissipated energy or the work done on the system for a displacement Δx , translates to

$$I = \int_{path} \gamma \dot{x} \Delta x'' = \int_{path} \phi_{\Delta x_j} \Delta x'' \quad (31)$$

over any arbitrary path j in which the motion takes place. The integral I becomes a functional of $\phi_{\Delta x}$, where $\phi_{\Delta x} = \gamma \dot{x}$ denotes a continuous closed curve in the complex plane, representing changes in dissipative force with respect to a varying displacement Δx over a path. I in essence, is the accumulative action of dissipative forces, where the integral over a path inherently incorporates the time. Another way of interpreting the accumulative action I is the $\sum_{paths} (momentum \times displacement)$, dissipation originating from momentum

transfer between interacting bodies or particles. Functionals in general, are variable values which depend on a variable [$\tan(\phi) \approx f(\phi)$ here] running through a set of functions ($\phi_{\Delta x}$ here, that is dependent on an arbitrary path Δx and γ), or on a finite number of such variables which are completely determined by a definite choice of these variable functions. Dissipation being *maximum* at resonance following the analysis of section 1.5 above, fundamentally becomes a variational problem where the integral I is maximized, i.e., $\delta I = 0$ and $\delta^2 I < 0$.

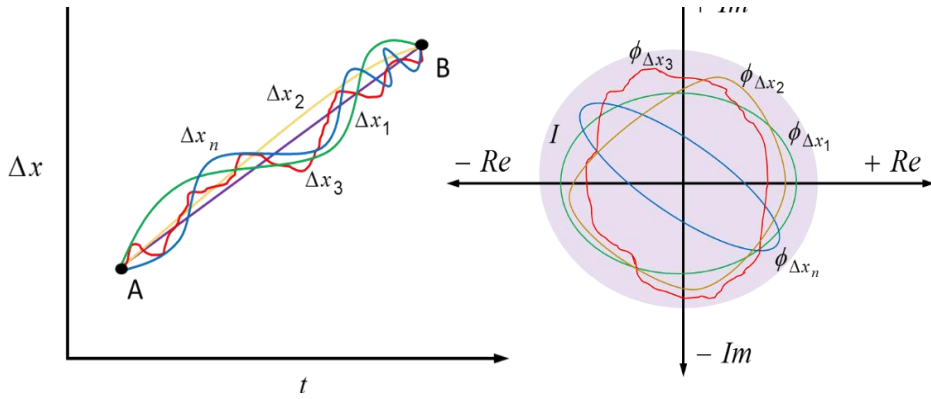


Fig 1.11| The evolution of $\dot{\chi}$ or $\phi_{\Delta x}$ in the real and complex plane as a function of path Δx_j

The mention or consideration of an arbitrary path is crucial here. As has been pointed out before, dissipation, that has its origin in the imaginary part $\chi''(\omega)$ of the response function $\chi(\omega)$, is not invariant under a time reversal $t \rightarrow -t$. The physical significance being that the imaginary $\chi''(\omega)$ encodes dynamical information of time dependent interactions during motion. In other words, $\chi''(\omega)$ knows the arrow of time. The physical significance of this time encoded information is the generic molecular scale interaction or collision processes that sum up to give the net dissipated energy in the system. Resonance is the condition when it is maximized. Dissipation, being a frequency dependent process, is invariably related to time as an inverse relation usually termed the relaxation time. This relaxation time is intertwined to ϕ in terms of an arbitrary path allowable in the motion. The physical quantity that links time and phase is wavelength, a parameter that defines a wave in a general sense. Dissipation thus provides a way to link particle motion to a wave character at the condition of resonance. From the aspect of wave character resonance can be defined as Eigen state solutions or Standing wave solutions.

The next chapter goes in-depth into discussing this paradigm as a single monograph communicated for a publication.

Dissipation in general is a path dependent process and the integral I gives a measure of the dissipated energy evolving in relation to the functional $\phi_{\Delta x}$ that is path dependent as discussed above. Interestingly, variational problems dealing with finding the extrema (maxima) of a functional, relate to finding a function that generates a closed curve with maximum area. Area is related to shape of an object in real space. In the case of dissipation, we are considered with finding the functional form $\phi_{\Delta x}$ that maximizes the area on a complex plane. In essence, $\phi_{\Delta x}$ represents the evolution of $\gamma \dot{x}$ or momentum transfer that is a function of shape, making dissipation inherently dependent on shape of the object in motion in real space. From the condition of resonance and response function, the integral I is maximum for $\phi = \pi/2$, where $\pi/2$ is dependent on a finite number of arbitrary paths - Δx each generating a closed curve $\phi_{\Delta x}$. Now, ϕ can be approximated as a summation of functionals $\sum_{paths} \phi_{\Delta x} = \phi$, where close to resonance the slope denoting the velocity \dot{x} deviates from the condition of linearity as explained before in Figure 1.9, making resonance a unique state of motion.

1.8 Application of the variational principle approach in practical dissipation studies at resonance

The inherent maximization property of dissipation at resonance as revealed by the analysis above has a profound significance in terms of understanding the nature of dynamics in a generic potential well. Studying dissipation at resonance gives a unique opportunity to

understand the general dynamics of a system. When dissipation is maximized in accordance to $\chi''(\omega)$ going to a peak, the stored energy in the system saturates with no variation as understood from the real $\chi'(\omega)$'s 0 crossing, and maximum change is for the dissipated energy. Physically from the system's perspective, it means that at resonance, the system is drawn to the potential well minima, dissipation promoting such a transition from a higher potential energy state, work being done on the system. From the perspective of the external action that drives the system to resonance, dissipation is the energy lost in achieving the potential minima. The resonance frequencies or Eigen solutions in general are the potential minima allowable in a system. For a particle undergoing resonance in a particular Eigen state (Eigen mode) under an external action, dissipation corresponds to either the cumulative sum of energy lost by a particle to attain the potential minima or alternatively, the energy needed by a particle to escape the metastable minima and transition to another Eigen state of lower potential energy. Thus from an alternate perspective, dissipation in conjunction with the stored energy at resonance, prevents the escape or transition of a particle from the potential minima intended to be achieved by an external action. An in-depth discussion of this argument is presented in the Section *II* where, the efficiency of this transition is discussed in the light of amplification factor or Q-factor at resonance as the ratio of the stored to the dissipated energy. The importance of phase ϕ accumulated in space and its role in the origin of standing waves at resonance has been proposed.

Dissipation can also promote transition between multiple potential wells or degenerate states in a system predominantly at the nanoscale, where the generic assumptions of continuum breaks down. Sections *III and IV* goes into in-depth study of

such effects presenting two published monographs with relevance to transitional effects brought about by dissipation. The monographs describe the utilization of dissipation properties at resonance in the design of novel sensitive sensors.

Monograph 1: Submitted in Journal for publication

II. Standing wave revisited: accumulated phase and resonance amplification

Arindam Phani[†], Charles Van Neste, Thomas Thundat[†]

Department of Chemical and Materials Engineering,
University of Alberta, Edmonton, Alberta T6G 1H9, Canada

[†]Correspondence to: phani@ualberta.ca, thundat@ualberta.ca

Standing wave revisited: accumulated phase and resonance amplification

Arindam Phani[†], C. W. Van Neste, Thomas Thundat[†]

Department of Chemical and Materials Engineering,
University of Alberta, Edmonton, AB T6G 2V4, Canada.

[†]Correspondence to: phani@ualberta.ca, thundat@ualberta.ca

Abstract:

Resonance amplification is attributed to standing waves formed by the superposition of a forward and a reflected wave, which accounts for an amplification that is only 2 times the amplitude of individual waves. However, in most cases achieved amplification or Q at resonance is much higher than 2. In fact, resonance amplification is always studied in the light of achieved high Q for high frequency sensitivity. What leads to a high Q or a higher amplitude at resonance is never paid attention to. In this paper, we revisit the fundamentals of the origins of standing waves. We carefully reconsider standing wave definition from the aspect of the phase ϕ in time and space, and comment on the resonance amplification factor from a hypothesis-formulated in terms of measured ϕ in space. This time-phase evolution in space, we explain as a continuous accumulated phase $\Delta\phi_r$ within the physical bounds of a resonator. This we attribute to the apparent non-istropicity of space to the wave in resonance condition. Such an argument allows for the consideration of stored energy in a medium through which a wave tries to propagate, leading to a high Q. Comparison of our theoretical results and experimental data show an excellent match. In addition, the fundamental treatment undertaken here makes the formulation applicable to all resonating systems in a general way.

2.1 Introduction

The concept of resonance originates from the study of oscillating systems in classical mechanics, philosophically describing dynamics in a potential well, like in a gravitational or a harmonic field binding a particle elastically to origin. It is central to many physical theories in electromagnetism, optics, acoustics, and quantum mechanics, among others. Standing waves are at the heart of explaining the phenomenon (1, 2), resonance being treated as eigenvalue solutions (standing waves) of an eigenfunction (wavefunction or quantized energy state of a potential well). Understanding dynamics from the aspect of a wave description became central in linking the two seemingly scale-disjoint fields - classical and quantum with a broad applicability from atomic to cosmological scale in a general sense. Historically, formulations starting from Plank's work on energy of resonators (3) and Bohr's description of an atom (4) to Heisenberg's idea of quantization map (5) bear justice to this. Schrödinger's description of quantum numbers as eigenvalues of the wavefunction (6) and de Broglie's wave-particle duality being the forerunner in the field (7, 8). Interestingly, the time dependent form of Schrödinger's wavefunction, similar in form to a non-linear wave equation, yields from the classical à la the Hamilton-Jacobi equation (9–11). Feynman's path integral approach connected quantum mechanical behavior with such classical ideas as the Lagrangian or in particular, the indefinite integral of the Lagrangian in describing general Hamilton's principle (12, 13). All such seminal ideas bear testimony to some quantum phenomenon or measurements, though being argued against by Lamb (14). Some recent expositions relevant to both classical and quantum fields (15–20) rekindle interests in reconsidering the fundamentals in the context of classical resonance description. Hence, this revisit, where we reconsider the fundamentals

of wave functions and standing waves. We focus on results of electrical resonance in an open-ended wire, with relevance to our recent advances in single-wire power transmission (21–23). We re-explore the underlying phenomenon of standing waves and explain the elusive resonance amplification from a radically alternate perspective using a path integral approach similar in form to Feynman's quantum theory.

Resonance amplifies a small external action by orders of magnitude, while matching the frequency of the external action to a characteristic frequency of the system. The amplification character is exploited in ideas like in a resonant vibrating nanostring or graphene membrane (24, 25), or in micro/nano cantilevers (26–28) and extreme states in bridge resonators (29). The standing wave character finds applications in ordered capillary wave states (30, 31), in X-Ray standing wave techniques (32), and in dissipation sensing and spectroscopy (33) or even in quantum oscillators (34, 35). Resonance amplification has always been studied in the light of improving Q-factor for achieving higher frequency sensitivity. However, what leads to the higher Q or a higher amplitude at resonance is never paid attention to. Surprisingly, literature discussing standing waves and resonance together is not many and that too not directed towards explaining the resonance amplification factor, most crucial in describing the resonance character or the generic curvature of the potential energy well that drives the dynamics. A standard wave description of dynamics necessitates the condition that the curvature of the potential asymptote vanish locally ($\nabla^2 = 0$), stemming from translational and rotational invariance. This invokes the stationary phase condition $\partial\phi = 0$ (36), with ϕ a phase factor in time and space, central to any wave description. In an earlier work, the importance of Brownian noise phase in manipulating resonance Q was introduced (37). We carefully reconsider standing wave definition from

the aspect of ϕ in time and space, and comment on the resonance amplification factor from a hypothesis-formulated in terms of measured ϕ in space. This time-phase evolution in space, we explain as a continuous accumulated phase within the physical bounds of a resonator. Comparison of our theoretical results and experimental data show an excellent match. In addition, the fundamental treatment undertaken here makes the formulation applicable to all resonating systems in a general way. More specifically, we address the fundamental question concerning resonance - *How does the amplification come about and what determines the amplification factor of a resonant system?*

The relevance of the question has its roots in the familiar standing wave (SW) definition in physics texts – as the superposition of a forward wave ψ_F and its reflected counterpart ψ_R (reflected off a fixed or open boundary), both travelling with the same or almost the same velocity but in opposite sense (direction/time) in a homogeneous isotropic space. The resulting SW appears to be stationary in space r and oscillating in time t , r representing a 1D space dimension. Mathematically, a linear superposition of two waves can give a SW amplitude that is ‘2’ times the amplitude of individual waves. A finite wave velocity in the medium, though large, would restrict the SW packets to be incoherent in time in the strictest sense. Such a consideration renders the superposition argument weak in explaining resonance amplification by orders of magnitude in practical experiments even when energy is continuously pumped into the system, e.g., in classical mechanical resonators and in electrical resonant lines (38), since an inherent phase difference at the input cannot be overlooked altogether. Herein lies the relevance of the question from the fundamental aspect of a wave definition and wave reflections at resonance.

2.2 Waves in isotropic space and phase of a wave

Let us first consider what constitutes a wave in the standard definition. From wave theory (39), a travelling wave ψ can be derived as a solution of the homogeneous wave equation

$v^2 \nabla^2 \mathbf{a} = \mathbf{a}_{tt}$, for a generalized amplitude $\mathbf{a}(\mathbf{r}, t)$ and a constant velocity \mathbf{v} , more generally

as solutions of the normal form $\mathbf{a}_{\xi\eta} = 0$ ($\mathbf{a}_{\xi\eta} = \partial^2 \mathbf{a} / \partial \xi \partial \eta$), ξ and η representing curves called characteristics or advanced/retarded variables in the (\mathbf{r}, t) plane. The derived ψ is

often termed as a wavefunction. The imposition of a constant \mathbf{v} in the wave equation must satisfy the Laplacian

$\nabla^2 \mathbf{a} = 0$ at every point on the characteristics, demanding $\xi(\mathbf{r}, t)$ and $\eta(\mathbf{r}, t)$ constants. Physically this means a

priori assumption of isotropic space,

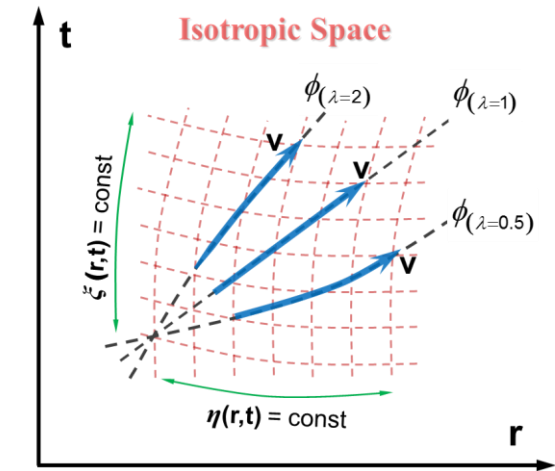


Fig 2.1| Schematic representing isotropic space

which has had profound implications on the properties of ψ 's in (\mathbf{r}, t) derived from the wave equation above. These can be reflected upon from the realization of a family of regular curves in (\mathbf{r}, t) , viz., $\phi \equiv \xi + \lambda \eta$ with λ , an arbitrary constant (Fig. 2.1). By a continuous deformation of $\lambda \in [-\infty, \infty]$ the ϕ curves, within the family of characteristics, can continuously warp/bend, maintaining uniformity and continuity for the isotropic assumptions. The physical significance of the family of curves ϕ is a distribution of phase fronts in (\mathbf{r}, t) , all supporting travelling wavefunctions with a constant velocity \mathbf{v} . This in essence defines emanating travelling waves in all directions from a point source that is independent of the medium. As a necessary condition for the solvability of the wave

equation that gives the family of travelling waves, a phase front within the family of curves defined by ϕ cannot be a tangent to the characteristics, like when $\lambda = 0$ or $\lambda = \pm\infty$, giving trivial solutions $\mathbf{a}_\xi = 0$ and $\mathbf{a}_\eta = 0$ on constants η and ξ respectively. By its nature, $\mathbf{v}^2 \nabla^2 \mathbf{a} = \mathbf{a}_{tt}$ is hyperbolic and so from chain rule the characteristics may be reduced to $\xi \equiv (\beta \mathbf{r} + \omega t)$ and $\eta \equiv (\beta \mathbf{r} - \omega t)$ in (\mathbf{r}, t) , with the generalized condition $\beta = \omega/\mathbf{v}$, ω being the angular frequency of perturbation/wave and β (wavenumber) describing the number of cycles the wave or perturbation completes per unit distance \mathbf{r} it travels. The intersection points of ξ and η in (\mathbf{r}, t) defines the wavefunction ψ completely as a function of the curves ϕ , giving $\psi_F = \mathbf{a}e^{i\phi}$ and $\psi_R = \mathbf{a}e^{-i\phi}$ as a non-trivial solution pair of $\mathbf{a}_{\xi\eta} = 0$ in the generalized complex form. A linear superposition of ψ 's on phase fronts ϕ and $-\phi$ describing a SW, indeed gives an amplitude that is '2' times the amplitude $\mathbf{a}(\mathbf{r}, t)$ of the individual waves following the identity $\psi_{SW} = \psi_F + \psi_R = 2\mathbf{a} \cdot \text{Re}(e^{i\phi})$. Intrinsically, the condition of a constant phase front ϕ implies $\partial\phi_r = 0$ from the assumptions of isotropic and homogeneous space as discussed above, forcing this limit. We introduce an alternate hypothesis stating that ψ_{SW} is not a result of superposition as above, rather it originates from the condition of an *accumulated phase* $\Delta\phi_r = \int_r \partial\phi_r \neq 0$, that is accrued in the path of a wave at resonance, and we corroborate this with experimental results. We establish a fundamentally new SW function Ψ_r dependent on $\Delta\phi_r$, that explains the general resonance character and predicts the elusive amplification factor of resonance. We quantitatively match the theoretical

predictions to time domain measurements in experiments. Interestingly, we are also able to deduce the standard superposition theory result of ‘2’ as a particular solution from our formulation with a certain generalized condition of the stationary phase $\Delta\phi_r = 0$, which is inadvertently imposed in the standard definition of reflection waves.

2.3 Phase from the consideration of non-isotropic space

We begin by noting that the family of phase fronts ϕ on which a wavefunction ψ is expressed, incorporates two descriptions: the spatial phase $\phi_s = \beta r$ and a temporal phase $\phi_t = \omega t$, all, which is required to reconstruct a wave’s envelope in (r, t) . These parameters demand rotation and dilatational invariance ($\beta, \omega = \text{const}$) for each complete cycle as demanded for the case of isotropic and homogenous media. This imposes the equivalence of ϕ_s and $\phi_t = 2\pi$ radians, giving $\phi = 0$

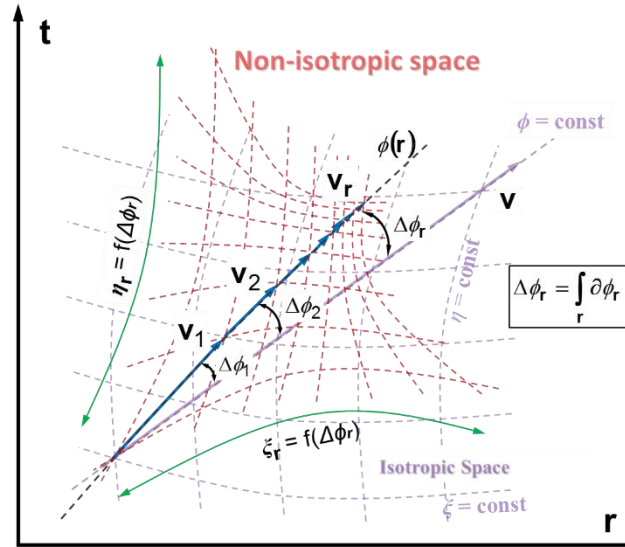


Fig 2.2| Schematic representing non-isotropic space

or an even multiple of 2π . Mathematically, it implies that $\psi = a e^{i\phi}$ reduces to a oscillating field with a maximum amplitude of a at every point in (r, t) , and that the separation of spatial and temporal phases over each cycle $\partial\phi_r = |\phi_s - \phi_t|$ is equal to 0 (ϕ being a constant), giving the condition of stationary phase $\Delta\phi_r = \int \partial\phi_r / r = 0$ over a

traversed wave path \mathbf{r} . This is Fermat's principle of least action in the most general form enforced for a travelling wave, satisfying a constant propagation velocity \mathbf{v} . Now let us reconsider, that for a SW, the condition $\Delta\phi_{\mathbf{r}} = 0$ might be a convoluted assumption in an attempt to associate a unique constant velocity to it. This is because the SW appears stationary in space (stationary state) from a relativistic frame. Our point of departure is a more holistic definition of this phase front ϕ accumulated along the wave path. This when considered in a broad sense, is analogous to a sum of contributions from each path having a phase $\phi[\mathbf{r}, \mathbf{t}]$ proportional to classical "action" $\mathbf{S} = \int_{\mathbf{T}} \mathbf{L}(\mathbf{r}, \dot{\mathbf{r}}, \mathbf{t})$ for a Lagrangian \mathbf{L} (2, 12).

The summation over paths will constitute a time period $\mathbf{T} = 2\pi/\omega$ for one cycle at resonance in the case of a SW. Normally, the condition $\Delta\phi_{\mathbf{r}} = 0$ is equivalent to an "action" minimization $\delta\mathbf{S} = 0$, ensuring the physical process of a wave travelling in space. In contraire, the starting point of our argument $-\Delta\phi_{\mathbf{r}} \neq 0$ for the case of a SW, need not enforce that condition. Physically, our argument would assert a non-isotropic space enforcing a non-equivalence of the spatial and temporal phases along the wave path that would manifest as non-constant coefficients (39), here, as non-constant wavenumber $\beta_{\mathbf{r}}$ and phase velocity $\mathbf{v}_{\mathbf{r}}$ in a relativistic frame. In context, the phase fronts would transform to a family of non-regular curves with variable gradient in space as, $\phi(\mathbf{r}) \equiv \xi_{\mathbf{r}} + \lambda_{\mathbf{r}} \cdot \eta_{\mathbf{r}}$, where $\lambda_{\mathbf{r}}$ can be a deformation function in \mathbf{r} , giving $\partial\phi_{\mathbf{r}} \neq 0$. We will elaborate on the general nature of $\lambda_{\mathbf{r}}$ and its connection to resonance in the next section. It must be noted here though, that the wave equation for a generalized real amplitude $\mathbf{a}(\mathbf{r}, \mathbf{t})$ with a constant velocity \mathbf{v} , has a family resemblance to other differential equations in physics like the heat

equation, diffusion equation and the hydrodynamics of incompressible and irrotational fluids; the constant \mathbf{v} translating to appropriate physical property constants. The basis of this similarity is the Laplacian $\nabla^2 \mathbf{a} = 0$ with small \mathbf{a} approximation. In resonant condition however, it is known that $\nabla^2 \mathbf{a} \neq 0$ and $\nabla \mathbf{a} \neq$ linear in \mathbf{r} , as in the measured logarithmic electrical potential along length in a helical coil (21, 23) or typical non-linear displacement field in a microcantilever (40). Clearly, such generic nonlinear amplitude fields cannot in the absolute sense support the travelling wave argument with a constant \mathbf{v} . We therefore theorize that $\nabla^2 \mathbf{a}$ in the SW condition should be a general function of $\Delta\phi_{\mathbf{r}}$, with the characteristic variables $\beta_{\mathbf{r}}$ and $\mathbf{v}_{\mathbf{r}}$ functions of $\Delta\phi_{\mathbf{r}}$ in space. The physical significance being a non-isotropic space from a relativistic frame of reference. The resulting wave function $\Psi_r = f(\mathbf{a}_{\mathbf{r}})$ will thus be a solution of the general class of an inhomogeneous wave/Telegrapher's equation $\mathbf{a}_{tt} + 2\gamma \mathbf{a}_t + \omega^2 \mathbf{a} - \mathbf{c}^2 \nabla^2 \mathbf{a} = f(\Delta\phi_{\mathbf{r}})$, with $f(\Delta\phi_{\mathbf{r}})$ denoting imaginary source functions in space similar to Huygens's secondary sources and γ denoting a generalized wave-damping factor. A comprehensive solution to the equation of this form is beyond the scope of this treatment, for which readers may refer to advanced mathematical treatments. Our goal is to reflect on the generalized functional form of Ψ_r in terms of $\Delta\phi_{\mathbf{r}}$ that can describe a SW, and establish its connection to motion or amplitude at resonance.

2.4 Phase at resonance

We start by considering oscillatory motion as a single complex-valued amplitude function $\mathbf{a} = \mathbf{x}e^{i\phi'}$, with a real-valued positive deflection \mathbf{x} in 1D and a generalized time phase ϕ'

describing the evolution of motion in time, the results being extendable to 3D. It is important at the onset to reflect on the nature of ϕ' as time phase only, since it originates as a parameter in the solution of the Euler-Lagrange equation of motion $\ddot{\mathbf{x}} + \gamma_n \dot{\mathbf{x}} + \omega_n^2 \mathbf{x} = \mathbf{X}_0 e^{i\omega t}$, with overdots denoting complete derivatives in time. At the condition of resonance, the oscillations in \mathbf{x} attains a maxima \mathbf{x}_n at $\omega = \omega_n$, the n^{th} eigenfrequency corresponding to system properties, \mathbf{X}_0 and ω being the amplitude and frequency of the external action. Understanding the evolution of time phase ϕ' in relation to damping factor γ_n for different eigenmodes (37) is crucial since their ratio denotes a timescale that is needed by the system to attain steady oscillations at ω_n . In essence, it gives the response time phase $\phi' = \gamma t$ of the oscillations with respect to the external drive phase ωt . The generalized amplitude response in ω from the equation of motion above

becomes $\mathbf{a}(\omega) = \frac{\mathbf{X}_0 \omega_n^2}{\omega_n^2 - \omega^2 - i\gamma\omega}$ with

$$\mathbf{a}(\omega) = \mathbf{x}_0 e^{i\phi'}, \quad (1)$$

giving the familiar maxima amplitude at the fundamental eigensolution ω_0 ($n = 0$)

$$\mathbf{x}_0 = \frac{\mathbf{X}_0 \omega_0^2}{\left[(\omega_0^2 - \omega^2)^2 + \gamma^2 \omega^2 \right]^{1/2}} \quad (2)$$

and phase lag with respect to external action

$$\phi' = \gamma t = \tan^{-1} \left(\frac{\gamma\omega}{\omega_0^2 - \omega^2} \right). \quad (3)$$

In general for all n , in the limit of $\omega \rightarrow \omega_n$, the complex amplitude $a_n \rightarrow iX_0 \omega_n / \gamma_n$ and the unwrapped phase $\phi'_n \rightarrow (n\pi + \pi/2)$ ($\forall n = 0, 1, 2, \dots$), physically signifying a time phase change at resonance. Nevertheless, it is required to understand here, what an eigensolution means in terms of wave perturbation in (r, t) and how ϕ'_n relates to the generalized phase fronts ϕ of the wave definition above. Answering the former would directly lead to the latter.

This may be explained by considering resonance as an eigenvalue problem of an oscillating surface containing the characteristics ξ and η , the surface acting as a space-time fabric and its local deformations constituting a wave. For pure harmonic oscillations, the customary eigenfunction expansion form of the homogenous wave equation reduces to $\nabla^2 a + \beta_n^2 a = 0$, with eigenfunctions as non-trivial solutions that satisfy the boundary condition $a(\omega) = 0$, β being the corresponding eigenvalue of the problem. Eigenvalues exist for $\beta_n^2 > 0$ and for β_n real, namely an infinite number. In the simplest case, each eigenvalue has an associated eigensolution. In general, $\beta_n = \omega_n / v$ denotes the n^{th} eigenvalue. The real character of β within conditions of homogeneity signify *absorption free or non-dissipative oscillations* within the boundaries $a(\omega) = 0$. The boundaries in essence are nodal lines or curves on which displacements are stationary, while tangents at the points of intersections in (r, t) trace out the family of regular phase fronts ϕ in space-time that can support a travelling wave. The eigenvalue corresponding to a boundary is thus analogous to the parameter ‘wavenumber’ in a wave description (both represented as β here for consistency). By definition, it is a constant for an eigensolution ω_n at

resonance, otherwise denoting infinite wave vectors with corresponding different wavelengths. For a generalized complex $\mathbf{a}(\omega)$, Green's theorem gives the spectral density

$$\int \mathbf{a} \cdot \mathbf{a}^* d\sigma = 1 \quad (\text{analogous to}$$

probability density) or the energy density in between the nodal bounds, σ representing the surface density of nodal lines in (\mathbf{r}, t) with ϕ' denoting

the isogonal angles between them at the point of intersections. Higher eigenmode thus have a lower energy density between the bounds. Essentially, the nodal lines exhibit bounds of a plane of uniform local curvature in a homogeneous isotropic space with σ denoting the density of eigenfunctions or allowable wave solutions. Travelling waves from a freely oscillating scalar point source satisfy the condition of infinite eigenfunctions, whence $\phi' \rightarrow 0$, and thus the local tangent to a boundary at the point of intersection in the plane coincide with a constant curve of the form $\phi = \xi + \lambda\eta$ (Fig 2.3). In general, the magnitude of ϕ' in radians for \mathbf{m} intersecting nodal lines, is given by π/\mathbf{m} (39) and may be looked upon as the time phase which from (3) reduces to $\mathbf{m} = 2$ for the fundamental eigenmode $\mathbf{n} = 0$. We restrict our discussions here with respect to fundamental mode only relevant to experiments conducted.

Travelling wave (infinite eigenfunctions)

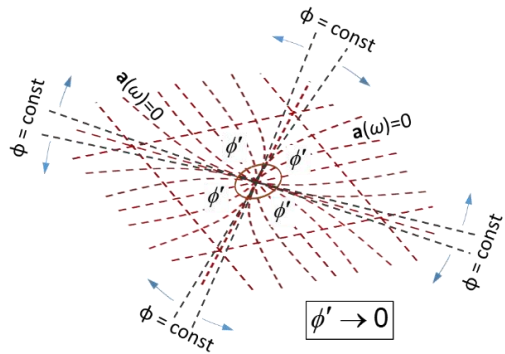


Fig 2.3| Relation of time phase ϕ' and phase front ϕ

2.5 The condition of accumulated phase and physical significance

The condition of stationary phase, i.e., the derivative of the phase $\partial\phi_r$ accumulated along the wave path $\int_r \partial\phi_r = 0$ is satisfied for infinite eigenfunctions (travelling waves) where

indeed the tangent to nodal lines coincide with the constant phase fronts. Evidently, this is not valid at the fundamental, more specifically the case of quarter SW, since it is understood from (3) that $\phi' = \gamma t$ changes by $\pi/2$ with respect to the external action phase ωt that created the perturbation in the first place. This signifies that the number of nodal lines gets restricted to two at the open-end bound of the system. ϕ' essentially is a time phase by definition without a spatial character. Resonance condition introduces that spatial character to originate in (\mathbf{r}, t) . Since the wave has a travelling character at the source point, the tangents to the nodal lines should coincide with a constant phase front to initiate a travelling wave at $\mathbf{r} = 0$, but gradually should transform to orthogonal boundaries in \mathbf{r} (Fig 2.4), by a continuous deformation of the phase front describable by non-regular curves $\phi(\mathbf{r}) \equiv \xi_{\mathbf{r}} + \lambda_{\mathbf{r}} \cdot \eta_{\mathbf{r}}$ as discussed before. Physically, at resonance, the space-time (\mathbf{r}, t) fabric can be viewed to be infinitely stretched at the source end while infinitely compressed at the open-end boundary, $\lambda_{\mathbf{r}}$ being a compressional factor in \mathbf{r} . Such a condition arises in the quarter SW condition because the path of the wave or perturbation is curtailed by a compression of the physical space, allowing only a fraction of an oscillation in space. Consequently, the condition of stationary phase need not be enforced in \mathbf{r} , since the wave path as should have been followed by that initial perturbation in space is never completed. In other words, the

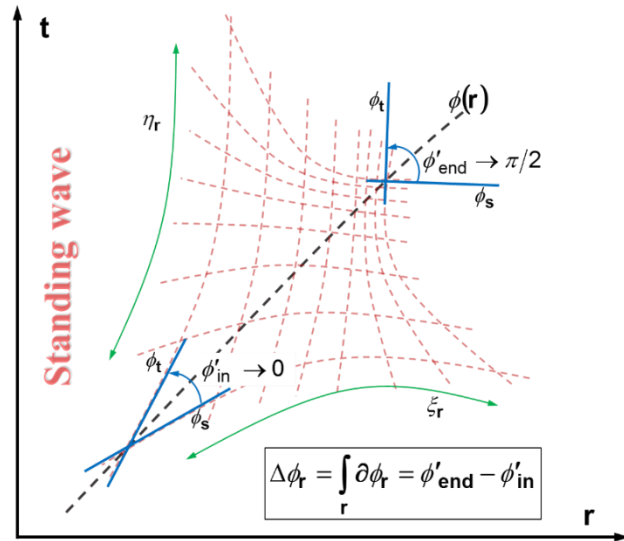


Fig 2.4| Standing wave schematic assuming non-isotropy describing the accumulated phase

accumulated phase $\int_{\mathbf{r}_1}^{\mathbf{r}_2} \partial \phi_{\mathbf{r}}$ for a path may and should deviate from the mathematical

condition of minima that interprets least action. Going by this argument, a SW envelop may emerge as a perturbation in space with gradual accumulated time phase over the

physical bound of a resonator, giving $\Delta\phi_{\mathbf{r}} = \int_{\mathbf{r}_{\text{initial}}}^{\mathbf{r}_{\text{final}}} \partial \phi_{\mathbf{r}} = \pi/2$ (limit case) following (3) or

more generally $\Delta\phi_{\mathbf{r}} = \phi_{\text{end}} - \phi_{\text{in}} < \pi/2$ (leaky resonance with multiple eigenmodes - less spectral density at higher mode), with $\Delta\phi_{\mathbf{r}}$ continuously differentiable in \mathbf{r} . The argument of an accumulated phase in space would mean that the perturbation constituting a wave would gradually change from a propagating state to a stationary state in space (in the medium) depending on the functional form of $\Delta\phi_{\mathbf{r}}$ in path $\mathbf{r}_{\text{initial}} \rightarrow \mathbf{r}_{\text{final}} \equiv \sum_{\text{all paths}} \mathbf{r}_1 \rightarrow \mathbf{r}_2$;

$\mathbf{r}_1 \rightarrow \mathbf{r}_2$ representing an infinitesimal path.

2.6 The standing wave function in terms of accumulated phase

Enforcing the above-argued condition $\int_{\mathbf{r}_{\text{initial}}}^{\mathbf{r}_{\text{final}}} \partial \phi_{\mathbf{r}} \neq 0$ and invoking Hamilton's variational

principle in a general sense, resonance can be defined as an integral sum of complex valued amplitudes $\mathbf{a}_{\mathbf{r}}$ corresponding to accumulated phases $\int_{\mathbf{r}_1}^{\mathbf{r}_2} \partial \phi_{\mathbf{r}}$ in the medium for a path

$\mathbf{r}_1 \rightarrow \mathbf{r}_2$. A net classical SW wavefunction in space thus emerges

$$\Psi_{\mathbf{r}} = \int_{\mathbf{r}_{\text{initial}}}^{\mathbf{r}_{\text{final}}} \mathbf{x}_0 e^{i\Delta\phi_{\mathbf{r}}} , \quad (4)$$

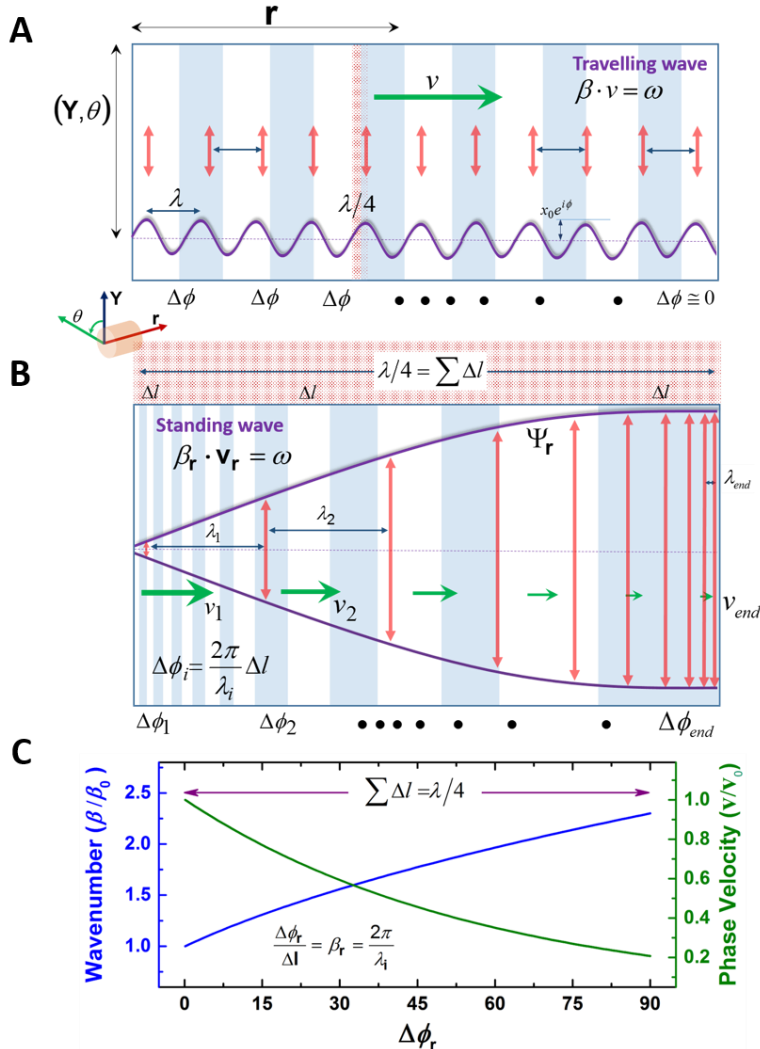


Fig 2.5| Implications of accumulated phase and the resulting standing wave description: **A.** The case of a travelling wave in isotropic space, where β and \mathbf{v} , both are constants giving $\beta \cdot \mathbf{v} = \omega$, a constant for a general propagating wave. **B.** The accumulated phase renders the medium non-isotropic in space, signifying that the perturbation would take a longer time to traverse in space (time dilation), which in other words would mean that the perturbation was slowing down in space. Relativistically, to the wave its velocity remains constant, while the effective path length Δl contracts (length contraction) because of the accumulated phase $\Delta\phi_r$. From an inertial frame however, Δl appears expanded. It thus enforces the condition that β and \mathbf{v} both become

functions of $\Delta\phi_r$ from an observers frame of reference outside, and should be related hyperbolically to satisfy the condition $\beta_r \cdot \mathbf{v}_r = \omega$, the resonance frequency or the eigensolution defining the SW case. **C.** Under the conditions of accumulated phase, the familiar wavenumber $\beta = 2\pi/\lambda$ in a propagating wave reduces to a propagation factor $\beta_i = \Delta\phi_r/\Delta l = 2\pi/\lambda_i$, with $\sum \Delta l = \lambda/4$ in case of a quarter SW with all paths

λ_i analogous to the compressional or deformation factor $\lambda(\mathbf{r})$ in our generalized definition. Since λ_i compresses in \mathbf{r} , β_i gradually increases with $\Delta\phi_r$ giving the very essence of a wave having to go through more number of cycles to travel the same physical length space Δl losing its propagation quality and transforming to a standing or stationary state. Alternatively, the perturbation seems to slow down in space with a gradual reduction in phase velocity \mathbf{v}_r . This fundamental change in the wave description on consideration of the accumulated phase $\Delta\phi_r$ at sub-wavelength scales implying the SW function (4), has profound implications in general.

as an accumulated sum of perturbation histories $\mathbf{a}_r = \mathbf{x}_0 e^{i\Delta\phi_r}$ in space, the SW envelop representing “the entire motion” in a time period T corresponding to a path $r_{\text{initial}} \rightarrow r_{\text{final}}$. Mathematically, (4) is closely similar to Schrödinger’s wave function in Feynman’s path integral form (12), here describing a *time independent* SW envelope in the classical limit. For the fundamental eigenmode, the time dependent oscillation envelop reduces to $\Psi_{r,t} = \left(\int_{r_{\text{initial}}}^{r_{\text{final}}} \mathbf{x}_0 e^{i\Delta\phi_r} \right) e^{i\omega_0 t}$, ω_0 describing the fundamental eigenfrequency. The phase proportional to classical ‘action’ \mathbf{S} (Planck units) in Feynman’s path integral form, translates to a generalized accumulated phase function here, elucidating the resonance character (mode shape) in the classical regime (Fig 2.5).

2.7 Significance of accumulated phase in resonance amplification factor α

In case of resonance in an electrical wire (the specific case we study here), the action accounting for a response amplitude \mathbf{x} translates to a measurable electrical potential \mathbf{V}_r effected by a charge distribution in the wire. Using (4) and the fact that \mathbf{x} can be represented in terms of \mathbf{a} as $\mathbf{x} = \mathbf{a} e^{-i\Delta\phi}$, the measurable potential \mathbf{V}_r in \mathbf{r} would be given by the solution of the Laplacian

$$\frac{1}{\mathbf{V}} \frac{\partial^2 \mathbf{V}}{\partial \mathbf{r}^2} = \mathbf{e}^{-i\Delta\phi}, \quad (5)$$

considering that the perturbations from the external action are restricted to (Y, θ) plane and the wave envelope extends along \mathbf{r} (Fig 2.5). The solution of the differential equation (5) which we propose is a classic Cauchy problem with $\mathbf{V}(\mathbf{r}, 0) = \mathbf{V}_0 \cos(\phi_{\text{in}})$ and $\frac{\partial \mathbf{V}}{\partial \mathbf{t}}(\mathbf{r}, 0) = -\mathbf{V}_0 \sin(\phi_{\text{in}})$, ϕ_{in} being the measurable phase at the input and $\mathbf{V}_0 = \mathbf{V}(0, t)$ is the

potential at the input. We subject our hypothesis to test in experiments with a straight wire connected to a grounded source at one end, tuned to the SW frequency of the wire, while kept open/free at the other end. The results in Fig. 2.6 support our hypothesis of accumulated phase and its role in the origin of SW profile. It is clear that the solutions to (5) is in a general complex form $\mathbf{V}_r + i\mathbf{V}'_r$ describing a complex potential well or commonly a generalized potential in physics, with $\text{Re}(\mathbf{V}_r) = \mathbf{V}_r \propto (\omega \mathbf{q})_n^2$ and the $\text{Im}(\mathbf{V}_r) = \mathbf{V}'_r \propto (\gamma \mathbf{q} \dot{\mathbf{q}})_n$ for the n^{th} eigenmode, continuously differentiable in \mathbf{r} , $\mathbf{q}(t)$ and $\dot{\mathbf{q}}(t)$ being generalized coordinates and velocities at every point of the trajectory of motion in configurational space. From the aspect of a complex generalized potential it is easier to invoke Hamilton's variation principle in configuration space, which in our case constitutes the SW envelop (Fig 2.5), the trajectory of motion not necessarily resembling an unique path $\mathbf{r}_{\text{initial}} \rightarrow \mathbf{r}_{\text{final}}$ over which SW function Ψ_r is defined. In our definition (4),

$$\mathbf{r}_{\text{initial}} \rightarrow \mathbf{r}_{\text{final}} \equiv \sum_{\text{all paths}} \mathbf{r}_1 \rightarrow \mathbf{r}_2, \mathbf{r}_1 \rightarrow \mathbf{r}_2 \text{ being small infinitesimal paths in configurational space.}$$

Here lies the significance of our path integral formulation. The complex nature of the potential solution of (5) results in a generalized complex Hamiltonian $\mathcal{H} = \left[\frac{1}{2} \dot{\mathbf{q}}^2 + \mathbf{V}_r \right] + i\mathbf{V}'_r$ for unit mass, describing the dissipative system at resonance condition with a real spectrum (41). It is understood that \mathbf{V}'_r in general, contributes to the accumulated phase factor $\Delta\phi_r \equiv \tan^{-1}(\mathbf{V}'_r / \mathbf{V}_r)$ in the SW envelop Ψ_r in (4). From the aspect of energy, the real part of \mathcal{H} within the square brackets account for the stored component, typically a function of the eigenvalues β_r of the SW function, while the

imaginary part represent the dissipated component, a function of \mathbf{V}_r in the (\mathbf{r}, t) plane.

Evidently both the real and imaginary parts of \mathcal{H} are functions of $\Delta\phi_r$ from (5) and would

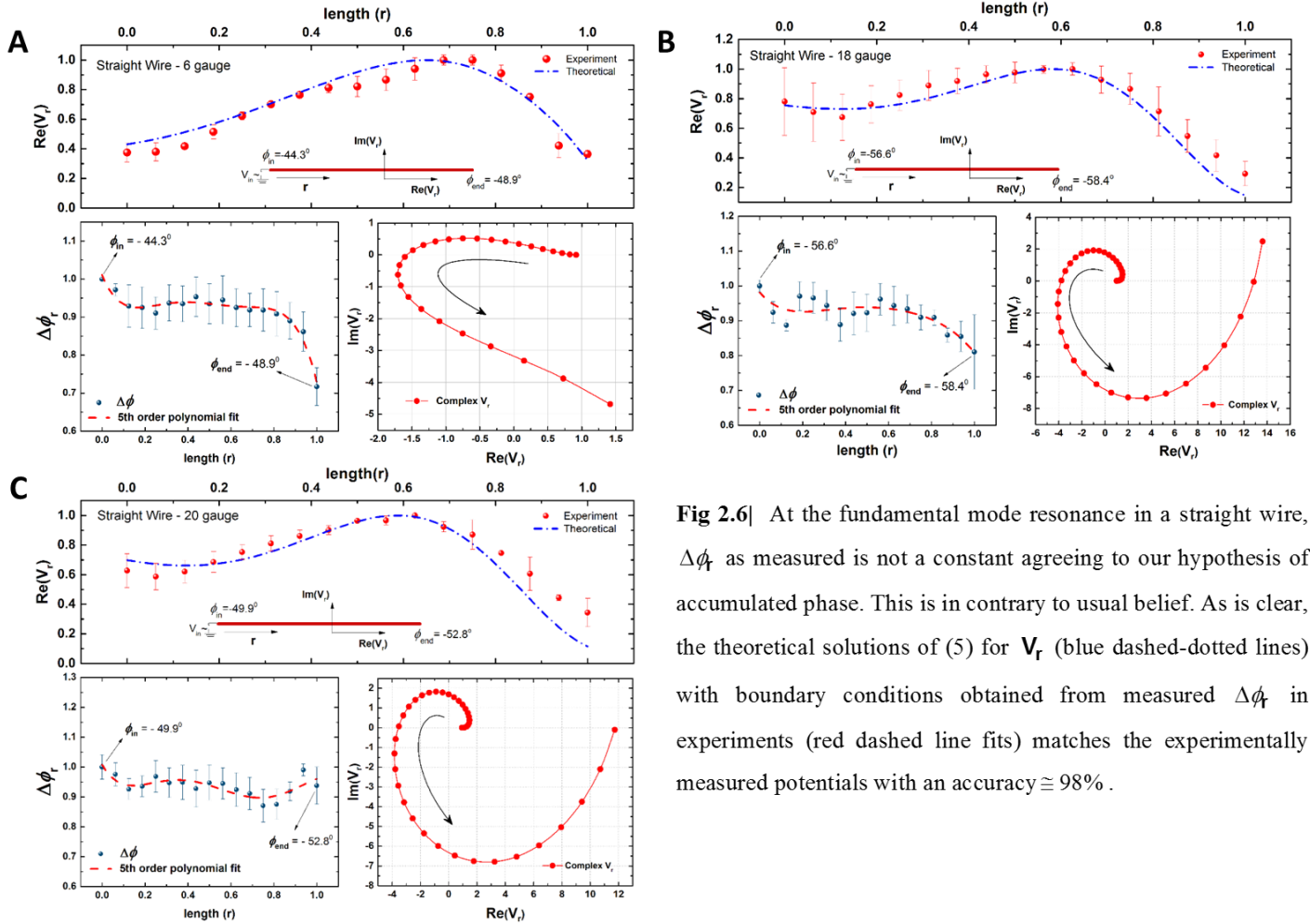


Fig 2.6| At the fundamental mode resonance in a straight wire, $\Delta\phi_r$ as measured is not a constant agreeing to our hypothesis of accumulated phase. This is in contrary to usual belief. As is clear, the theoretical solutions of (5) for \mathbf{V}_r (blue dashed-dotted lines) with boundary conditions obtained from measured $\Delta\phi_r$ in experiments (red dashed line fits) matches the experimentally measured potentials with an accuracy $\geq 98\%$.

follow the generalized condition of $\Delta\phi_r \equiv (n\pi + \pi/2)$ for the n^{th} eigenmode ($\forall n = 0, 1, 2\dots$). When plotted in phase space (Fig 2.6), the imaginary part of the solution of (5) in \mathbf{r} traces out diverging spirals elucidating the resonance character of amplification in a general sense. It must be pointed out here that the spiral nature in general also represents the phase space evolution in time, $\Delta\phi_r$ essentially being a time phase $\propto \gamma_n t$ for the n^{th} eigenmode. The phase-space spirals (Fig. 2.6) also reveals the general amplification character at resonance. This can be expressed in terms of amplification factor α as the ratio of the

energy stored to loss in \mathbf{r} from the generalized Hamiltonian \mathcal{H} . The emergence of α as measured in our experiments for varying $\Delta\phi_r$ (Fig. 2.7) can be represented as a cumulative sum of β_r/v_r in \mathbf{r} , where β_r and v_r are related hyperbolically as depicted in Fig. 2.5.

From results discussed earlier (21) we can deduce the magnification factor

$$\alpha = \sum_{r_{\text{initial}}}^{r_{\text{final}}} \beta_r / v_r = \sum_{r_{\text{initial}}}^{r_{\text{final}}} e^{2/\lambda_r \cdot \Delta\phi_r}, \quad (6)$$

plotted in Fig. 2.7, elucidating the general amplification character as a function of the accumulated phase. Here, $\lambda_r = 2\pi v_r / \omega_0$ is the effective space compression factor in \mathbf{r} as perceived by the wave. In the limit of $\Delta\phi_r \rightarrow 0$, inadvertently imposed by the argument of a travelling wave, $\alpha \rightarrow 2$, reducing to the standard wave reflection theory result.

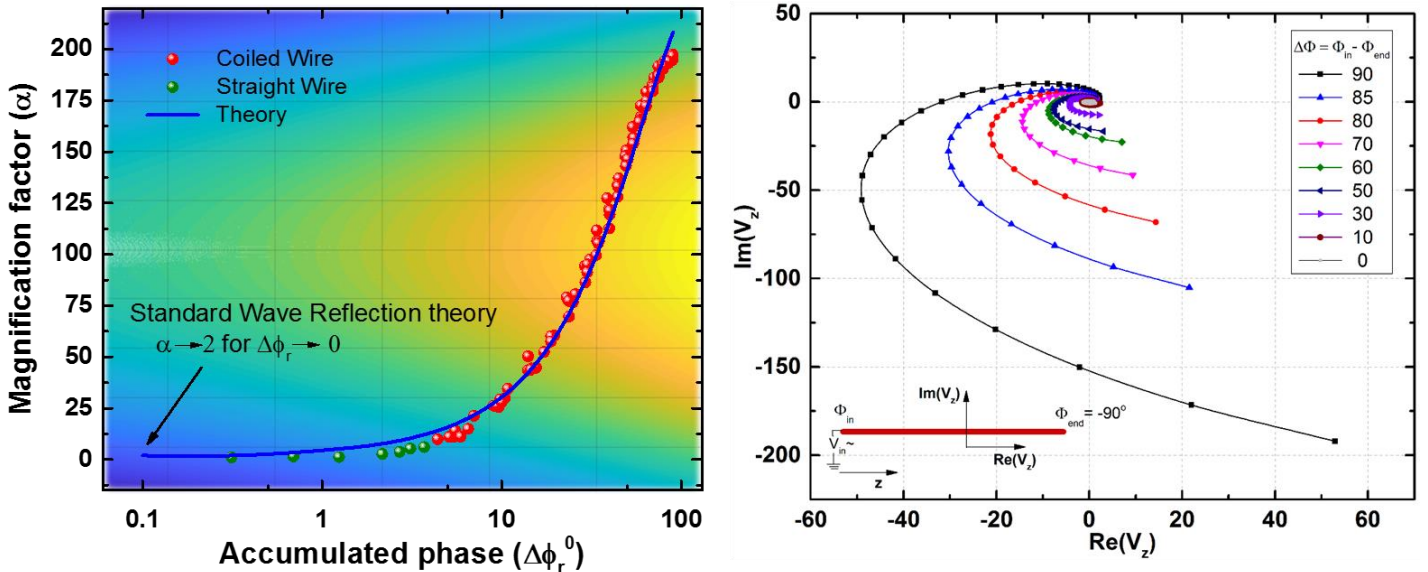


Fig 2.7| A. The match of experimental measured data to theoretical fit obtained from equation (6). The standard wave reflection amplification factor $\alpha = 2$ obtained with the condition of $\Delta\phi_r = 0$ as in a standard definition of wave is highlighted. The background color inlay represents the complex wave field in 2D as a function of accumulated phase $\Delta\phi_r$. **B.** Simulated plots of the complex potential vs the real potential as a function of $\Delta\phi_r$. The generic higher amplification character with higher accumulated phase is evident.

2.8 Physical analogy of accumulated phase in the wire

A small potential applied at one end of a wire breaks down the electron-cloud symmetry inside the metal wire with respect to the positive charge centers in the metal lattice (Fig. 2.8). For a time dependent potential, this symmetry breakdown oscillates in time and for small enough values of $\Delta\phi_r \approx 0$, the breakdown in electron cloud symmetry is also small, leading to uniform scattering at each cross section resulting in an uniform resistance. Resistance is reflected in broadening of γ or the width of resonance in frequency space, γ essentially being a measure of the scatterings of free electron with the deformed electron cloud. In result, a constant propagation factor β emerges, where $\beta \cdot \mathbf{v} = \omega$ is a fundamental condition defining the wave that propagates with a phase velocity \mathbf{v} . The assumption of this constant scattering resistance, restricts \mathbf{V}_r to be linear from the possible

solutions of the Laplacian $\frac{\partial^2 \mathbf{V}_r}{\partial \mathbf{r}^2} = 0$. As a direct result, the solution corroborates to Ohm's

law of resistances in a wire. Also, both β and \mathbf{v} become constants at resonance condition when ω is a constant as discussed before. For the oscillations to follow the applied potential (external action) in phase with no magnification, the condition of stationary phase has to be satisfied closely i.e., $\int_r \partial\phi_r \cong 0$. Resonance breaks this symmetry leading to equation (5) as a function of accumulated phase.

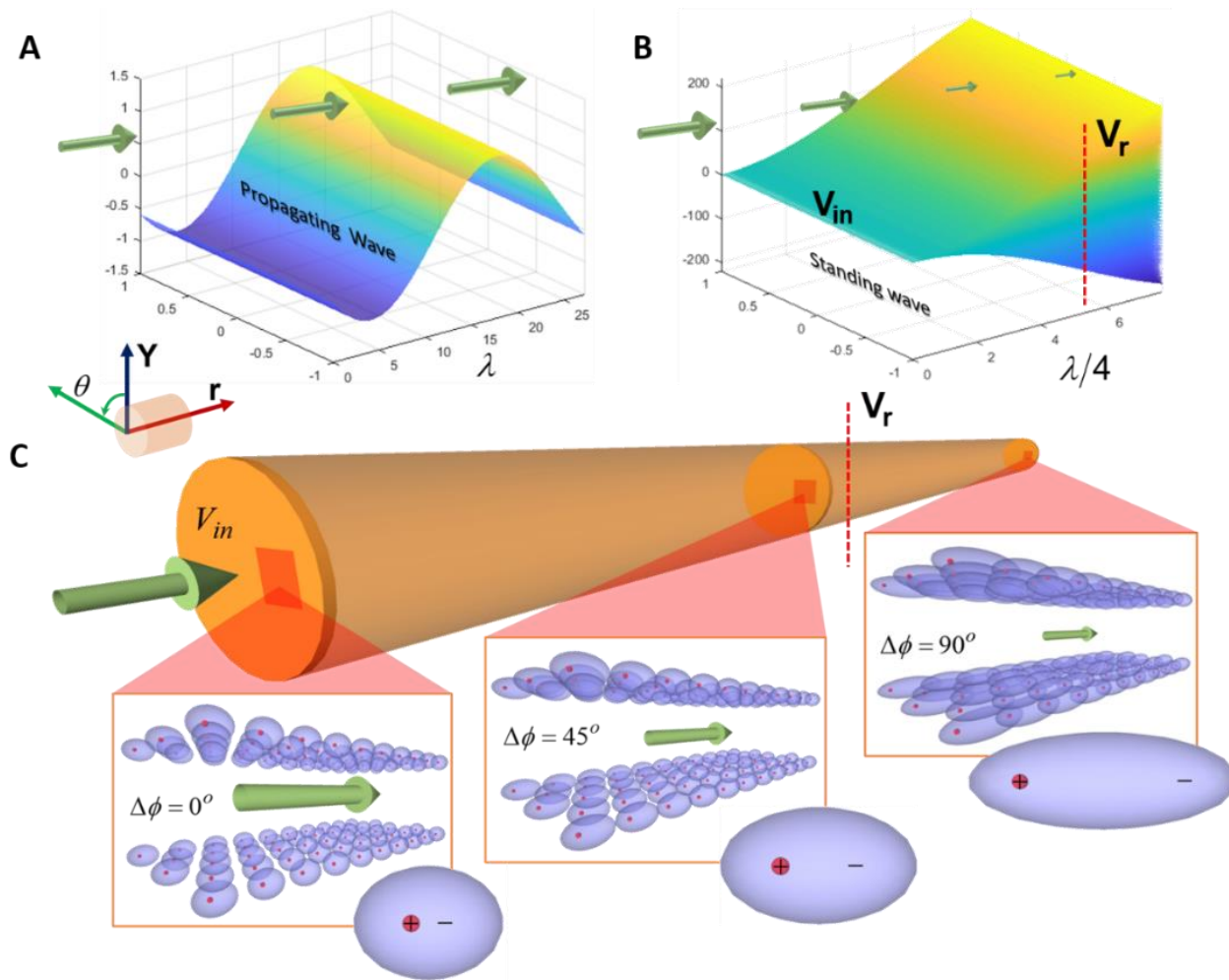


Fig 2.8| Resonance breaks the electron cloud symmetry at the SW frequency creating a nonlinear dependence of the potential explainable through the condition (4) and the phase dependent solution of (5), the deformation being dependent on the accumulated phase. The condition $\int \partial\phi_r \rightarrow \pi/2$ makes the electron cloud

deformation extreme. The higher asymmetric electron cloud takes a higher finite time to make its effect felt as a function of space in the metal lattice, hence the accumulated phase. The greater overlap of electron cloud changes the charge distribution in space making them static charges rather than moving charges as in the usual case of $\Delta\phi_r = 0$. The medium thus appears non-isotropic to the perturbation or wave, with the functional form of $\Delta\phi_r$ being a measure of the non-isotropicity. The distributed charges leads to more storage of energy and lesser dissipation for reduction in charge flow. The stored energy corresponds to the imaginary part of the solution of (5) which when plotted in phase space makes evident the accumulated phase that diverges out in spirals rather than collapsing onto the real axis forming a circle or an ellipse.

2.9 Conclusions and Discussions

By correctly predicting the resonance amplitude from our treatment, we conclude that the SW amplitude Ψ_r at a point in space is a result of summation of perturbations over all time

deducible through the generalized accumulated phase $\Delta\phi_r = \int_{r_{\text{initial}}}^{r_{\text{final}}} \partial\phi_r$ in space, integrating

all the perturbation histories. Our model also deduces the standard superposition result 2 of the wave reflection theory. It is paradoxical that from our argument, a seemingly classical phenomenon like a SW can be explained by an equation that is equivalent in form to the quantum equations formulated by Feynman, while the classical à la the Hamilton-Jacobi equation propounds a non-linear wave equation similar to Schrödinger's quantum form with an additional potential term dependent on the wave function. Our treatment here tries to bridge the two in terms of a generalized approach of *accumulated phase* considering a non-isotropic space in the resonance condition as perceived by a wave that tries to propagate through the medium from the source. In a broader context, we can extend the notion of dissipated energy as our perception of the visible universe, radiations from events in the past. The fundamental assumption of non-isotropicity in a resonance/cyclical model of the universe would allow the consideration of a stored energy component in the vast cosmos. This may provide clues to unravelling the riddles of dark matter and dark energy.

2.10 Discussion on single wire electrical power transfer using resonance

The underlying physics in all forms of energy transfer is *the potential gradient between two points in space*. Science have exploited this common paradigm to transfer energy efficiently, meant to flow from higher potential to lesser potential in a medium. From its inception electrical energy flow using wire as a medium has also followed the same

fundamental ideology (42). At the turn of century, conversion from direct current (DC) single wire power-lines to AC mode posed a fundamental limitation due to unavoidable spatial and temporal phase dependence restricting efficient energy transfer. Traditionally alternating (AC) electrical power has been transmitted through two wires where one serves the equipotential line and other the common ground wire. However, an alternate approach for transferring electric energy may be using a single wire using resonance. Resonance allows the generation of this gradient even in a single wire, which this communication establishes from the first principle. At the onset, it is essential to point out that this should not be confused with the commonly used single wire transmission where the earth acts as a return path, as envisaged by Tesla in late 1800's. In true single wire electrical transmission, there is no secondary wire. Tesla's coinage - "transmission through one wire," has remained elusive and a subject of interest among few researchers since his pioneering experiments. Nearly all subsequent demonstrations of his single wire transmission or variations thereof, are qualitative and require high driving voltages, making power transfer to devices unsafe near people. However through resonance a large gradient, proportional to the amplification factor α , can be generated between two ends. A load connected in series in between this gradient can drive real power. This brings us back to the fundamental question of the necessity of a physical return path for transferring electrical energy from one point to the other. The basic idea of such energy transfer relies on transferring real power through a conducting medium to a load, which is maintained at the same potential gradient as that of the two wires employed in such power transmission. Essentially, in electrical terminology it involves considering a load in parallel to the two-port output, where the two ports; source and the load by virtue of the connection made thus,

maintain a constant potential gradient allowing the flow of energy. Considering a load in parallel necessitates that the gradient in potential be a real quantity for maximum power transfer. At resonance however, the gradient is a function of the phase gradient in space as established in the discussions below and is independent of the phase angle. In fact higher the phase angle, higher is the amplification or the storage to dissipated energy internally. A higher phase gradient thus becomes a marker of increased efficiency of transfer.

The phase gradient is a result of variance in spatial impedance in electrical terminology. Impedance behaves like an incompressible fluid. In fluids, you can transfer power by an applied pressure as in hydraulic systems. The viscosity of a fluid stores the information of relative displacement of molecules corresponding to the applied pressure, and sum of all the relative motions is perceived on the other end as an action or flow. Therefore, viscosity is out of phase to the flow in time and hence acts like a memory element. In electrical system, the flow element is current, hence the memory element is the capacitance storing the information of flow i.e the charges. Thus, the displacement of charges is same as fluid motion in hydraulics. Capacitance can maintain the information so long the voltage is present and if it oscillates in time, the charges oscillate too. The displacement of charges thus results in the power transfer rather than the flow itself. The amplification factor as a function of accumulated phase in space thus dictates the efficiency of energy transfer in the single wire power transmission technique (21 – 23).

ACKNOWLEDGEMENTS

We would like to acknowledge the support and funding of the Canada Excellence Research Chairs (CERC) Program and the Faculty of Engineering at the University of Alberta.

REFERENCES

1. G. Taylor, *Proc. R. Soc. London A, Math. Phys. Sci.* **218**, 44–59 (1953).
 2. H. Goldstein, C. Poole, J. Safko, *Classical Mechanics. Book* (2007), pp. 1–646.
 3. M. Planck, *Eight Lectures on Theoretical Physics* (Columbia University Press, New York, ed. 1st, 1915).
 4. N. Bohr, *Philos. Mag. Ser. 6.* **26**, 857–875 (1913).
 5. I. J. R. Aitchison, D. A. MacManus, T. M. Snyder, **1370**, 999–1008 (2004).
 6. E. Schrodinger, *Collected papers on Wave Mechanics* (Blackie & Son Ltd., London and Glasgow, 1928).
 7. L. De Broglie, *Nature.* **112**, 540 (1923).
 8. L. De Broglie, *Nature.* **118**, 441–442 (1926).
 9. W. R. Hamilton, *Phil. Trans. R. Soc. Lond.* **124**, 247–308 (1834).
 10. W. R. Hamilton, *Philos. Trans. R. Soc. London.* **125**, 95–144 (1835).
 11. S. H. Benton, *The Hamilton-Jacobi equation: a global approach* (Academic press, New York, 1977).
 12. R. P. Feynman, A. Hibbs, *Quantum mechanics and path integrals* (McGraw-Hill, New York, ed. 1, 1965).
 13. R. P. Feynman, *Phys. Rev.* **80**, 440–457 (1950).
 14. W. E. Lamb, *Am. J. Phys.* **69**, 413 (2001).
 15. W. P. Schleich, D. M. Greenberger, D. H. Kobe, M. O. Scully, *Proc. Natl. Acad. Sci.* **110**, 5374–5379 (2013).
 16. J. Slater, *Phys. Rev.* **51**, 846 (1937).
 17. R. M. More, E. Gerjuoy, *Phys. Rev. A.* **7**, 1288–1303 (1973).
 18. H. J. Korsch, F. Physik, U. Kaiserslautern, in *Resonances : The unifying route towards the formulation of dynamical processes* (Springer Verlag, Berlin, 1987), pp. 253–278.
 19. J. Harris *et al.*, *Nat. Phys.* **11**, 629–634 (2015).
 20. A. Benucci, R. A. Frazor, M. Carandini, *Neuron.* **55**, 103–117 (2007).
 21. C. W. Van Neste *et al.*, *Wirel. Power Transf.* **1**, 75–82 (2014).
 22. C. W. Van Neste *et al.*, *Wirel. Power Transf.* **3**, 117–125 (2016).
 23. A. K. Pickering *et al.*, *Wirel. Power Transf.* **2**, 134–142 (2015).
-

24. J. S. Bunch *et al.*, *Science* (80-). **315**, 490–493 (2007).
 25. C. Chen *et al.*, *Nat. Nanotechnol.* **4**, 861–867 (2009).
 26. L. Tetard, A. Passian, T. Thundat, *Nat. Nanotechnol.* **5**, 105–109 (2010).
 27. L. Tetard *et al.*, *Nat. Nanotechnol.* **3**, 501–505 (2008).
 28. D. W. Dareing, D. Yi, T. Thundat, *Ultramicroscopy*. **107**, 1105–1110 (2007).
 29. F. W. Beil *et al.*, *Phys. Rev. Lett.* **100**, 2–5 (2008).
 30. B. Christiansen, P. Alstrom, M. T. Levinsen, *Phys. Rev. Lett.* **68**, 2157–2160 (1992).
 31. A. J. Yule, Y. Al - Suleimani, *Proc. R. Soc. A Math. Phys. Eng. Sci.* **456**, 1069–1085 (2000).
 32. J. Zegenhagen, A. Kazimirov, *The X-Ray Standing Wave technique: Principles and Applications* (World Scientific, 2013).
 33. K. Prashanthi, A. Phani, T. Thundat, *Nano Lett.* **15** (2015), doi:10.1021/acs.nanolett.5b02557.
 34. K. C. Schwab, M. L. Roukes, *Phys Today*. **July**, 36 (2005).
 35. A. D. O'Connell *et al.*, *Nature*. **464**, 697–703 (2010).
 36. R. N. Bhattacharya, I. Basu, *Comput. Phys. Commun.* **16**, 167–173 (1979).
 37. A. Mehta, S. Cherian, D. Hedden, T. Thundat, *Appl. Phys. Lett.* **78**, 1637–1639 (2001).
 38. F. E. Terman, *Trans. IEEE*. **53**, 21–24 (1934).
 39. A. Sommerfeld, *Partial differential equations in physics* (Academic Press, New York, 1949).
 40. J. E. Sader, *J. Appl. Phys.* **84**, 64 (1998).
 41. B. Bagchi, R. Roychoudhury, *J. Phys. A Math. Gen.* **33**, L1–L3 (2000).
 42. J. H. Poynting, *Philos. Trans. R. Soc. London*. **175**, 343–361 (1884).
-

Monograph 2: Published in Scientific Reports

III. A nanostructured surface increases friction exponentially at the solid-gas interface

Arindam Phani^{1*}, Vakhtang Putkaradze^{1,2*}, John E. Hawk¹, Kovur Prashanthi¹, Thomas Thundat^{1*}

¹Department of Chemical and Materials Engineering, ²Department of Mathematical Statistical Sciences, University of Alberta, Edmonton, Alberta T6G 1H9, Canada

*Correspondence to: phani@ualberta.ca, putkarad@ualberta.ca, thundat@ualberta.ca

Scientific Reports 6, Article number: 32996 (2016)

doi:10.1038/srep32996

Published online: 06 September 2016

Copyright © 2016 Nature Publishing Group

A nanostructured surface increases friction exponentially at the solid-gas interface

Arindam Phani^{1*}, Vakhtang Putkaradze^{1,2*}, John E. Hawk¹, Kovur Prashanthi¹, Thomas Thundat^{1*}

¹Department of Chemical and Materials Engineering, ²Department of Mathematical Statistical Sciences, University of Alberta, Edmonton, Alberta T6G 1H9, Canada

*Correspondence to: phani@ualberta.ca, putkarad@ualberta.ca, thundat@ualberta.ca

Abstract: According to Stokes' law, a moving solid surface experiences viscous drag that is linearly related to its velocity and the viscosity of the medium. The viscous interactions result in dissipation that is known to scale as the square root of the kinematic viscosity times the density of the gas. We observed that when an oscillating surface is modified with nanostructures the experimentally measured dissipation shows an exponential dependence on kinematic viscosity. The surface nanostructures alter solid-gas interplay greatly, amplifying the dissipation response exponentially for even minute variations in viscosity. Nanostructured resonator thus allows discrimination of otherwise narrow range of gaseous viscosity making dissipation an ideal parameter for analysis of a gaseous media. We attribute the observed exponential enhancement to the stochastic nature of interactions of many coupled nanostructures with the gas media.

Keywords: Nanostructured surface friction, Surface nanomechanical effect, Nanostructure enhanced dissipation, Viscosity of gases, Energy loss in mechanical resonators.

3.1 Introduction

Solid-gas interface interactions are central to physical processes such as adsorption, catalysis, oscillatory dynamics, stochastic interactions relevant to thermodynamics, atomic and molecular manipulation, viscous drag on nanoparticles and many other fields(43–48).

Dissipative effects from viscous drag, originating from the solid-gas interactions, play an important role in recent advances in micro-nano resonator technology(49–56). Viscosity in general is related to momentum transfer originating from collisions of fluid molecules with surfaces. Thus, viscous friction(57), is always present resulting in energy loss (dissipation), unless the motion occurs in absolute vacuum, which is a theoretical abstraction. The general premise of studying viscous friction at micro- and nano-scales in the continuum assumption has been Stokes' drag equation(58, 59), which states that the damping losses are proportional to the viscosity of the fluid when the other flow parameters such as velocity and length scale are held constant. However, this law of friction starts showing deviations at the nanoscale, prompting the need to understand the role of viscous interactions at nanoscale interfaces arising from the solid-fluid interactions(50, 60–77).

To elaborate on the flow of fluid at the nanoscale in the Stokes flow regime, the physical length scale a is of the orders of nanometers and the typical velocity u is of the order of mm or μm per sec. In such systems, viscous forces dominate over inertial forces, as expressed by the dimensionless Reynolds number $Re = \frac{ua}{\nu}$, ν being the media's

kinematic viscosity, with $Re \ll 1$, and where $\nu = \frac{\eta}{\rho}$, the ratio of η , the dynamic viscosity and ρ , the density of the fluid. For uniformity in all further discussions the term viscosity has been used to mean kinematic viscosity ν . This very low Reynolds number regime is

most relevant for vibrating nanomechanical oscillators or surfaces modified with nanoscale structures, where the effective flow is across nanostructure boundaries. Since the viscous terms dominate the inertial terms in this Stokes regime, the equation of motion shows a linear dependence on velocity, and the dissipation terms are proportional to viscosity. For an incompressible fluid motion without external forces, the Stokes equation is

$$\nu \Delta \mathbf{u} - \frac{1}{\rho} \nabla p = \mathbf{0}, \quad (1)$$

with $\nabla \mathbf{u} = 0$ inside the fluid and $\mathbf{u} = 0$ on the solid-fluid interface, where Δ is the Laplace operator, ρ is the fluid density assumed constant and p is the pressure. In this approximation, the viscous drag on any finite object moving through the fluid will be proportional to the velocity of the object and the viscosity, with a coefficient depending on the object's shape. It should be noted that the shape coefficient may depend weakly on Re due to Oseen's corrections as we shall utilize below for the case of a cylinder moving through the flow. Nevertheless, the main dependence of the friction force acting on an object in Stokes' approximation must be linear (or almost linear) in viscosity and velocity. The effect of viscous drag in the Stokesian regime can be studied by the measure of damping experienced by a mechanical resonator, where the motion generates oscillatory flows at the interface. The damping can be characterized by the Q-factor of the resonator, proportional to the inverse of the rate of decay of vibrations per period. Energy loss from viscous drag reduces the Q of the system, which depends on the interactions of the resonator surface with the medium.

For liquids, the variations in viscosity can be significant, by several orders of magnitude. For gases, however, that variation is much smaller. This is because the mean free path of molecules in gases ($\sim 67\text{nm}$ in normal conditions) is large compared to the

inter-molecular distances ($\sim 3 - 4\text{nm}$ in the same conditions) and the interaction forces between molecules decay rapidly with increasing distance. The values for gas viscosity thus tend to be small and change relatively little as compared to liquids. In addition, the dynamic range of variation for kinematic viscosity between different gases is relatively small, within an order of magnitude. For example, viscosity of H_2 is $8\mu\text{Pa} \cdot \text{sec}$ while that of CO_2 is $14.8\mu\text{Pa} \cdot \text{sec}$. Viscosities of gases also show little variation with temperature(57).

This small dynamic range of gas viscosity limits observable variations in interactions with a surface, since its effect on dynamical change is correspondingly small. We shall also note that oscillating shear flows over a surface lead to power-law dependences of drag on viscosity, which is also a slowly varying function. Thus, viscosity is not used as a parameter in characterizing vapors or gas media and in most sensing applications. Instead, most resonator sensors in air rely on resonator frequency shift induced by mass loading as a reliable sensor parameter. A resonator with a high resonance frequency, operating in vacuum can detect single molecules in special circumstances. In general, atto-gram sensitivity can be observed with micro and nanoscale mechanical resonators in high vacuum. The higher loss in energy due to fluid drag at the nanoscale necessitates operation in vacuum to increase the Q of resonance in order to obtain a high resolution in frequency variations. However, it has been reported that the improvement in Q at higher vacuum for nano-cantilevers is rather moderate(49, 60, 62). This would suggest that it is difficult to use the change of gas viscosity as a measuring tool, whether by a macro- or a nano-scale device.

3.2 Objectives and key results of the work. We report that in contrast to existing results for single oscillators at the nanoscale, modifying an oscillating surface with a forest of nanoscale features, like vertical slender nanorods or nanobristles (Fig 3.S1), magnifies viscous interactions with the ambient media by up to three orders of magnitude as compared to the non-modified (bare) surface. This was observed with surface nanostructures having typical spacing between them in the order of 50-60 nm (Fig 3.1a), which is around the mean free path (mfp) of the gas phase molecules. As far as we are aware of, the studies of enhancement of dissipation from such surface nanostructuring has not been addressed in the literature. More interestingly, we observe an enhancement showing an *exponential* sensitivity to viscosity change, drastically deviating from the linear dependence as predicted by the premise of Stokes' theory and its modifications.

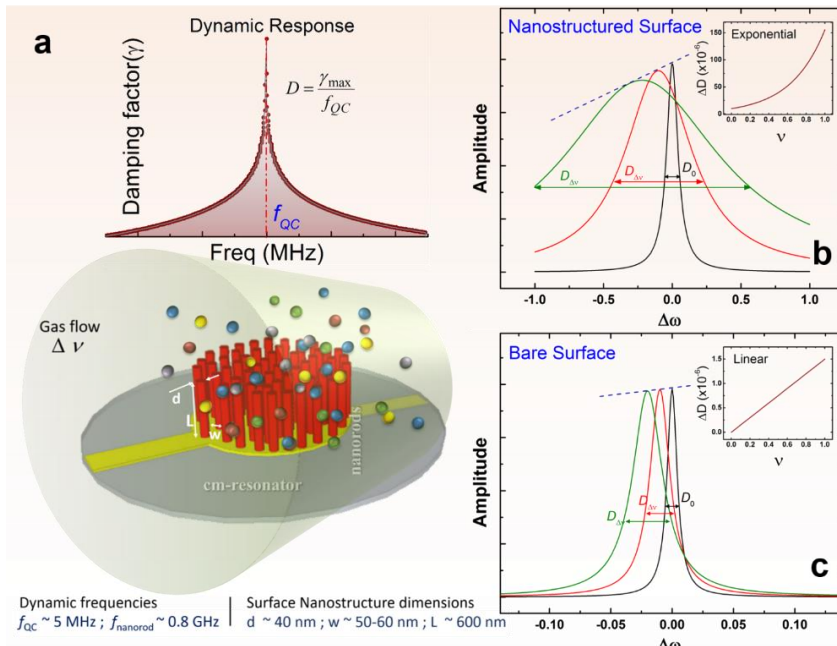


Figure 3.1| Experimental Schematic with key result. (a) A typical measured graph of dissipation (top) and an artist's impression of a nanostructured resonator surface interacting with gas molecules (bottom). (b) Amplitude response graphs for a nanostructured surface for three measurements of increasing viscosity of ambient gas (black, red, green) showing the exponential variation of the dissipation D on viscosity (inset). (c) Amplitude response graphs for a bare surface for similar three measurements of increasing viscosity of ambient gas (black, red, green) showing the linear variation of D on viscosity (inset). The blue dotted lines joining the amplitude peaks in (b) and (c) represent the same relative change in amplitudes in both cases.

dissipation D on viscosity (inset). (c) Amplitude response graphs for a bare surface for similar three measurements of increasing viscosity of ambient gas (black, red, green) showing the linear variation of D on viscosity (inset). The blue dotted lines joining the amplitude peaks in (b) and (c) represent the same relative change in amplitudes in both cases.

3.3 Experimental design. A schematic of the experimental realization (Fig. 1a) in the context of studying such surface nanostructuring effect in a quartz crystal (QC) oscillator is shown along with the key result (Fig 3.1b). Use of macroscopic, commercially available QC oscillators offers many advantages such as easy readout, simplicity, high base Q-factor in air, large surface area for increased molecular interactions, and low cost. The nanoscale modification of QC surface combines the advantages of both nano and macro devices and serves as a bridge between the nano and macro world. The closely spaced nanostructures increase the mechanical interaction between gas molecules and surface, leading to an exponential dependence on viscosity, as we report.

In contrast, the change observed for an unmodified bare surface is consistent with the Stokes' equation, and is orders of magnitude smaller. For small variations in the kinematic viscosity, Stokes' theory predicts the linear change (see schematic on Fig 3.1c). Our measurements of the response of the bare QC surface (Fig 3.2b) attests to solutions of Stokes' equation for an oscillating surface (Stokes' second problem(78)), which predicts damping rates D as slow varying nonlinear functions of media properties. Typically for shear flows, D scales as $\nu\rho$ where vibrations generate thick viscous layers(66, 72, 76), or as $\rho\sqrt{\nu}$ when the viscous layers are thin^{9,19,36}. In the Stokesian regime in air, the viscous layer is thin and hence the relative change in $D(\nu, \rho)$ can be approximated with a high accuracy as $\frac{\Delta D}{D} \approx \frac{1}{2} \frac{\Delta \nu}{\nu} + \frac{\Delta \rho}{\rho}$ for small (few per cent) relative changes in ρ and ν , relevant to media characterization. For more general functions of $D(\nu, \rho)$ involving higher order terms, the changes in $\frac{\Delta D}{D}$ would still remain linear in small relative changes of

parameters. More complex theories based on Stokes' flows can be derived, and they all point to a *linear* dependence of dissipation on small relative changes in the ambient media. This contradicts our results for nanostructured resonators, which we will analyze below in detail.

3.4 Measured quantities and presentation of results. All our results are presented in terms of the dissipated to stored energy per cycle at resonance as

$$D = \frac{1}{Q} = \frac{E_{diss}}{E_{stored}} = \frac{\int_0^T \vec{F}_{visc} \cdot \vec{x} dt}{E_{kinetic} + E_{potential}} = \frac{\int_0^T \gamma \dot{x}^2 dt}{\frac{1}{2T} \int_0^T (\dot{x}^2 + \omega_0^2 x^2) dt} = \frac{\gamma \int_0^T \omega_0^2 x^2 dt}{\frac{1}{T} \int_0^T \omega_0^2 x^2 dt} = \frac{\gamma}{f}, \quad (2)$$

from simultaneous measurements of f and γ in an experiment (Fig. 1a) where $\vec{F}_{visc} = \gamma \dot{x}$ is the viscous drag force, γ the damping factor and where $f = 2\pi/\omega_0$ is the resonance frequency in sec^{-1} , T being the time period of oscillations. The motion in this case is assumed to be along the x direction with \dot{x} and \ddot{x} denoting the 1st and 2nd order time derivatives respectively.

We note here, that the obtained D from experimental impedance analysis and $\frac{1}{Q}$ obtained independently from the Lorentzian fit (see Fig 3.S3 in Supplementary materials) are identical with accuracy to an order of 10^{-7} (Fig 3.S4 in Supplementary text). This serves as an additional verification of the accuracy of our measurements. Therefore, we can consider both D or $\frac{1}{Q}$ as identical. It is easier to cast the results in terms of D since it is easier to analyze the total dissipation in the system as the linear addition of internal dissipation and that originating from boundary media interactions.

3.5 Experimental results of dissipation enhancement for nanostructured interface.

Our work reports an *exponential* sensitivity of dissipation for various gas media with a nanostructured resonator, which is drastically different from previous results. The enhancement effect was studied in detail by conducting systematic experiments for various media conditions (Fig 3.2a), allowing a dynamic range of up to 30% variations in kinematic viscosities. The experimental kinematic viscosities for different media conditions were computed using literature reference and has been included in the supplementary materials (S5). Previous works report similar surface nanostructuring effects, attributing enhanced sensitivity to increased surface area for higher molecular adsorption and mass loading on an oscillator(80, 81). Our approach of dissipation analysis reveals a drastically different paradigm, namely, the exponential change in damping for even few percent relative changes in media kinematic viscosity ν (Fig 3.2a). The data in Fig 3.2 includes the change of viscosity corresponding to different gas media and also due to change of temperature(57) in the same gas media. A crucial result is the observed exponential dependence of dissipation on temperature of a fixed gas as well, as shown in Fig 3.2a, with data collapsed on to the same normalized scale of kinematic viscosity change. For a detailed experimental setup and operation, refer to the section *Experimental Methods* below. All normalized x-axis scales represent relative changes of corresponding ‘variable’ as in $\left(\frac{\Delta \text{ variable}}{\text{variable}_{\min}} \right)$. The observed enhancement effect of nanostructuring is shown to resolve viscosity changes substantially better compared to non-nanostructured surfaces at even normal atmospheric conditions (Fig 3.2b, 3.2c), effectively broadening the detection range of the otherwise narrow range of viscosities of gases. In comparison, the resonance frequency variations of

the resonator are orders of magnitude lower (Fig 3.3). Error bars shown on all experimental data points represent 5% of absolute variation. It is also interesting that the change in damping is drastic for even modest changes in the resonance amplitude a (Fig 3.4), making the dissipation response strongly non-linear, even though the resonator itself is operating in the purely linear regime. For a standard linear resonator, the dissipation would have varied proportional to the resonance amplitude. In contrast, nanostructuring of the surface creates a drastic exponential decrease with the resonance amplitude.

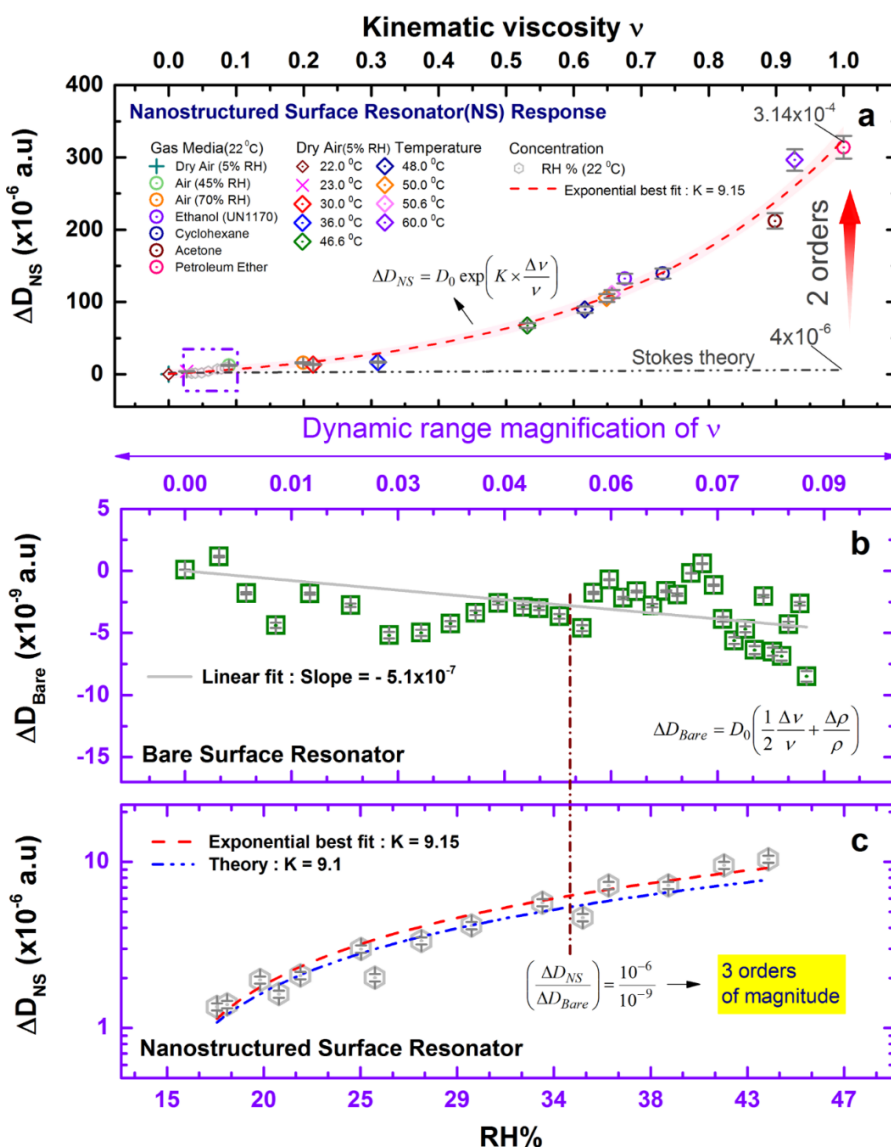


Figure 3.2| Damping with varying media conditions. (a) Results of experiments for a wide range of viscosities for different gases at a fixed temperature, and also temperature dependence for a single gas. 2 orders of magnitude deviation from Stokes' theory shown with a Red arrow. Panels (b) and (c) show the effective magnification of dynamic range of ν as a measurement parameter, where 3 orders of dissipation enhancement as compared to a bare surface are highlighted.

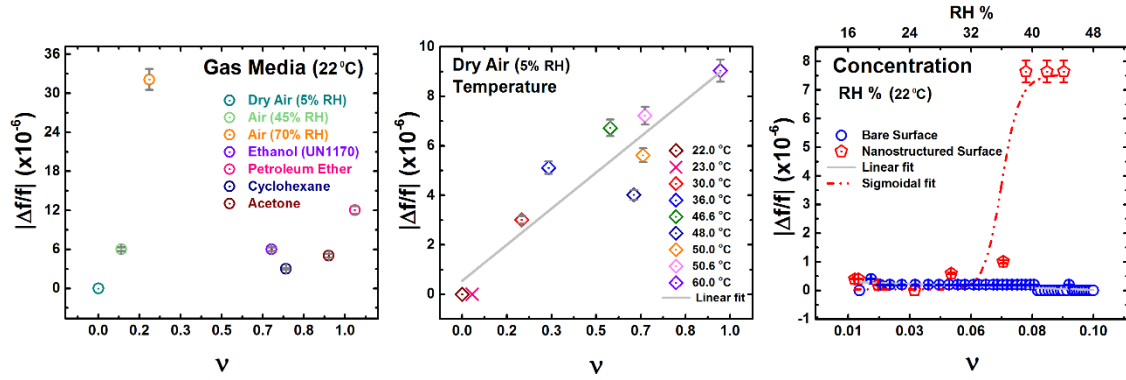


Figure 3.3| Observed absolute relative frequency changes $|\Delta f/f|$. Resonance frequency f measured in dry air at normal temperature and pressure conditions for the lowest drive input. All variations in frequency correspond to the expected values with orders of magnitude of 10^{-6} .

We note here that the dissipation has contributions from resonator's internal friction, and friction with external media as $D = D_{int} + D_{ext}$. It is known that friction with external media (D_{ext}) depends on both shape factor and media-boundary interactions. For small amplitudes, D_{ext} is the dominating factor for a nanostructured resonator surface as revealed in the experimental results (Fig 3.4). However, for higher resonance amplitudes, the boundary-media dissipation component becomes small, and the internal dissipation D_{int} can no longer be neglected, exhibiting a residual dissipation in our system. This residual dissipation has been included in the exponential fits of Fig 3.4 of all presented data related to the amplitude dependence. In the enhancement case shown on Fig 3.2, this residual dissipation D_{int} is negligible compared to the boundary-media dissipation term.

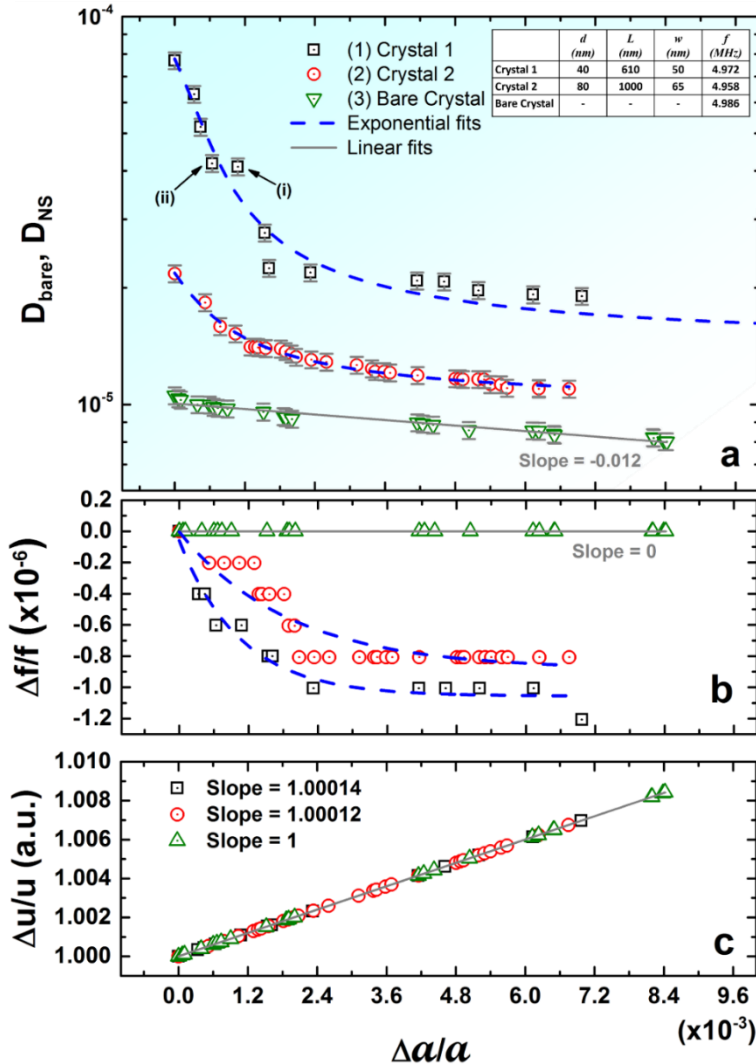


Figure 3.4| Damping for a single vapor concentration vs normalized changes resonance amplitude. (a) Shows high sensitivity of the dissipation for a nanostructured resonator vs an equivalent resonator with a non-structured surface. Dashed blue line shows exponential fit corroborating to our theory. As a representative for detailed analysis check Fig 3.S3 for data points (i) and (ii). (b) The corresponding frequency variations, commonly used as a measuring parameter, shows substantial enhancement for nanostructured case, and remains in the order of ppm. (c) The variations of velocity are linearly proportional to the change in amplitude, with the slope being very close to 1, as expected.

3.6 Limiting Sensitivity: Relevance to sensing applications.

Our work shows that nanostructuring a surface allows probing the most fundamental physical aspects of ambient gases, such as its continuity, using a macro-device, acting as a bridge between the nano and macro world. Such active non-continuum probing resolves the changes in viscosity better for magnified viscous effects at the interface, effectively broadening its dynamic range (Fig 3.2b). We show experimentally that such enhanced resolution cannot be achieved with non-modified surfaces (Fig 3.2c).

It is imperative to provide an estimate of the maximum possible sensitivity achievable by a measuring device, based on such nanostructuring, using dissipation as an observable parameter. Such an estimate is most relevant for cases of a non-adsorbing analyte in very low concentrations such as highly volatile organics. As the data shows (Fig 3.3), using frequency as a measuring parameter for the sensor in normal conditions is challenging in such a case as it is orders of magnitude smaller and does not follow any established trend for small changes in media. It is also known that for dominant boundary-media viscous interactions the resonance frequency is not independent of the damping forces. So, deducing changes in the media through resonator's dynamics solely from the aspect of resonance frequency shift can be difficult where the adsorption effects are small. In our work, for high enough changes in relative humidity, the observed change in the resonance frequency is in the parts per million order conforming to previous works(80, 81). On the other hand, damping shows the relative change of several orders of magnitudes, making the damping in surface nanostructured resonators to be approximately $10^8 - 10^9$ times more sensitive to ambient changes compared to the frequency shift (*i.e.*, factor of $10^2 - 10^3$ in dissipation vs 10^{-6} in frequency).

To elaborate on this point, the changes in dissipation are expected to come from the probability of molecular interactions and fluctuations in a cell bounded by the nanostructure walls, and this method does not necessitate adsorption of the molecules on the resonator to effect a change in resonator's behavior. Let us consider the volume space, marked in yellow in Fig 3.5, contained in-between adjacent nanorods (cell), and suppose α is the concentration of an added analyte expected to induce a change in the perceived media. Then, at each point in time, the probability that a cell would have an analyte

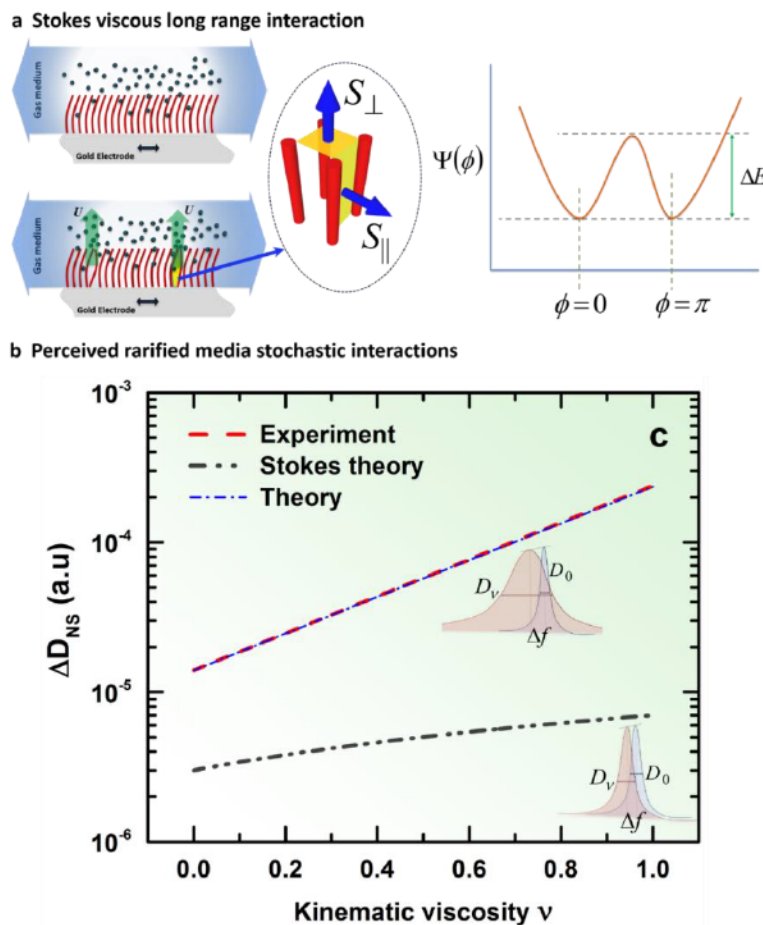


Figure 3.5| Illustration of the mechanism for spontaneous out-of-phase rod dynamics enhancing dissipation. (a) Illustrating in-phase motion of the rods, only the friction of the motion parallel to the resonator contributes to dissipation. (b) Two incidents of out-of-phase motion of the rods create a strong motion transversal to the resonator, enhancing the dissipation. The potential function $\Psi(\phi)$ defining the energy of a given state, having the minima at $\phi = 0$ and $\phi = \pi$ with the potential barrier separating the two states (the in-phase and out-of-phase) being ΔE . (c) Compiled graphical comparison of experiment and theoretical analysis.

molecule in it is ${}^1P = \alpha$, and not to have that molecule is ${}^0P = 1 - \alpha$. After a characteristic viscous timescale $\tau_m = L^2/\nu$, the molecules of the analyte will escape the cell, making the events that are separated by τ_m time apart statistically independent. After an elapsed time $T' = n\tau_m$ encompassing n independent events of going in/out of a cell (equivalent to one event from n independent cells), the probability of a cell not to experience the effect of presence of an analyte molecule will be ${}^0P_n = (1 - \square)^n = e^{-T'/\square_m}$ assuming $\alpha \ll 1$ and $n \gg 1$. For a typical time scale of one QC period at resonance, $T' \Leftrightarrow \tau_n = 1/f$, the number of cells that are actively experiencing the effect of analyte molecules becomes

$N_s = N_r \left(1 - e^{-\alpha \tau_n / \tau_m}\right) = N_r (\alpha \tau_n / \tau_m)$ for $\alpha \rightarrow 0$, with N_r being the total number of cells per unit area. The limit sensitivity of the system, as measured by concentration of molecules, is then given as $\frac{N_s}{N_r} = \alpha \frac{\tau_n}{\tau_m}$. With the current experimental apparatus, measurement accuracy of D is guaranteed to be better than 0.02% which gives $\alpha \approx 2 \times 10^{-5}$ (~10 parts per million - ppm) for $\tau_n / \tau_m \approx 10$ typical to our system. However, the accuracy of the measurement of D , as shown in the Supplementary Section 3.S3, fits the alternative measurement of the width of Lorentzian within 10^{-7} , (Fig 3.S3 and 3.S4), giving the expected minimum concentration measurable with this setup to be 10^{-8} (~10 parts per billion - ppb), if one were to assume that the accuracy of the measurements illustrated in Figures 3.S3 and 3.S4 persisted for all experiments. In principle, the limit of the accuracy is given by mean average fluctuation of number of molecules in a cell (about $\pm 3\%$ for 10^3 molecules in a cell between nearest neighbor rods), taken for $N_r = 10^8$ independent cells/ mm^2 , giving an estimate of $\alpha \approx 10^{-9}$ (ppb). Of course, such idealistic experiment to perceive variations in ppb level will require much more accurate measurements from the aspect of electrical impedance accuracy, though not unachievable; and may require controlled conditions such as low temperature etc. This limiting value of measurable concentrations is of great importance for design of devices that can achieve ppb accuracy even at normal conditions.

3.7 Theoretical analysis of the results.

We shall now focus on a theoretical understanding of the system to explain the experimental results obtained. For a plausible explanation of the exponential dependence

of the dissipation on parameters, we suggest the following theory based on dynamical transitions between two co-existing states at resonance, in-phase and out-of-phase motion of nanostructures with the motion of the resonator base. We base this theory on the assumption that most of the dissipation comes from the out-of-phase motion, with the transition between the states occurring due to the stochastic transitions between the multiple steady states and Stochastic Resonance (SR) effect(82–84). Indeed, such a consideration of stochastic transition is relevant since the nanostructure dimensions and distances between them are smaller than the *mfp* of the gas phase molecules.

State I: In-phase motion of nano-structures. It is well known that the resonator motion would generate oscillating flows at the interface, *i.e.* nanostructure boundaries in our case, with $\Re e \sim 10^{-6}$ and the corresponding dynamic viscous length scale(85)

$$\delta = \sqrt{\frac{2\nu}{\omega_0}} \sim 10^{-6} m, \text{ which is much greater than both the width } w \sim 50 - 60 nm \text{ between}$$

a nearest neighbor nanostructure, and also the *mfp* of the gas molecules. Thus, due to shear flow, the viscous interaction from each nanorod would extend laterally over many neighboring nanorods on the surface, resulting in a strong bias towards the in-phase steady motion of the nanorods with the base (Fig 3.5a), similar to swimming microorganisms(86, 87), clustered stereocilia during spontaneous oscillations of hair bundles in cochlear outer hair cells(63), or Kuramoto oscillators(88). The resulting viscous friction between the rods from the oscillating-flow would then account for the energy loss in the form of damping in experiments. This loss energy scale can be estimated as the work of friction force per period of oscillation(85), given by $\Delta W = 2\pi\nu\rho CLu^2 / f$, where $C = 2/\log(7.4/\Re e)$ is the Oseen's drag coefficient correction for low $\Re e$ flow past a rigid cylinder(85) with L and

d as defined in Fig 3.1a and u being the characteristic flow velocity. This energy dissipation expression essentially leads to Stokes-like drag formulations(52, 60, 62, 64, 69, 71, 79), predicting a *linear* dependence of dissipation D on the small relative changes in viscosity ν . This predicted result is expressed graphically in Fig 3.2a by the gray dash-dotted line highlighting the 2 orders of magnitude deviation from experimental results. We also studied more complex considerations of Stokes flows with off-set boundaries to account for the nanostructured surface, leading to a similar, essentially linear estimate of resonator friction dependence on viscosity. However, our experimental results deviate significantly from this Stokesian regime. Thus, there must be another state of the system with drastically enhanced dissipation. This other state, at resonance, we can relate to with the out-of-phase motion of the nanostructures.

State II: Out-of-phase motion. Because of inherent randomness in the system, a spontaneous off-phase motion of some neighboring pairs of nanorods generating flow transversal to the resonator plane may occur (Fig 3.5b). With first order approximation, let us consider the volume space $V = Lw^2$ bounded by counter-moving walls of the nanorods (cell) (Fig 3.5). The in-phase moving walls of the cell do not change the volume contained between them and thus generate no additional flow velocity. The out-of-phase motion leads to an effective volume change between two such nearest neighbors as $dV/dt = U \cdot S_{\perp}$, thus generating velocity U of the gas, with $S_{\perp} = w^2$ being the cross sectional area of the cell normal to the surface of the crystal (Fig 3.5), w being the distance between rods. This would account for localized energy of the fluid moving in the out-of-phase cell as

$$\Delta E = V \cdot \rho \cdot U^2 / 2 , \quad (3)$$

ρ being the gas density, assumed constant for incompressible flow. For the typical dimension of the nanorods and operational vibrational amplitude $a \sim 4\text{nm}$ (See Supplementary Section S7), the mean free path of the molecules is $l_* \approx 67\text{nm} \gg a$. Since the resonance amplitude is comparable with the intermolecular gas distances ($3 - 4\text{nm}$), there is a high rate of impact between the molecules and the nanostructures. In addition, the impacted molecules are much more likely to collide with another nearest neighbour nanorod than another molecule. We can approximate this fact by positing the effective amplitude of motion of molecules to be $a_{eff} \approx l_*$. With this consideration, we can approximate the time rate of volume change for off-phase motion as

$$dV/dt = S_{||} \cdot f \cdot a_{eff} = L \cdot w \cdot f \cdot a_{eff}, \quad (4)$$

$S_{||} = Lw$ giving the cross-sectional area in the direction parallel to the crystal surface (Fig 3.5) and f being the frequency as defined before. This time rate of change of the volume may cause the gas to move in and out of the domain bounded by the walls with a typical velocity $U = \frac{dV/dt}{S_{\perp}} = L \cdot f \cdot a_{eff}/w$. It thus follows from equations (3) and (4), that the energy gain necessary to go from in-phase to out-of-phase motion with the base is $\Delta E = \rho L^3 a_{eff}^2 f^2$. As the distance between the rods is comparable to molecular mfp , the lubrication-type friction caused by impacts between the molecules can be considered small compared to that arising from the stochastic interactions with the walls. Thus, the main contribution to dissipation can be assumed to be originating from the friction encountered by the rods themselves(75, 85).

Transition between the states due to stochastic dynamics. The existence of these two states, representing the two possible steady states of the system at resonance, can be considered as the first step towards a more complex theoretical analysis. In reality, there is a continuum of states corresponding to the intermediate configurations of flow. The states can be viewed in terms of effective variable ϕ representing the on and off-phase transition of an individual cell, with $\phi = 0$ being the in-phase state and $\phi = \pi$ being the out-of-phase state. Then, ΔE is the energy barrier the system needs to overcome in order to transition from the in-phase to the out-of phase state, as schematically illustrated by a double-well potential on Figure 3.5, the minima of the potential representing the two possible states. The transition between the states is driven by the molecular impacts which are much faster (\sim picosecond) compared to both the time scale of oscillations of the crystal (\sim microsecond) and the resonance of the nanorods (\sim nanosecond). The dynamics of the transition between the states can then be modeled in terms of stochastic dynamics of a bi-stable system(82–84) with the noise intensity ζ (i.e., the noise autocorrelation function) being proportional to ΔW , which is precisely the viscous loss due to the molecules impacting the rods.

3.8 Key result on the Theoretical Analysis and relevance to experimental data.

For detailed theoretical analysis to be undertaken later, one will proceed with finding a stochastic dynamics model of motion between the different states. Such a model will necessarily include the dynamical assumptions of the state ϕ as a function of generalized time, the potential $\Psi(\phi)$ describing the energy of a given state, a periodic forcing and a noise. Such theory will be crucial for understanding of the dynamics close to the resonance, however, for now, we would like to postpone such detailed discussions for subsequent

work when the nature and functional form of different terms is more clear. Here, we take a more general approach and outline the results that will be common for such models, and which are of relevance to our experiments. The primary ingredient of the theoretical model is the potential function $\Psi(\phi)$ defining the energy of a given state, having the minima at $\phi = 0$ and $\phi = \pi$ with the potential barrier separating the two states being ΔE (Fig 3.5) as we have illustrated. Then, independent of the exact functional form of the chosen $\Psi(\phi)$, the noise-induced hopping between the states may be described in the form of Kramers rate (89, 90)

$$r_K \propto \exp\left(-\frac{\Delta\Psi}{\zeta}\right), \quad (4)$$

as long as the potential $\Psi(\phi)$ satisfies the above constraints of being a smooth function with two given minima. Surprisingly, this general fact is sufficient to provide an excellent explanation of all available experimental data. Indeed, with the majority of the states being in the in-phase state, Kramers' law, coupled with the assumption of a finite lifetime of the off-phase state, leads to describing the number of cells in the off-phase state following the Gibbs probability distribution as

$$p = p_0 \exp\left[-\frac{\Delta E}{\Delta W}\right] = p_0 \exp\left[-\frac{L^2 f}{4\pi C\nu} \left(\frac{a_{eff}}{a}\right)^2\right]. \quad (5)$$

This is precisely the consequence of the existence of two states as estimated above, with ΔW playing the role of the amplitude of the noise ζ in (4). The exponent in square brackets above incorporates parameters of the integrated multi-scale resonator into a single

dimensionless constant $K = \frac{1}{4\pi} \frac{L^2 f}{C\nu} \left(\frac{w}{a}\right)^2$ where $a_{eff} \approx w$, a_{eff} being the effective amplitude of motion of molecules on impact with the rods as described before.

Now, assuming that most dissipation comes from the in-phase energy scale, with the off-phase energy scale resulting in the enhancement as a function of minute media viscosity ν variations, from (5) above we obtain

$$\Delta D = D_0 \exp\left(\frac{1}{4\pi} \frac{L^2 f}{C\nu} \left(\frac{w}{a}\right)^2 \cdot \frac{\Delta\nu}{\nu}\right) = D_0 \exp\left(K \cdot \frac{\Delta\nu}{\nu}\right), \quad 6)$$

with D_0 being the dissipation for the smallest kinematic viscosity in the experiments.

While much needs to be done to derive a complete stochastic dynamics model from the first principles, we believe that this preliminary result coming from rather general assumptions leads to some encouraging insights. Indeed, the theoretical prediction (6) is in agreement with the exponential experimental trend presented on Fig 3.2a and 3.2c, providing an excellent match to the data with no fitting parameters. The best fit of the graph in Fig 3.2a provides $K = 9.15$ and theoretical prediction (6) yields $K \approx 9.1$ where we have taken $a = 4nm$ from experimental data analysis (supplementary materials S7). The high value of the dimensionless parameter K determines the amplification or scaling factor e^K for unit changes in $\frac{\Delta\nu}{\nu}$, showing exponential sensitivity to small variations in viscosity in our experiments. In the absence of surface nanostructuring, the system ceases to have a second stable state where expressions (4) and (5) are no longer valid, and a continuum energy scale similar to ΔW , relevant to the system, can explain the linearity in response for small relative variations in flow parameters(52, 62, 79). This is confirmed by our experiments (Fig 3.2b) where indeed, for a bare surface, the motion is in the continuum

regime and expected change in dynamics from Stokes' drag is linear, $\Re e$ being a slow varying function on media kinematic viscosity ν .

The theoretical prediction (6) for small changes in motion is further substantiated by the exponential dependence of dissipation on resonance amplitude (Fig 3.4). If we assume the simplest linear dependence of a_{eff} on Δa , from (6) we arrive to the exponential dependence of D on $\frac{\Delta a}{a}$ (supplementary materials S8), shown with the dashed line as an experimental best fit in Fig 3.4. Here a in the denominator is the resonance amplitude obtained for the lowest input drive energy. More sophisticated models of dependence of a_{eff} on Δa with higher order terms can be derived by considering collisions of gas phase molecules and the nanorods varying as a power law, essentially leading to the same results. The most interesting fact is the apparent higher exponential rate of change of dissipation as a function of $\frac{\Delta a}{a}$ for the surface with nanostructures having diameter and width lesser than the *mfp* of the gas phase molecules (Fig 3.4 Crystal 1). We shall note that the system with larger nanorods separated by a larger distance experience slower decay of D with the amplitude (Fig 3.4 Crystal 2). While the experimental limitations do not allow us to test the continuously changing dimensions of the nanorods, we believe that these results illustrate that, as the dimensions slowly increase with respect to the *mfp*, the effect of dissipation enhancement correspondingly diminishes, eventually yielding a linear dependence on viscosity as expected by Stokes' theory (Fig 3.4a). Thus, even preliminary analysis for our system based on quite general assumptions are of substantial interest, and further elaboration of the theory will be considered in details in our upcoming work.

3.9 Discussion on time and length scales.

We shall note that, the probabilistic consideration of interactions at the solid-gas interface, because of the nanostructures, inherently incorporates two non-dimensional scaling

parameters: a time scale ratio $\frac{L^2 f}{\nu} = \frac{\tau_m}{\tau_n} = \Omega$ and the other a spatial scale ratio

$$\left(\frac{a_{eff}}{a}\right)^2 = \Pi. \text{ The orders of magnitude of these two scale ratios gives a measure of}$$

separation of the two energy state basins considered in our model. Here, τ_m is the molecular motion time scale related to the kinematic viscosity ν and τ_n is the time scale of motion of the surface or the nanorods. The ratio $\tau_n/\tau_m = 1/\Omega > 1$ signifies the extent of collisions with gas molecules experienced by a nanorod per period of its motion or the rate of molecular fluctuations within a cell bounded by nearest neighbor nanorods. We have, typically, $\Pi \gg 1$ for our system, that changes depending on the grafting density on the surface. Their product $K = \Omega \Pi$ (~ 10 for typical order of magnitudes in our system) affords a large change of p in (5) with respect to small changes in media defining the sensitivity. Theoretical estimate based on the physics of statistical fluctuations of the number of molecules in a cell bounded by the nanorods gives limiting sensitivity of the order of parts per billion (ppb) concentrations even at normal temperature and pressure conditions, on the introduction of an analyte, which can in principle be achieved by this method. Our experimental results demonstrate measurement sensitivity of the order of ppm as presented (Fig 3.2a, 3.2c), when a single analyte is introduced in the system with a carrier gas.

3.10 Conclusions.

Damping in nanomechanical resonators has traditionally been regarded as an impediment to sensitivity. We show that for oscillating surfaces modified with nanoscale structures, dissipation offers a wealth of information on the nature of mechanical interactions of molecules with surfaces. We also present a theoretical model based on two bi-stable states and two energy scales, showing encouraging agreements with experiments. We envision that a future development of theoretical studies incorporating ideas of Stochastic Resonance will be of particular interest. We believe that in the future, the analysis of dynamics of multitude of coupled nanostructures in complex gas mixtures may play an important role in non-adsorption based, physical detection of chemicals.

3.11 Materials and Methods

3.11.1 Surface Nanostructuring.

In our experiment, we use a standard AT cut QC from International Crystal Manufacturing (ICM) Co. Inc. (USA) as a test platform. First step involves sputter coating a 10nm thick ZnO seed layer only on one electrode surface using a mask, the coated area contributing to the effective response change in our case. We used hydrothermal(80) process for growing the ZnO nanorods on the sputter coated surface. The involved chemicals are: Zinc nitrate hexahydrate ($\text{Zn}(\text{NO}_3)_2 \cdot 6\text{H}_2\text{O}$, 98%) and Ammonium hydroxide (28 wt% NH_3 in water), purchased from Sigma–Aldrich. The crystals are put in $\text{Zn}(\text{NO}_3)_2 \cdot 6\text{H}_2\text{O}$ solution with its pH being modified to 10.6 by adding 2.3 ml of the ammonia solution. The solution is put in an oven at 90°C for 3hrs and the pH of the solution is constantly maintained by a sealed environment reaction vessel. The 3hr growth gave us our desired dimensions. After

hydrothermal growth, the crystals were rinsed with de-ionized water and ethanol, and then dried in a vacuum oven. Estimations verified through Field Emission Scanning Electron microscopy (Fig 3.S1) show a mean nanorod length L of $611\text{nm} \pm 10\%$ with mean diameters d of the order of $43\text{nm} \pm 10\%$. The dimensions and growth kinetics strongly depends on the seed layer thickness and average roughness. Nanorod density measured at different locations is 18 ± 2 nanorods per μm^2 giving a typical area coverage of about 12% per $1\mu\text{m}^2$ of electrode surface area. Such a coverage density is essential to effect limit sensitivity \sim parts per billion as has been discussed in supplementary information.

3.11.2 Flow system for analyte introduction.

A schematic of experimental procedure as shown (Fig 3.6) allows varying of ambient media properties in the flow cell by the introduction of various gas molecules using carrier gas (dry-air) bubbling, with flow maintained at 50 sccm - standard cubic centimeters per minute for all cases. The variance in the media properties is achieved through 0.1 wt% analyte-water mixtures or by controlled temperature variations in the same dry air environment. The relative humidity for all experiments with different analytes and temperature is maintained at 5%. For same percentage by weight analyte solutions in water and the fixed flow rate, the relative change in kinematic viscosity is unique to an analyte depending upon the relative vapor pressures. For calculations on mixture viscosities in experiments refer section in supplementary information.

3.11.3 Impedance measurement.

The nanostructure modified QC is driven into shear mode vibration and the dynamic dissipation factor as in our analysis (Eq. 1) is measured as an electrical impedance

parameter $\gamma = \frac{\phi_s}{X_s} = \frac{\phi_s}{1/\omega c_s} = \omega \phi_s c_s$, where ω is the drive frequency, ϕ_s is the

equivalent series resistance and c_s is the equivalent series capacitance. At resonance (Eq.

1) $D = \frac{\gamma_{\max}}{f_{QC}} = 2\pi \phi_s c_s$ gives the measure of dissipated energy. The measurements are

done employing Agilent 4294A Impedance Analyzer with nominal impedance accuracy of $\pm 0.08\%$ at 100Hz. Drive signal from analyzer's internal oscillator is swept over a moderately low bandwidth (5 kHz) with the sweep time of 30 sec for viscosity dependence experiments. Variations of impedance parameters monitored as a function of the drive frequencies, reflect the equivalent impedance based mechanical dissipation in the system.

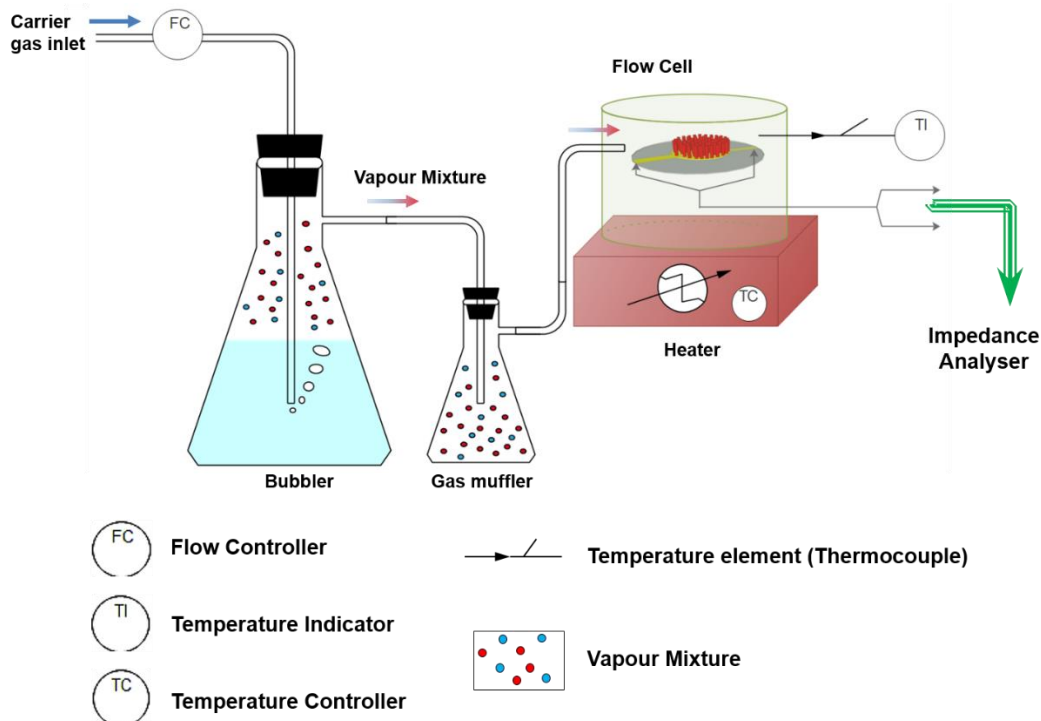


Figure 3.6| Experimental Schematic

REFERENCES

1. *Surface and Interface Science: Vol 5 & 6.* (Wiley-VCH Verlag & Co., 2015).
2. Adamson, A. W. & Gast, A. P. *Physical Chemistry of Surfaces.* (John Wiley and Sons, 1997).
3. Min, Y., Akbulut, M., Kristiansen, K., Golan, Y. & Israelachvili, J. The role of interparticle and external forces in nanoparticle assembly. *Nat. Mater.* **7**, 527–538 (2008).
4. Pelton, M. *et al.* Damping of Acoustic Vibrations in Gold Nanoparticles. *Nat. Nanotechnol.* **4**, 492–495 (2009).
5. Tam, C. K. W. The drag on a cloud of spherical particles in low Reynolds number flow. *J. Fluid Mech.* **38**, 537 (1969).
6. Gieseler, J., Novotny, L. & Quidant, R. Thermal nonlinearities in a nanomechanical oscillator. *Nat. Phys.* **9**, 806–810 (2013).
7. Li, M., Tang, H. X. & Roukes, M. L. Ultra-sensitive NEMS-based cantilevers for sensing, scanned probe and very high-frequency applications. *Nat. Nanotechnol.* **2**, 114–20 (2007).
8. Oden, P. I., Chen, G. Y., Steele, R. A., Warmack, R. J. & Thundat, T. Viscous drag measurements utilizing microfabricated cantilevers. *Appl. Phys. Lett.* **68**, 3814–3816 (1996).
9. Rodahl, M. *et al.* Simultaneous frequency and dissipation factor QCM measurements of biomolecular adsorption and cell adhesion. *Faraday Discuss.* **107**, 229–246 (1997).
10. Rodahl, M., Höök, F., Krozer, A., Brzezinski, P. & Kasemo, B. Quartz crystal microbalance setup for frequency and Q-factor measurements in gaseous and liquid environments. *Rev. Sci. Instrum.* **66**, 3924 (1995).
11. Spletzer, M., Raman, A., Wu, A. Q., Xu, X. & Reifenberger, R. Ultrasensitive mass sensing using mode localization in coupled microcantilevers. *Appl. Phys. Lett.* **88**, 254102 (2006).
12. Widom, A. Krim, J. Q factors of quartz oscillator modes as a probe of submonolayer-film dynamics. *Phys. Rev. B* **34**, 1403 (1986).
13. Xu, Y., Lin, J.-T., Alphenaar, B. W. & Keynton, R. S. Viscous damping of microresonators for gas composition analysis. *Appl. Phys. Lett.* **88**, 143513 (2006).

14. Cleland, A. N. & Roukes, M. L. Noise processes in nanomechanical resonators. *J. Appl. Phys.* **92**, 2758–2769 (2002).
15. Sutherland, W. LII. The viscosity of gases and molecular force. *Philos. Mag. Ser. 5* **36**, 507–531 (1893).
16. Stokes, G. G. On the effect of the Internal friction of fluids on the motion of pendulums - Section III. *Trans. Cambridge Philos. Soc.* **IX**, 8 (1850).
17. Rayleigh, Lord. LXXXII. *On the motion of solid bodies through viscous liquid.* *Philos. Mag. Ser. 6* **21**, 697–711 (1911).
18. Bhiladvala, R. B. & Wang, Z. J. Effect of fluids on the Q factor and resonance frequency of oscillating micrometer and nanometer scale beams. *Phys. Rev. E* **69**, 036307 (2004).
19. Chen, Y., Zhang, C., Shi, M. & Peterson, G. P. Slip boundary for fluid flow at rough solid surfaces. *Appl. Phys. Lett.* **100**, 1–5 (2012).
20. Karabacak, D. M., Yakhot, V. & Ekinci, K. L. High-Frequency Nanofluidics: An Experimental Study Using Nanomechanical Resonators. *Phys. Rev. Lett.* **98**, 254505 (2007).
21. Kozlov, A. S., Baumgart, J., Risler, T., Versteegh, C. P. C. & Hudspeth, A. J. Forces between clustered stereocilia minimize friction in the ear on a subnanometre scale. *Nature* **474**, 376–9 (2011).
22. Martin, M. J. & Houston, B. H. Gas damping of carbon nanotube oscillators. *Appl. Phys. Lett.* **91**, 103116 (2007).
23. Ortiz-Young, D., Chiu, H.-C., Kim, S., Voïtchovsky, K. & Riedo, E. The interplay between apparent viscosity and wettability in nanoconfined water. *Nat. Commun.* **4**, 2482 (2013).
24. Sader, J. E. Frequency response of cantilever beams immersed in viscous fluids with applications to the atomic force microscope. *J. Appl. Phys.* **84**, 64 (1998).
25. Saviot, L., Netting, C. H. & Murray, D. B. Damping by bulk and shear viscosity of confined acoustic phonons for nanostructures in aqueous solution. *J. Phys. Chem. B* **111**, 7457–7461 (2007).
26. Jeffrey, D. J. & Onishi, Y. Calculation of the resistance and mobility functions for two unequal rigid spheres in low-Reynolds-number flow. *J. Fluid Mech.* **139**, 261 (1984).

27. Tamada, K. & Fujikawa, H. The steady two-dimensional flow of viscous fluid at low reynolds numbers passing through an infinite row of equal parallel circular cylinders. *Q. J. Mech. Appl. Math.* **10**, 425–432 (1957).
28. Thompson, P. A. & Troian, S. M. A general boundary condition for liquid flow at solid surfaces. *Nature* **389**, 360–362 (1997).
29. Tuck, E. O. Calculation of unsteady flows due to small motions of cylinders in a viscous fluid. *J. Eng. Math.* **3**, 29–44 (1969).
30. Van Eysden, C. A. & Sader, J. E. Frequency response of cantilever beams immersed in viscous fluids with applications to the atomic force microscope: Arbitrary mode order. *J. Appl. Phys.* **101**, (2007).
31. Voisin, C., Christofilos, D., Del Fatti, N. & Vallée, F. Environment effect on the acoustic vibration of metal nanoparticles. *Phys. B Condens. Matter* **316-317**, 89–94 (2002).
32. Verbridge, S. S., Ilic, R., Craighead, H. G. & Parpia, J. M. Size and frequency dependent gas damping of nanomechanical resonators. *Appl. Phys. Lett.* **93**, 20–23 (2008).
33. Yamamoto, K. & Sera, K. Flow of a rarefied gas past a circular cylinder. *Phys. Fluids* **28**, 1286 (1985).
34. Yum, K., Wang, Z., Suryavanshi, A. P. & Yu, M. F. Experimental measurement and model analysis of damping effect in nanoscale mechanical beam resonators in air. *J. Appl. Phys.* **96**, 3933–3938 (2004).
35. Yakhot, V. & Colosqui, C. Stokes' Second Problem in High Frequency Limit: Application to Nanomechanical resonators. *J. Fluid Mech.* **586**, 249–258 (2007).
36. Schlichting, H. & Gersten, K. *Boundary layer Theory*. (Springer-Verlag, 1999).
37. Ekinci, K. L., Karabacak, D. M. & Yakhot, V. Universality in oscillating flows. *Phys. Rev. Lett.* **101**, 1–4 (2008).
38. Joo, J., Lee, D., Yoo, M. & Jeon, S. ZnO nanorod-coated quartz crystals as self-cleaning thiol sensors for natural gas fuel cells. *Sensors Actuators B Chem.* **138**, 485–490 (2009).
39. Anderson, H., Jönsson, M., Vestling, L., Lindberg, U. & Aastrup, T. Quartz crystal microbalance sensor designI. Experimental study of sensor response and performance. *Sensors Actuators B Chem.* **123**, 27–34 (2007).

40. Gammaitonni, L., Hänggi, P., Jung, P. & Marchesoni, F. Stochastic resonance. *Rev. Mod. Phys.* **70**, 223–287 (1998).
41. Badzey, R. L. & Mohanty, P. Coherent signal amplification in a nanomechanical oscillator via stochastic resonance. *AIP Conf. Proc.* **850**, 1675–1676 (2006).
42. Benzi, R., Sutera, A. & Vulpiani, A. The mechanism of stochastic resonance. *J. Phys. A Math. Gen* **14**, 453–457 (1981).
43. Batchelor, G. *Introduction to Fluid Dynamics*. (Cambridge University Press, 1983).
44. Elfring, G. & Lauga, E. Hydrodynamic Phase Locking of Swimming Microorganisms. *Phys. Rev. Lett.* **103**, 088101 (2009).
45. Golestanian, R., Yeomans, J. M. & Uchida, N. Hydrodynamic synchronization at low Reynolds number. *Soft Matter* **7**, 3074 (2011).
46. Kuramoto, Y. Cooperative Dynamics of Oscillator Community. *Prog. Theor. Phys. Suppl.* **79**, 223–240 (1984).
47. Martin, M. J. & Houston, B. H. Gas damping of carbon nanotube oscillators. *Appl. Phys. Lett.* **91**, (2007).
48. Kramers, H. A. Brownian motion in a field of force and the diffusion model of chemical reactions. *Physica* **7**, 284–304 (1940).
49. Hänggi, P., Talkner, P. & Borkovec, M. Reaction rate theory: Fifty years after Kramers. *Reviews of Modern Physics* **62**, (1990).

Acknowledgements

This research has been funded by Canada Excellence Research Chair (CERC) for Oil-Sands Molecular Engineering at University of Alberta. V.P was also partially supported by the National Sciences and Engineering Research Council (NSERC) Discovery grant and University of Alberta Centennial Fund. We thank Dr. Charles Van Neste for discussions and technical assistance, Dr. Dongkyu Lee for discussions regarding fabrication of nanorods and Dr. Ravi Gaikwad for the SEM images.

Author Contributions

A.P synthesized, characterized, designed and performed all experiments. J.E.H wrote machine interface codes in LabVIEW and was involved in study design and data interpretation, K.P was involved in study design and data interpretation, A.P, V.P, and T.T were involved in study design, data interpretation and theoretical analysis, and wrote the manuscript. All authors discussed results and commented on the manuscript.

Additional information

Supplementary information accompanies this paper.

Correspondence and requests for materials should be addressed to A.P., V.P. or T.T.

Competing financial interests: The authors declare no competing financial interests.

Supplementary Materials

S1. FE-SEM of nanostructured surface

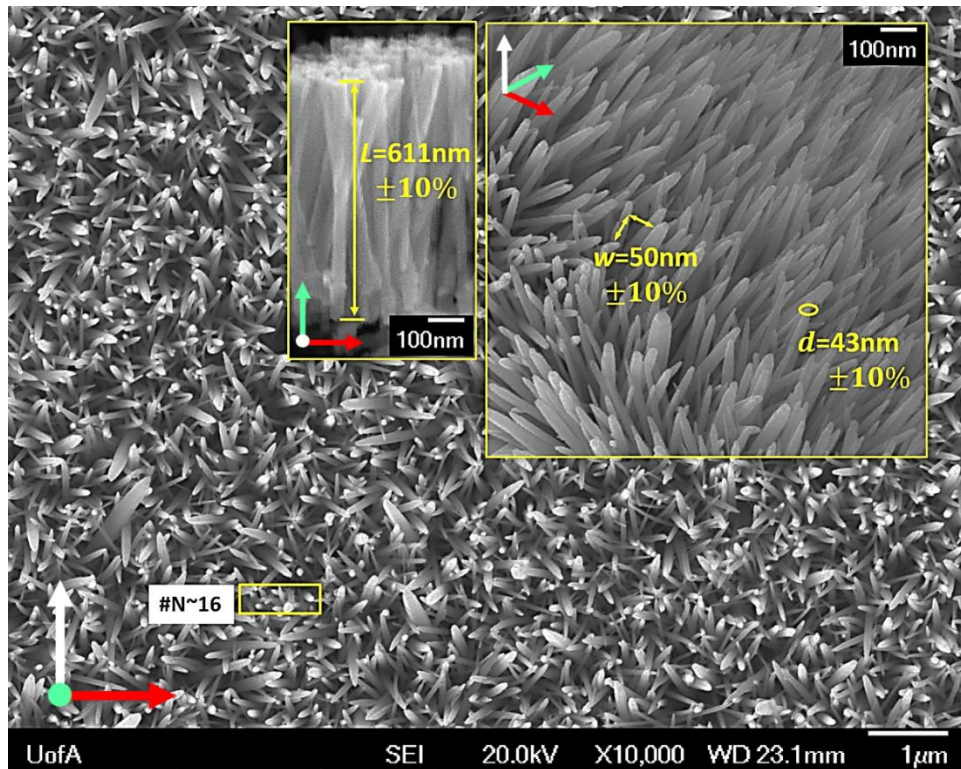


Figure 3.S1| FE-SEM image of nanostructured QC with embedded scale-bars.

S2. XRD analysis of nanostructured surface:

Fig 3.S2 presents the XRD analysis of ZnO nanorods grown on QC. All the diffraction peaks could be indexed to hexagonal phase of ZnO with polycrystalline grain orientations (JCPDS: 36-1451). No characteristic peaks from other impurities are detected, which indicates the purity of grown ZnO nanorods. The Au (200) peak corresponds to Au layer on QC. Since the ZnO nanorods are polycrystalline in nature, the piezoelectricity of ZnO nanorods is insignificant due to mutual cancellation of induced strain, therefore, less likely to impact the dynamic response of the QC resonator.

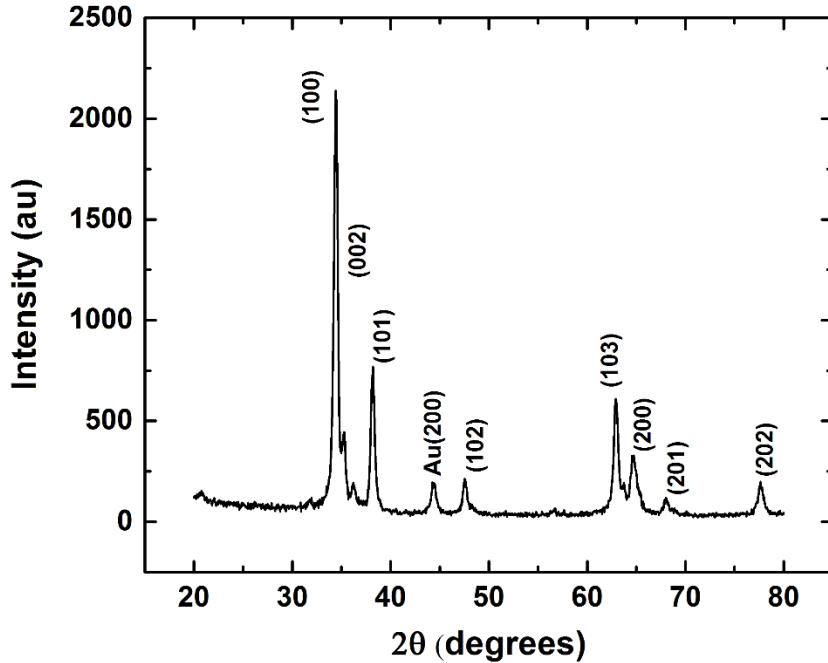


Figure 3.S2| XRD-analysis of nanostructured QC.

S3. Measured data accuracy analysis and estimation

Conventional models^{1–4} regard the QC as an electrical resonator obeying the equation of a driven damped simple harmonic mechanical oscillator

$$\ddot{x} + \gamma\dot{x} + \omega_0^2 x = A \cos(\omega t) \quad (\text{S1})$$

where we have denoted resonant frequency $\omega_0 = \sqrt{k/m_{eff}}$, k the stiffness, γ the effective dissipation coefficient and m_{eff} the effective mass with A and ω , the drive amplitude and frequency respectively. In the electrical analogue, x acquires the meaning of electric charge q , γ the relative resistance \wp per unit inductance ℓ and spring stiffness defined as $k = 1/c$ with c being the capacitance.

The simultaneous measurement of damping factor γ and resonance frequency f_{QC} allows the estimation of non-dimensional damping D as $D = \frac{\gamma_{\max}}{f_{QC}}$. We shall note here that the dissipation D is measured directly from the experiments as illustrated in Fig 3.1a in main

text, whereas Q -factor is estimated from the width of the Lorentzian peak of the amplitude response (Fig 3.S3 below). From general theory, one expects that, independent of the type of measurement, $Q=1/D$. This is substantiated by the plot of normalized values of Q vs $1/D$, with data points lying on a straight line with slope 1 (Fig 3.S4). The highest intercept value, and deviation of the slope from 1, obtained in the fits corresponds to the accuracy in the experiments $\sim 10^{-7}$. This attests to the high accuracy of our experiments.

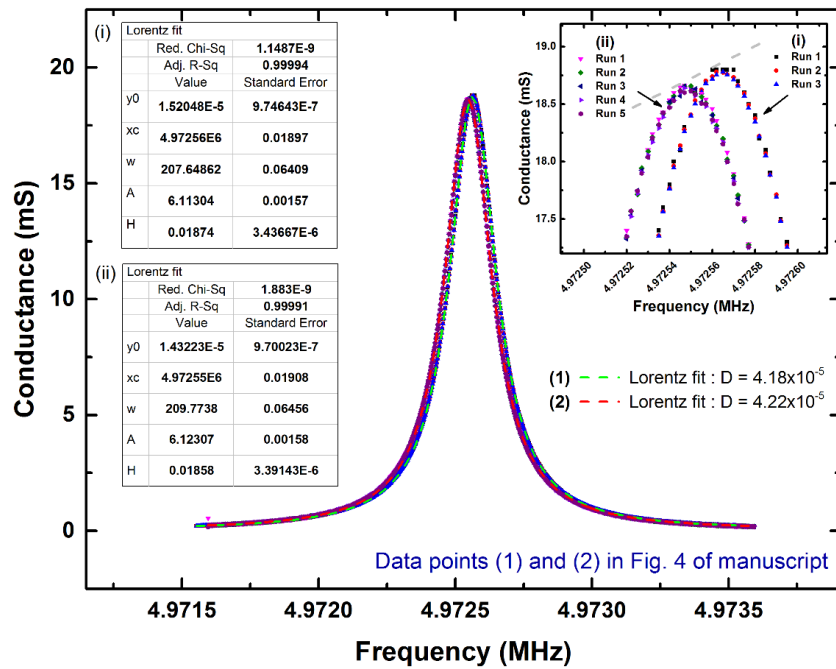


Figure 3.S3| Conductance vs Frequency response of the Nanostructured QC resonator for small changes in input drive energy.

Figure 3.S3 shows the Lorentzian fit for a particular measurement giving an estimate of the Q -factor. Data points for the Q factor and dissipation D from experiments have been analyzed in this way to estimate measurement accuracy, as represented in Fig 3.S3 above and for generating Fig 3.2a in the main article.

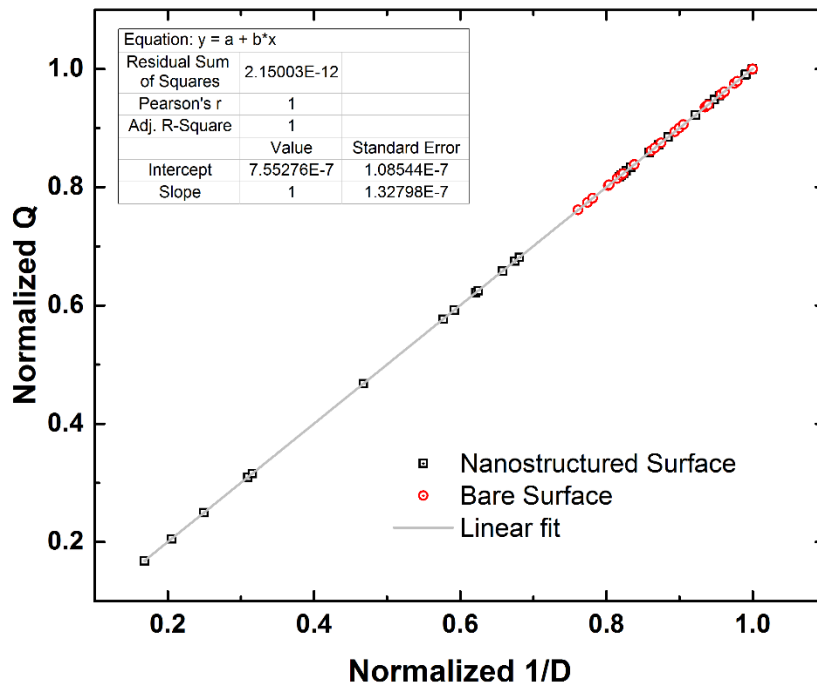


Figure 3.S4| Accuracy analysis of measured data.

S4. Dissipation responses for different gas media

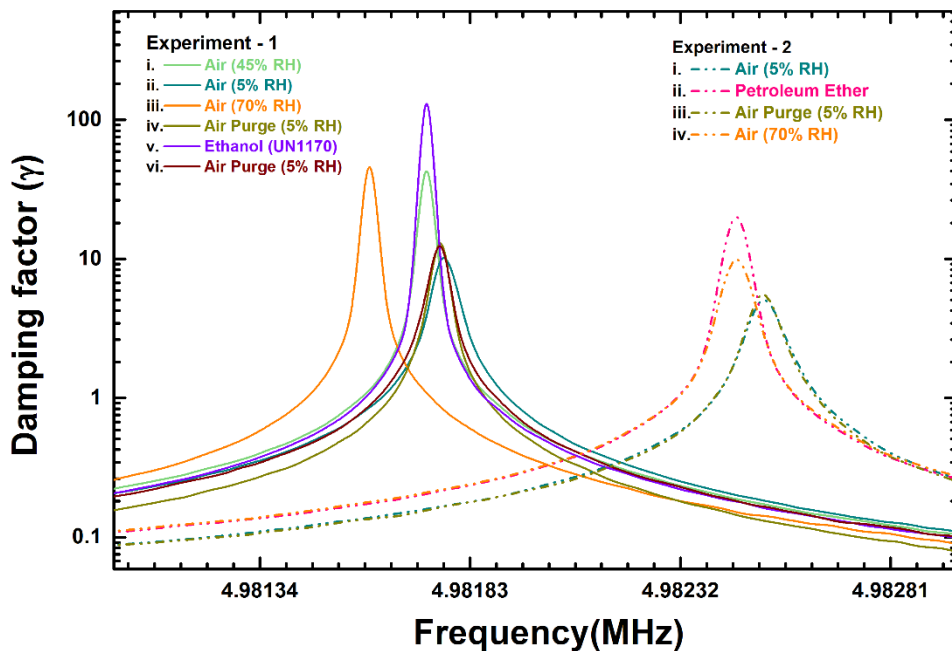


Figure 3.S5| A representative set of dissipation measurements for different gas media as done in sequence. Note that each graph is obtained as a concatenated fit of multiple readings similar to that presented in Fig 3.S3 above.

S5. Estimation of gas mixture viscosities

There are two possible ways to bring about a change in the viscosity ν as a function of the media properties. One way is to change the medium, for example by saturating the air with the vapor of a chemical up to a particular concentration level (ppm levels in our case), or, alternatively, replacing the air altogether by another gas. In the case of complete replacement, the effective variation in ν of the medium is relatively easier to compute following

$$\frac{\nu_{vapour}}{\nu_{dry-air}} = \left(\frac{\rho_{dry-air}}{\rho_{vapour}} \right) \cdot \left(\frac{\eta_{vapour}}{\eta_{dry-air}} \right) \quad (S2)$$

For mixtures however, it is more complex. The changes in viscosity ν_m in a mixture can be estimated from well-established theoretical and experimental work on the subject⁵⁻⁹. For a complex vapor mixture of air and volatile chemicals, air molecules of the fluid medium around the nanorods are replaced by molecules of the vapor, depending upon its partial vapor pressure and hence its number density and molar mass, which results in an effective change in kinematic viscosity $\Delta\nu$. The experimental viscosity mixture of up to 3 components ν_m may be calculated using⁶

$$\nu_m = \frac{\nu_1}{1 + \frac{1-x_1}{x_1} \left(\frac{1.385\nu_1}{\rho_1 D_{1m}} \right)} + \frac{\nu_2}{1 + \frac{1-x_2}{x_2} \left(\frac{1.385\nu_2}{\rho_2 D_{2m}} \right)} + \frac{\nu_3}{1 + \frac{1-x_3}{x_3} \left(\frac{1.385\nu_3}{\rho_3 D_{3m}} \right)}, \quad (S3)$$

with x_i being the mole fraction of component i determinable from the vapor pressure at normal temperature and pressure conditions, ρ_i being the vapor density of component i .

The diffusion coefficient D_{im} of component i into a mixture of 2 and 3 is defined as

$$D_{im} = \frac{1-x_i}{\frac{x_2}{D_{i2}} + \frac{x_3}{D_{i3}}}, \quad (S4)$$

as derived from Maxwell's equations for diffusion⁶. The diffusion coefficient of two component mixture is derivable from¹⁰

$$D_{12} = \frac{1.858 \times 10^{-3} T^{3/2} \sqrt{\frac{1}{M_1} + \frac{1}{M_2}}}{p \sigma_{12}^2 \Omega_c} \quad (S5)$$

where, p is the pressure in atm., M is the molar mass, T is the absolute temperature in Kelvin and $\sigma_{12} = 1/2(\sigma_1 + \sigma_2)$ is the average collision diameter. Also, Ω_c is the temperature dependent collision integral and is assumed to be 1 in our calculations considering non-interacting molecules. The values of σ_i are obtained from literature data⁸ or computed based on molar volume and density.

S6. Estimation of gas viscosity at different temperatures

The variation of kinematic viscosity as a function of temperature is expected and has been a subject of interest for many years. The kinematic viscosity of air for different temperatures as in our experiments are computed from¹¹ using 120 as the Sutherland's constant.

S7. Estimation of vibration amplitude at 5mV drive from impedance measurement

The key to understanding our results and theoretical formulation lies in the fact that in the parameter regime we are operating, which is indeed described in Reference³, the amplitude is proportional to the measured conductance G ($\text{Re}(Y)$, the *Admittance*). More precisely, from equation (2) in Reference³, page 4519 and using our notation, (see also Appendix section in Reference⁴) we conclude that $a \propto G$. Thus, the quantity $\Delta a/a$ is *exactly equal* to $\Delta G/G$. In our experiment (using their notation), G is measured with a ppm accuracy by the impedance analyzer as

$$G = \frac{2\phi}{V} \dot{u} = \frac{2\phi}{V} f u, \quad (\text{S6})$$

where V is the drive voltage across the crystal, f is the frequency at resonance, u is the lateral displacement (a in our case) at the crystal surface, \dot{u} is the lateral speed, and $\phi = \frac{A_q e_{26}}{d_q}$ is a crystal factor. The consideration of conductance G , the $\text{Re}(Y)$ is valid here since the entire analysis is done with respect to magnitudes at zero phase at resonance.

The crystal shear amplitude or lateral surface amplitude a in our representations of resonance amplitude can be estimated from impedance measurements as has been

discussed in literature^{3,4} using appropriate parameters. A quick calculation using values for our used crystal: $A_q = 4.084 \times 10^{-6} m^2$ (equivalent electrode surface area, with 12% per μm^2 (Fig 3.S1) coverage with nanorods), $e_{26} = 9.54 \times 10^{-2} Cm^{-2}$ ³ and $d_q = 333 \times 10^{-6} m$

$$2\phi = 2 \times \frac{4.084 \times 10^{-6} m^2 \times 9.54 \times 10^{-2} Cm^{-2}}{333 \times 10^{-6} m} = 0.002337 Cm^{-1}. \quad (S7)$$

From measured conductance $G \sim 18.5 \times 10^{-3} S$ (Fig 3.S3) at 5mV input drive, and at resonance $f = 4.972 MHz$,

$$u = a = \frac{1}{2} \times \frac{18.5 \times 5 \times 10^{-6}}{0.002337 \times 4.972 \times 10^6} = \frac{1}{2} \times 7.521 \times 10^{-9} m = 3.9 nm \sim 4 nm. \quad (S8)$$

The final factor of 1/2 is for considerations of the motion of the nanorod with respect to its center axis as relevant to our oscillating nanorod theoretical model. This is the estimate used in our theoretical model, providing the excellent match to the experimental data without the need of fitting parameters.

S8. Explanation of exponential amplitude dependence

Equation (2) in text can also explain the exponential nature of D with respect to the changes in the amplitude at resonance. If we assume the simplest possible linear dependence $a_{eff} = w + z\Delta a$, with Δa being deviation from the smallest resonance amplitude for the lowest input drive energy, equation (2) yields, for small changes of Δa

$$D = D_0 \exp \left[2K \left(1 - \frac{a}{w} z \right) \frac{\Delta a}{a} \right] = D_0 \exp \left[-\lambda \frac{\Delta a}{a} \right], \quad (S10)$$

where $\lambda = 2K \left(\frac{a}{w} z - 1 \right)$, z being a non-dimensional fitting parameter in experiments and D_0 being the dissipation for the smallest amplitude. Further development of the theory can be done, assuming more accurate expression for a_{eff} that is nonlinear in $\left(\frac{\Delta a}{a} \right)$, giving essentially the same results.

REFERENCES

1. Rodahl, M. *et al.* Simultaneous frequency and dissipation factor QCM measurements of biomolecular adsorption and cell adhesion. *Faraday Discuss.* **107**, 229–246 (1997).
2. Rodahl, M., Höök, F., Krozer, A., Brzezinski, P. & Kasemo, B. Quartz crystal microbalance setup for frequency and Q-factor measurements in gaseous and liquid environments. *Rev. Sci. Instrum.* **66**, 3924 (1995).
3. Johannsmann, D. Viscoelastic, mechanical, and dielectric measurements on complex samples with the quartz crystal microbalance. *Phys. Chem. Chem. Phys.* **10**, 4516–4534 (2008).
4. Kanazawa, K. K. Mechanical behaviour of films on the quartz microbalance. *Faraday Discuss.* **107**, 77–90 (1997).
5. Brokaw, R. S. *NASA Technical Note: Viscosity of gas Mixtures*. (1968).
6. Buddenberg, J. W. & Wilke, C. R. Calculation of Gas Mixture Viscosities. *Ind. Eng. Chem.* **41**, 1345–1347 (1949).
7. Davidson, T. A. *A Simple and Accurate Method for Calculating Viscosity of Gaseous Mixtures*. (1993).
8. Neufeld, P. D. Empirical Equations to Calculate gas mixture viscosities as a function of the Transport Collision Integrals Ω . *J. Chem. Phys.* **57**, 1100 (1972).
9. Reid, R. C., Poling, B. E. & Prausnitz, J. M. *The Properties of Gases and Liquids*. (McGraw-Hill, 1987).
10. Cussler, E. L. *Diffusion mass transfer in fluid systems*. (Cambridge University Press, 1997).
11. Sutherland, W. LII. The viscosity of gases and molecular force. *Philos. Mag. Ser. 5* **36**, 507–531 (1893).

Monograph 3: Published in Nanoletters

IV. Photothermal electrical resonance spectroscopy of physisorbed molecules on a nanowire resonator

Kovur Prashanthi*, Arindam Phani, and Thomas Thundat*

Department of Chemical and Materials Engineering,
University of Alberta, Edmonton, Alberta T6G 1H9, Canada

*Correspondence to: kovur@ualberta.ca and thundat@ualberta.ca

Nano Lett., 2015, 15 (8), pp 5658–5663

DOI: 10.1021/acs.nanolett.5b02557

Publication Date (Web): July 28, 2015

Copyright © 2015 American Chemical Society

Photothermal electrical resonance spectroscopy of physisorbed molecules on a nanowire resonator

Kovur Prashanthi*, Arindam Phani, and Thomas Thundat*

Department of Chemical and Materials Engineering, University of Alberta, Edmonton Canada.

*E-mail: kovur@ualberta.ca and thundat@ualberta.ca

ABSTRACT: Mid infrared (IR) photothermal spectroscopy of adsorbed molecules is an ideal technique for molecular recognition in miniature sensors with very small thermal mass. Here, we report on combining the photothermal spectroscopy with electrical resonance of a semiconductor nanowire for enhanced sensitivity, selectivity, and simplified readout. Wide band gap semiconductor Bismuth Ferrite (BiFeO_3 , BFO) nanowire, by virtue of its very low thermal mass and abundance of surface states in the band gap, facilitates thermally induced charge carrier trapping in the surface states, which affects its electrical resonance response. Electrical resonance response of the nanowire varies significantly depending on the photothermal spectrum of the adsorbed molecules. We demonstrate highly selective detection of mid IR photothermal spectral signatures of femtogram (fg) level molecules physisorbed on a nanowire by monitoring internal dissipation response at its electrical resonance.

KEY WORDS: *Nanowire sensors, nanowire resonators, photothermal spectroscopy, infrared sensor, molecular recognition, temperature-induced dissipation in nanowires*

4.1 Introduction

Nanosensor platforms such as nanowires¹⁻⁵ and nanocantilevers^{6,7} are topics of active research because of their potential as a miniature sensor platform with unprecedented sensitivity for applications ranging from health-care to national security. In general, molecular adsorption-induced changes in nanosensor physical properties serve as the sensor signal. Imparting chemical selectivity for small molecule detection to these sensor systems for reversible detection has been a challenge. Commonly used method of using immobilized chemoselective coatings often results in high false positives due to the generic nature of reversible chemical interactions. Hence, developing concepts that do not require immobilized chemical interfaces are very attractive. One such technique that exploits the very high thermal sensitivity of a bi-material microcantilever is photothermal cantilever deflection spectroscopy where IR excitation of adsorbed molecules and the subsequent non-radiative decay results in mechanical bending of the cantilever⁸⁻¹⁰. Nanomechanical deflection of the cantilever as a function of excitation wavelength shows the molecular vibrational characteristics of the adsorbates^{9,10}. This nanomechanical spectrum is complementary to that obtained with conventional IR spectroscopies such as FTIR. Thermo-mechanical detection of spectroscopic signals does not rely on Beer-Lambert principle, and, therefore, the relative intensities of the peaks are complementary to that of conventional IR spectra. However, the locations of the peaks (energy, $h\nu$) match very well with that of conventional spectroscopies, making nanomechanical spectroscopy highly selective and sensitive. Another advantage of the technique is that it works for physisorbed molecules, making sensor regeneration at room temperature easy^{9,10,8}.

The sensitivity of detection in the nanomechanical spectroscopic technique depends on the thermal mass of the sensor. Therefore, lowering the thermal mass of the detector could result in superior sensitivity in chemical sensing. Since a nanowire has a very small thermal mass, it can be an ideal sensor for photothermal spectroscopy. However, measuring nanomechanical bending of a nanowire caused by bi-material effect is very challenging using optical readout techniques. In general, monitoring nanomechanical motion of nanostructures such as nanoribbons and nanocantilevers, effected by small temperature changes, require complex and bulky equipment^{7,11-13}.

In this letter, we introduce a method of combining photothermal spectroscopy of physisorbed molecules on a semiconductor nanowire with its electrical resonance response for unprecedented selectivity and sensitivity. This technique, therefore, combines the selectivity of mid IR spectroscopy and sensitivity offered by electrical resonance phenomenon. Wide band gap materials such as bismuth ferrite (BiFeO_3 or BFO) have high density of surface states in their band gap, which are filled up to the Fermi level¹⁴⁻¹⁶. Due to the high surface-to-volume ratio of a BFO nanowire, its electrical properties are significantly influenced by the electrical nature of the surface states^{17,16}. Changing the temperature of the nanowire modulates the occupation of these surface states. Since the thermal mass of a nanowire is extremely small, absorption of very small quantities of heat can result in large changes in its temperature and in turn cause changes in the carrier population/depopulation of the surface states. Alternatively, small internal changes in heat from phonon excitations can effect similar repartitioning of surface states. This fact can be used to an advantage where by illuminating the nanowire with pulsed light, we show, can modulate the population-depopulation of these surface states depending on excitation and

relaxation of molecular vibrations of the adsorbed molecules. A slight variation in temperature from non-radiative relaxation induces changes in the surface state population further changing the electrical properties of the nanowire, which can be detected by monitoring the electrical resonance response of the nanowire.

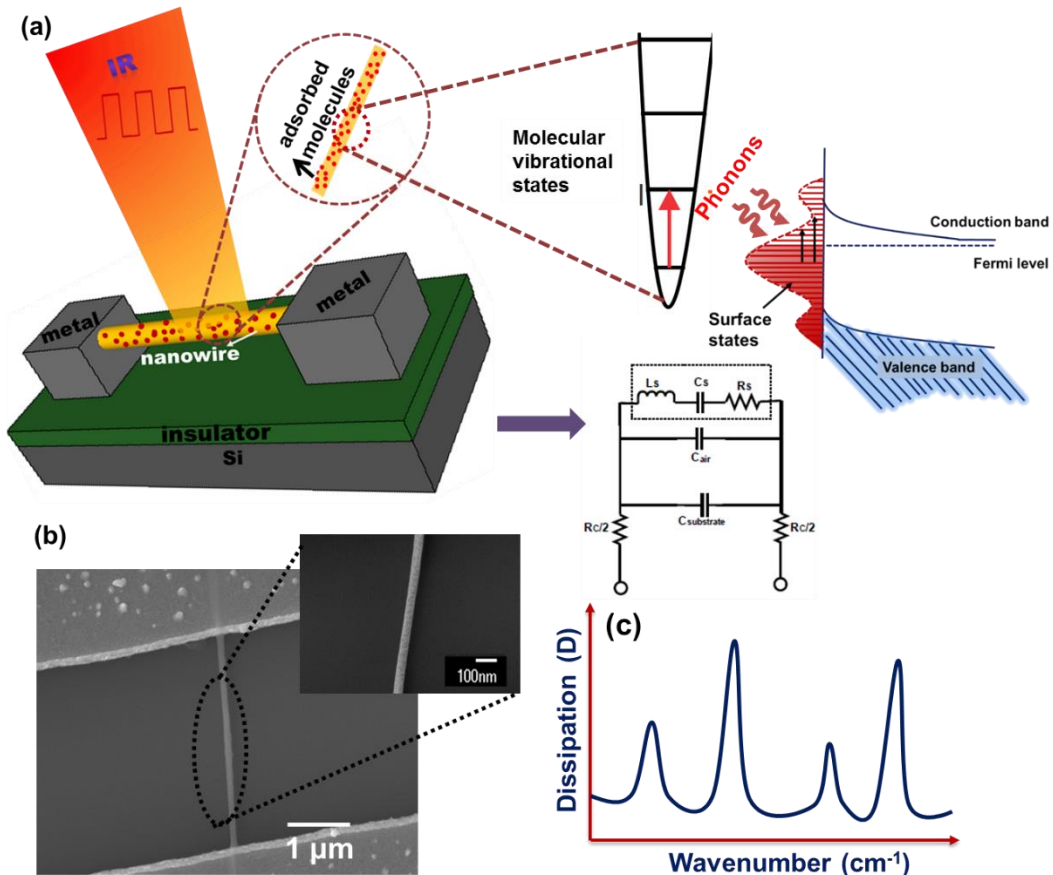


Figure 4.1| (a) Schematic representation nanowire resonator with equivalent electrical circuit model (please refer to section 1b, Supplementary Information) and the concept of coupling electrical resonances of the nanowire with optical excitation for high selectivity and high sensitivity chemical sensing, (b) SEM images of BFO nanowire, (c) dissipation (D) IR spectrum of adsorbed molecules. Electrical resonance frequency of the nanowire changes due to molecular adsorption, enabling detection of f_g levels of adsorbed mass. Resonant IR excitation of adsorbed molecules produce large changes in the dissipation of nanowire resonator due to population-depopulation of surface states by thermally generated carriers.

4.2 Experimental Technique

A schematic of our photothermal electrical resonance spectroscopy (PERS) technique is illustrated in Figure 4.1. A suspended BFO nanowire (3-20 μ m in length with a radius of 100 nm) electrically connected to metal (Pt/Ti) electrodes forms the electrical nanowire resonator (Figure 4.1a). A scanning electron microscopy (SEM) image of BFO nanowire is shown in Figure 4.1b. Any change in the electrical properties of the nanowire changes the electrical resonance frequency of the circuit. The electrical resonance frequency of a nanowire also changes due to molecular adsorption (capacitive loading) as well as from changes in temperature due to optical excitation of the adsorbed molecules (surface state population-depopulation). However, these changes in the electrical resonance frequency are too small for high sensitivity detection. We have realized that though the changes in resonance frequency are small, the resonance response of dissipation is extremely sensitive to changes in temperature changes. Only dissipation shows significant variations due to IR excitation of adsorbed molecules on the nanowire resonator. We record this dissipation signatures at electrical resonance of nanowire as a function of incident mid IR wavelengths, and they correspond to a dissipation spectrum (photothermal electrical resonance spectrum or PERS) unique to excited vibrational states of physisorbed molecules (Figure 4.1c).

4.3 Analysis of Results

A nanowire behaves analogous to an electrical series *RLC* resonant circuit (Figure 4.1a) with effective inductance *L* and a non-ideal capacitance *C*, showing resonance frequency

$$f_{res} = \frac{1}{2\pi\sqrt{LC}} \quad \text{in the MHz regime as measured (See Supplementary Section 1). The}$$

corresponding response timescale, $\tau = \frac{1}{f_{res}}$ (tens of ns) as obtained from the resonance analysis, essentially becomes the timescale of changes in electrical characteristics due to increased thermal energy of ΔQ arising from phonon-assisted transitions. Cantilever-based photothermal sensors, having higher thermal mass, are typically slow (ms) and they fail to track ΔT at a fast enough timescale (ns). Electrical resonance of nanowires makes that fast tracking (ns) possible and has the effect of enhancing the detection of heat changes arising from phonon-transitions internally. The very low thermal mass of the suspended nanowire effectively results in a high rate of change in temperature $\frac{\partial T}{\partial \tau} \uparrow$ as a function of time. In essence, the energy from any phonon relaxation gets dissipated internally and it is possible to monitor the dynamic dissipation at resonance as a ratio of energy dissipated to energy of excitation per cycle. This dimensionless quantity known as dissipation (in electrical terms it called D-factor) can be measured for different IR incident wavelengths. The dissipation (or D-factor) has been used earlier as a sensor signal for differential detection of volatile chemicals.^{18,19} A detailed discussion on the electrical definition of D-factor is presented in Supplementary Section S1.

Absorption of IR energy resonantly excites vibrational states of molecules physisorbed on the nanowire. Non-radiative decay of these excited states cause thermal changes through multi-phonon relaxation processes. Such phonon-induced changes in heat ΔQ depend on the thermal-mass mC_p (m being the mass and C_p the thermal heat capacity) and result in a measurable temperature change $\Delta T = \Delta Q/mC_p$, scaling inversely with the detector thermal mass. In all conventional forms of detection, measurable ΔT relies on the change

in electrical property arising from this ΔQ . Inherent limitations on timescale responses thus poses a fundamental limit to the detection sensitivity of ΔQ over thermal noise originating from any such phonon interaction process. At bulk scales, the overall response time is long and it demands a high ΔQ or multiple non-radiative relaxations integrated over time to produce a steady state electrical property change. However, in a very low thermal mass nanosystems like nanowire, thermal changes can be significant and at a very small timescale. An electrical property change in a semiconductor nanowire is predominantly brought about by the distribution of carriers in its electronic states. A change in ΔQ which can bring about a change in the carrier distribution by populating vacant higher electronic states with thermally induced carriers, would change its electrical property.

4.4 Surface State Density and significance in dissipation response

The importance of surface-states in modulating responses of bulk semiconductor materials through surface charges was addressed in the early 1970's by Lagowski and Gatos^{20,21}. Catalan's review reveals prospects on similar grounds in semiconductor BFO²². Phonon de-excitations are usually in the form of a cascading multi-phonon assisted relaxation process reflected as internal dissipation^{23–25} and is attributed to phonon-phonon interactions or scattering. Defects in bulk or on the surface enhances it significantly^{26–28} and they play a crucial role at the nanoscale as in our method. For a system with high surface state density, there is a higher probability of coupling phonon relaxation energy (ΔQ)_{phonon} in promoting a charge carrier to an allowable vacant surface states above the Fermi level; traditionally termed charge capture or carrier trapping^{26–28}, which we exploit to our advantage by monitoring through electrical resonance. In the electrical domain, such carrier

repartitioning into different allowable surface states reflect a dominant capacitive reactance (X_C) change, as revealed in our experiments. The electrical parameter definitions are given in Supplementary Section 1.

4.5 Significance of low thermal mass

Higher thermal mass sensors have slow response time ($\sim ms$) as compared to low thermal mass systems as illustrated in Figure 4.2a, and hence their usual steady state electrical property change, used as a measurement signal, fails to track ΔT at a fast enough timescale. The dependence of external excitation energy $\Delta Q = i^2 R_S / f_{res}$ (R_S being the equivalent series resistance) on f_{res} , gives the relative thermal sensitivity $\Delta T/T = \Delta Q/Q$ of the nanowire electrical resonance as a function of relative timescale response $\Delta\tau/\tau$ at electrical resonance, showing an enhanced exponential sensitivity (Figure 4.2b), where $\tau = 1/f_{res}$. Such an increased sensitivity at timescales of the order of tens of ns in energy space, as evident more in Figure 4.2c makes sensitive discrimination of ΔQ possible even at normal conditions. Since the thermal-mass of the nanowire resonator is negligible, ΔT can be significantly greater than the thermal noise. The measured normalized dissipation (D/D_0) as shown in Figure 4.2b (inset) & 2c shows the temperature-induced effective changes in internal losses at the same timescale. The nanowire thus serves as an extremely sensitive thermal sensor and an electrical resonator platform, enabling recognition of adsorbed molecules through monitored variations in its dynamic impedance parameters.

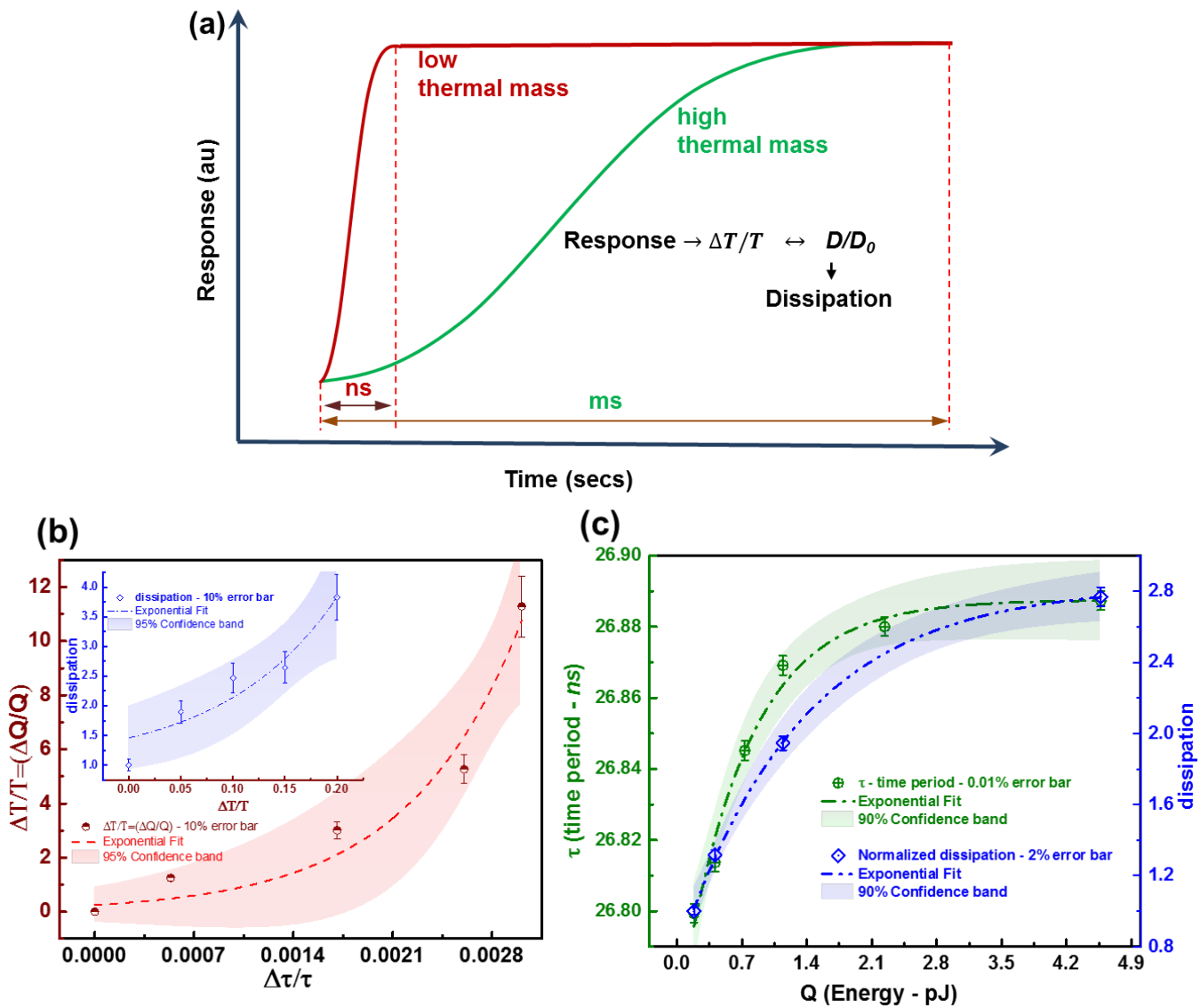


Figure 4.2| (a) Typical time response curve for low thermal mass and high thermal mass systems. (b) Thermal response sensitivity of nanowire resonator with low thermal mass analyzed at SRF as a function of external drive. Inset shows normalized changes in dissipation (D/D_0) as a function of relative changes above room temperature. (c) Time response (τ) variations as a function of heat energy (Q) floor corresponding to external drive; subsequent variations in normalized dissipation (D/D_0) of the nanowire resonator for the same energy fluctuations. Electronic state distribution in a material typically follows Boltzmann distribution and hence their variations as a function of energy all follow logarithmic trends, evident from thermal responses.

4.6 Demonstration of IR dissipation IR spectroscopy

To demonstrate the capabilities of the sensor platform, we have chosen commonly investigated explosive, cyclotrimethylene trinitramine (RDX) as model system. Since these explosive molecules bind to surfaces very easily, they remain on the nanowires for longer periods enabling repeated measurements. The changes in resonance frequency of a nanowire due to the adsorption of RDX are presented in Figure 4.3. As mentioned earlier, both resonance frequency and dissipation vary as a function of molecular adsorption due to mass loading (inset of Figure 4.3). A detailed analysis of experimental data on other set of nanowire resonators with similar trend has been presented in Supplementary Section S2. The higher surface area of a nanowire coupled with higher number of surface states promotes unprecedented mass resolution in detection. Adsorbed mass on the nanowire resonator from the resonance response shift and corresponding capacitance change is calculated as a function of charge donation or transfer from the adsorbed chemical species²⁹ of unknown mass and is estimated to be of the order of 10 fg . This estimated mass is also verified within the same order of magnitude (60 fg), assuming fractional two dimensional (2D) surface exposure of the nanowire to $0.4\mu\text{L}$ droplet (used in experiment). The factor of variation between the measured capacitance change and the surface area exposure estimation may be accounted for the non-uniform and different evaporation kinetics of solvent on the surface of the nanowire and the substrate (See Supplementary Section 3). It is possible that RDX adsorption on the nanowire cannot be in the form of a continuous layer, instead would be in the form of discrete islands on the nanowire surface and hence monolayer assumption would tend to overestimate the adsorbed mass. The technique thus

also opens up a novel way of estimating adsorbed mass from electrical property variation through dynamic dissipation study at resonance.

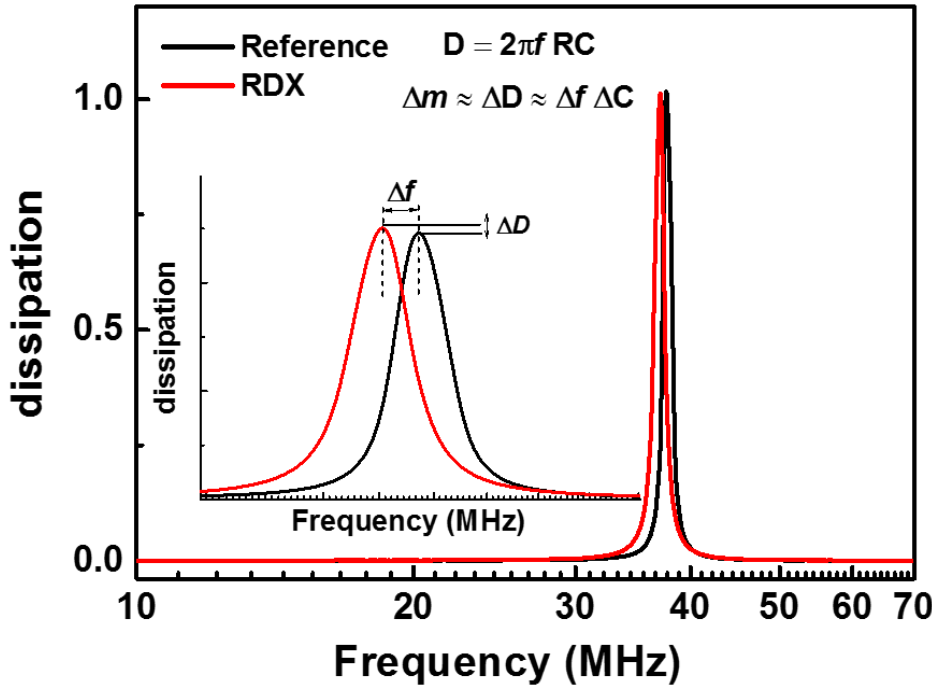


Figure 4.3| Electrical resonance of the nanowire resonator without and with adsorbed RDX molecules. The dissipation of the nanowire resonator also changes as a function of molecular adsorption. Inset of Figure 3 show higher magnification in the region of interest. Dissipation change proportional to adsorbed mass.

The variation in the amplitude of dissipation corresponding to IR absorption wavenumbers of RDX is shown in Figure 4.4a. The normalized dissipation, D/D_0 (corresponding to each IR wavenumber) as a function of relative timescale response, $\Delta\tau/\tau$ (Figure 4.4b) reveals an exponential nature of thermal response, where the change is from excited thermal phonons, which couple to the surface states of the nanowire through multi-phonon assisted relaxation processes. The higher dissipation as a function of IR is from phonon induced ΔT analogous to more effective internal dissipation as clear from Figure 4.2. In essence,

the thermally induced carrier repartitioning within the surface states change the way energy from external electrical drive gets dissipated and stored in the nanowire resonator per cycle of its oscillation at resonance. This resonance response variation, typical of the nanowire system employed, provides deeper insights on the thermal response characteristics (please refer to Figure 4.2), which is exploited here as a basis for our unique way of receptor free IR chemical discrimination. In electrical terms, the variations in the dissipation are from the changes in the effective capacitance of the nanowire. An increasing capacitance decreases the capacitive reactance, X_C (See Supplementary Section 4) and thus stores less energy per cycle. Effectively the dissipation increases showing higher dissipation. The variation in the capacitive reactance, affecting the nanowire response, reflects the variations in the charge state of surface energy levels of the semiconductor nanowire. It is believed that the observed increase in surface capacitance is a result of an increase in surface charge carriers (electrons or holes) in the unoccupied surface states of the BFO nanowire by multi-phonon process and has been reported previously for MOS thin films^{23,24}.

A systematic recording of the variations in dissipation as a function of incident IR wavelengths gives the spectrum of the adsorbed species, bringing selectivity. Experimentally observed spectrum of RDX molecules adsorbed on nanowire is presented in Figure 4.5a. Dissipation spectra as a function of IR wavelengths for the nanowire without the adsorbed analyte molecules becomes the reference or background signal in our analysis and is used for background corrections. Figure 4.5b shows comparison of PERS and FTIR spectra. The observed peaks in the dissipation signature match the FTIR spectra peak positions, showing selectivity and sensitivity of this approach. The line-widths of the

dissipation spectrum are much sharper and are primarily due to the low thermal mass and high electrical resonance frequency of the nanowire. Usually, the broadening of the peaks in conventional solid and liquid phase IR spectra is caused by the relaxation and dephasing of the vibrational excited states and indicates the complex fast dynamic interaction of the molecule with its environment. The high inherent nanowire resonance frequency along with the low thermal mass has the advantage of faster dynamic response as evident from discussions and results (Figure 4.2) and is reflected in the obtained spectra as unique sharp peaks with a significant low linewidth broadening compared to FTIR spectra (Figure 4.5b).

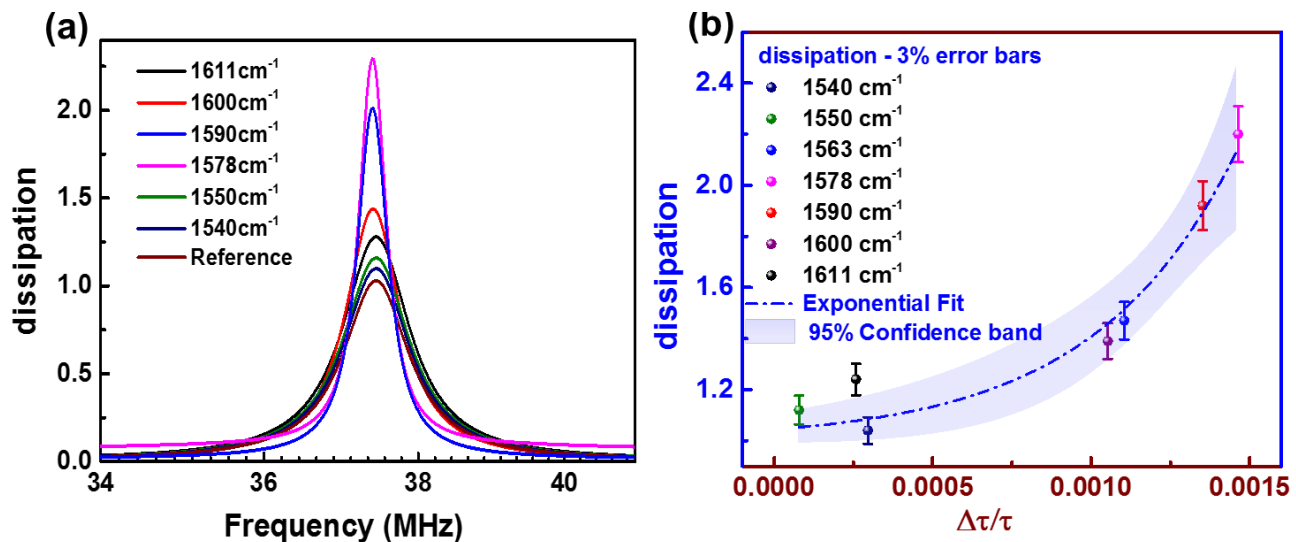


Figure 4.4| (a) Dynamic dissipation of the nanowire resonator with RDX molecules adsorbed on its surface and irradiated by IR. (b) Normalized dissipation (D/D_0) response of the nanowire resonator as a function of its response time. The selectivity in detection is through to the unique spectral absorption characteristics of the adsorbates in the mid-IR region. A variation in internal dissipation of the nanowire resonator is reflected by its dynamic dissipation in proportion to the small temperature changes due to IR absorption by adsorbates. The dynamic dissipation of the nanowire resonator with adsorbed molecules (without IR irradiation) served as the reference signal.

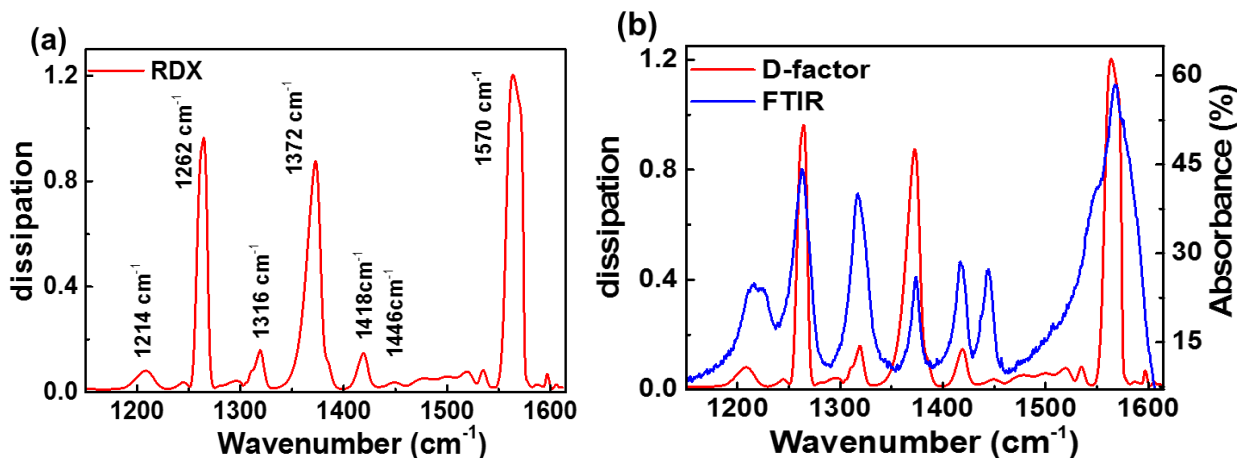


Figure 4.5| (a) PERS of RDX molecules adsorbed on nanowire (b) comparison PERS and FTIR spectroscopy of RDX molecules. The peaks on the measured PERS matches very well with the FTIR spectra of the analyte molecules. The observed high spectral resolution (linewidth) in PERS of the nanowire resonator is due to its extremely low thermal mass and fast response time *ns* significantly reducing thermal broadening compared to FTIR. FTIR absorbance \approx photon count; Dissipation from IR absorption is a complementary response in terms of phonon induced heat.

4.7 Conclusion

In conclusion, combining electrical resonance of a BFO nanowire with mid IR photothermal effect allows molecular recognition of *fg* levels of physisorbed molecules on a single BFO nanowire. IR excitation of the physisorbed molecules increases the temperature of the nanowire due to its low thermal mass. Because of the presence of high density of surface states on the nanowire, changes in temperature promotes carrier trapping which in turn changes the electrical resonance parameters of the nanowire. The BFO nanowire system described here utilizes the internal dissipation due to IR absorption by the adsorbed molecules and opens new opportunities for detecting minute amounts of surface adsorbed molecules on similar nanomechanical resonating platforms using dissipation as

the parameter. With optimization, this method provides exciting opportunities in developing a sensitive platform with superior selectivity performance.

4.8 Materials and methods

4.8.1 Preparation of BFO nanowire resonator:

BFO nanowire resonators with various electrode spacing are fabricated directly on pre-patterned substrates by electrospinning technique as reported in our previous work¹⁷. A gas injection system (GIS) available with motorized flexible *xyz*-drive was used for in situ platinum metal contact to these nanowires (RAITH150). The residues of explosive molecules of RDX was deposited on the nanowire resonator using the droplet evaporation method.

4.8.2 Chemicals:

The standard explosive RDX samples were purchased from AccuStandard, Inc. (New Haven, CT) and used without further purification. The standard concentration of each explosive is 1000 $\mu\text{g}/\text{mL}$ in MeOH:ACCN (1:1) as indicated by the manufacturer.

4.8.3 Dynamic impedance IR spectroscopy setup:

The IR radiation (pulsed at 200 kHz) from the quantum cascade laser (QCL) (Daylight Solutions UT-8) was focussed on the nanowire resonator. The laser peak power was in the range of 100–800 mW depending on the wavelength of operation. For UT-8, the peak power was 400 mW at 8.2 μm wavelength. The specified average power for this laser was up to 20 mW . The wavenumber of IR source was fixed at a specific value (range: 1630 cm^{-1} to 1150 cm^{-1}) and the corresponding dissipation parameters were measured. The impedance parameters of the nanowire resonator were measured using an Agilent 4294A

impedance analyzer having a frequency range of 40 Hz to 110 MHz with nominal impedance accuracy: +/-0.08 % at 100 Hz . The excellent high quality factor (Q) or D accuracy enables reliable analysis of low-loss components. The inherent high dynamic range of the equipment allows evaluation under actual operating conditions. A fixed ac test signal level $V_{rms} \sim 50 \text{ mV}$ was employed as input drive voltage for all the impedance measurements.

4.8.4 FTIR spectroscopy:

The explosive residues were characterized using a standard FTIR Thermo Scientific Nicolet Contihuum infrared microscope with a potassium bromide (KBr) beam splitter and a MCT-A (narrow band 650 cm^{-1} cut-off) detector microscope in reflection mode. The number of registered scans was 200 with resolution of 4 cm^{-1} .

ASSOCIATED CONTENT

Additional details on the electrical resonance of nanowire resonators, definitions of the electrical parameters, a detailed analysis of experimental data on other set of nanowire resonators and calculations of adsorbed mass on nanowire using electrical resonance. This material is available free of charge via the Internet at <http://pubs.acs.org>.

AUTHOR INFORMATION

Corresponding Author

*E-mail: kovur@ualberta.ca and thundat@ualberta.ca

Notes

The authors declare no competing financial interest.

ACKNOWLEDGEMENTS

This work was supported by Canada Excellence Research Chairs Program. The authors would like to acknowledge X. Liu in helping with IR setup and J.E.Hawk for developing automated data acquistion software which was used to collect the data.

REFERENCES

- (1) McAlpine, M. C.; Ahmad, H.; Wang, D.; Heath, J. R. *Nat. Mater.* **2007**, *6* (5), 379–384.
- (2) Penner, R. M. *Annu. Rev. Anal. Chem. (Palo Alto, Calif.)*. **2012**, *5*, 461–485.
- (3) Liu, H.; Kameoka, J.; Czaplewski, D. A.; Craighead, H. G. *Nano Lett.* **2004**, *4* (4), 671–675.
- (4) Patolsky, F.; Lieber, C. M. *Mater. Today* **2005**, 20–28.
- (5) Lieber, C. M. *MRS Bull.* **2012**, *36* (12), 1052–1063.
- (6) Yang, Y. T.; Callegari, C.; Feng, X. L.; Ekinici, K. L.; Roukes, M. L. *Nano Lett.* **2006**, *6* (4), 583–586.
- (7) Li, M.; Tang, H. X.; Roukes, M. L. *Nat. Nanotechnol.* **2007**, *2* (2), 114–120.
- (8) Krause, A. R.; Van Neste, C.; Senesac, L.; Thundat, T.; Finot, E. *J. Appl. Phys.* **2008**, *103* (9), 094906.
- (9) Kim, S.; Lee, D.; Liu, X.; Van Neste, C.; Jeon, S.; Thundat, T. *Sci. Rep.* **2013**, *3*, 1111.
- (10) Bagheri, M.; Chae, I.; Lee, D.; Kim, S.; Thundat, T. *Sensors Actuators, B Chem.* **2014**, *191*, 765–769.
- (11) Zhang, X. C.; Myers, E. B.; Sader, J. E.; Roukes, M. L. *Nano Lett.* **2013**, *13* (4), 1528–1534.
- (12) McCaig, H. C.; Myers, E.; Lewis, N. S.; Roukes, M. L. *Nano Lett.* **2014**, *14* (7), 3728–3732.
- (13) Hanay, M. S.; Kelber, S.; Naik, a K.; Chi, D.; Hentz, S.; Bullard, E. C.; Colinet, E.; Duraffourg, L.; Roukes, M. L. *Nat. Nanotechnol.* **2012**, *7* (9), 602–608.
- (14) Prashanthi, K.; Thakur, G.; Thundat, T. *Surf. Sci.* **2012**, *606* (19-20), L83–L86.
- (15) Prashanthi, K.; Thundat, T. *Scanning* **2013**, *36*, 224–230.
- (16) Prashanthi, K.; Dhandharia, P.; Miriyala, N.; Gaikwad, R.; Barlage, D.; Thundat, T. *Nano Energy* **2015**, *13*, 240–248.
- (17) Prashanthi, K.; Gaikwad, R.; Thundat, T. *Nanotechnology* **2013**, *24* (50), 505710.

- (18) Weimar, U.; Göpel, W. *Sensors Actuators B Chem.* **1998**, *52* (1-2), 143–161.
- (19) Amrani, M. E. H.; Persaud, K. C.; Payne, P. A. *Meas. Sci. Technol.* **1999**, *6* (10), 1500–1507.
- (20) Lagowski, J.; Balestra, C. L.; Gatos, H. C. *Surf. Sci.* **1972**, *29*, 213–229.
- (21) Gatos, H. C. *J. Vac. Sci. Technol.* **1973**, *10* (1), 130.
- (22) Catalan, G.; Scott, J. F. *Adv. Mater.* **2009**, *21* (24), 2463–2485.
- (23) Garetto, D.; Randriamihaja, Y. *IEEE Trans. Electron Devices* **2012**, *59* (3), 610–620.
- (24) Garetto, D.; Randriamihaja, Y. M.; Zaka, A.; Rideau, D.; Schmid, A.; Jaouen, H.; Leblebici, Y. *Solid. State. Electron.* **2012**, *71*, 74–79.
- (25) Garetto, D.; Randriamihaja, Y. *IEEE Trans. Electron Devices* **2012**, *59* (3), 621–630.
- (26) Henry, C. H.; Lang, D. V. *Phys. Rev. B* **1977**, *15*, 989–1016.
- (27) Burt, M. *J. Phys. C Solid State Phys.* **1979**, *4827*.
- (28) Ridley, B. *J. Phys. C Solid State Phys.* **1978**, *2323*.
- (29) Ahuja, B. L.; Jain, P.; Sahariya, J.; Heda, N. L.; Soni, P. *J. Phys. Chem. A* **2013**, *117* (27), 5685–5692.

Supplementary Information:

S1. Equivalent circuit model for the nanowire resonator

The device behaves as a typical electrical series RLC circuit as shown in Scheme 1a where its typical component values drive it to a resonance frequency of the order of tens of MHz.

R_s , C_s & L_s are representations of equivalent components as measurable through the impedance analyzer. The nanowire suspends freely in air at a height of 100 nm from the substrate surface and hence the air capacitance C_{air} , as seen by the two electrodes, does not show a dominant effect in determining the resonance frequency of the equivalent circuitry.

Also typical value of the substrate capacitance $C_{substrate}$ along with the contact resistances $R_c/2$ at the electrodes, exhibits a resonance frequency in the order of few KHz only, with no nanowire drawn between the electrodes. This ensures that our device response at the MHz frequency regime is that of the nanowire and not dominated by changes on the substrate or the changes in medium around it. The effective dominant dissipation change used in our study can be explained in terms of the ratio of the lost to stored energy through its frequency dependant effective complex impedance parameters. The response of the nanowire resonator recalls to mind the response of a non-ideal capacitive element following Scheme 1b where, it is well known that at SRF, the capacitive and inductive

reactance values become equal $\left(X_C = \frac{1}{\omega C_s} = X_L = \omega L_s \right)$ and the device becomes

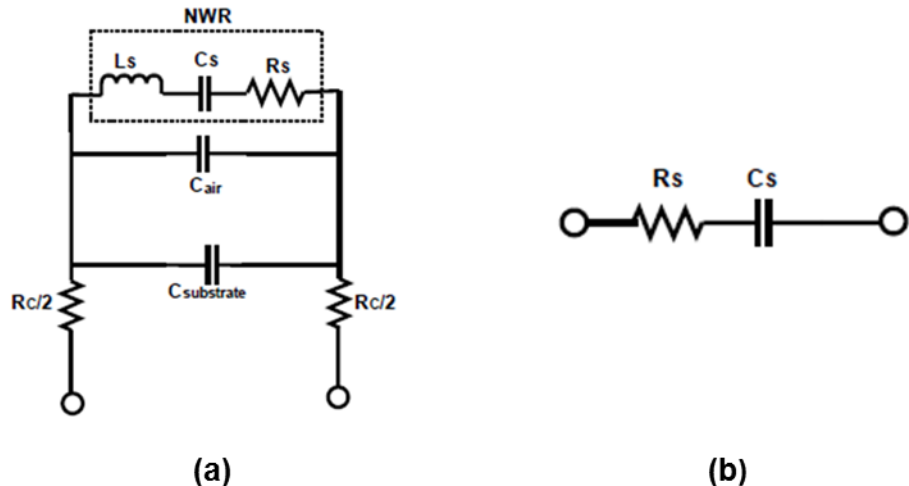
predominately resistive (R_s), ω being the self-resonating frequency (SRF). The inductance L_s variation, in one of the employed fabricated nanowire resonator, as a function of frequency (Figure 4.S1a) is negligible as is evident from its response curve,

conclusively implying that the reactance change of the resonator circuit tends to be dominantly capacitive. Following the same argument, the capacitance response of the nanowire resonator (Figure 4.S1b), indeed also exhibits maximum variation at SRF justifying the series equivalent model (Scheme 4.1b). Evidently, in such a non-ideal capacitive element at SRF, the storage of energy per cycle is through its capacitive reactance X_C while the dissipation is through its effective frequency dependent series resistance component R_s .

The observed electrical resonance response of the employed nanowire resonator, promptly recalls the characteristics of a non-ideal capacitive element with an effective inductance in series. At the self-resonating frequency (SRF), $\omega = 2\pi f_{res}$, the capacitive reactance (X_C) and inductive reactance (X_L) exactly compensate each other $\left(X_C = \frac{1}{\omega C_s} = X_L = \omega L_s \right)$ making the device predominately resistive or dissipative. In effect, the storage of energy in such a non-ideal capacitive element at SRF is through X_C , per alternating cycle, while the dissipation is through its effective frequency dependent series resistive component R_s . R_s and X_C are representations in terms of the impedance parameters obtained from the impedance analyzer used in our study. Essentially, the ratio of the energy lost to that stored per cycle becomes a critical and sensitive measure of the quality of resonance. This ratio, commonly referred as the dissipation or D-factor (dimensionless) is given by

$$D = \frac{R_s}{X_C} = \frac{R_s}{1/\omega C_s} = \omega R_s C_s$$

The variations of resonance characteristics of the nanowire resonator are sensitively reflected by D-factor responses when subjected to external parameter variations, in turn reflecting changes in its internal dissipation. It should be noted, that for high enough temperature changes, R_s change can be significant in metal nanowire resonator as well reflecting similar dissipation trend.



Scheme 4.1| Equivalent RLC circuit model for nanowire resonator (with typical RLC values; $R \sim \Omega$, $L \sim 10^{-7} H$ and $C \sim nF$)

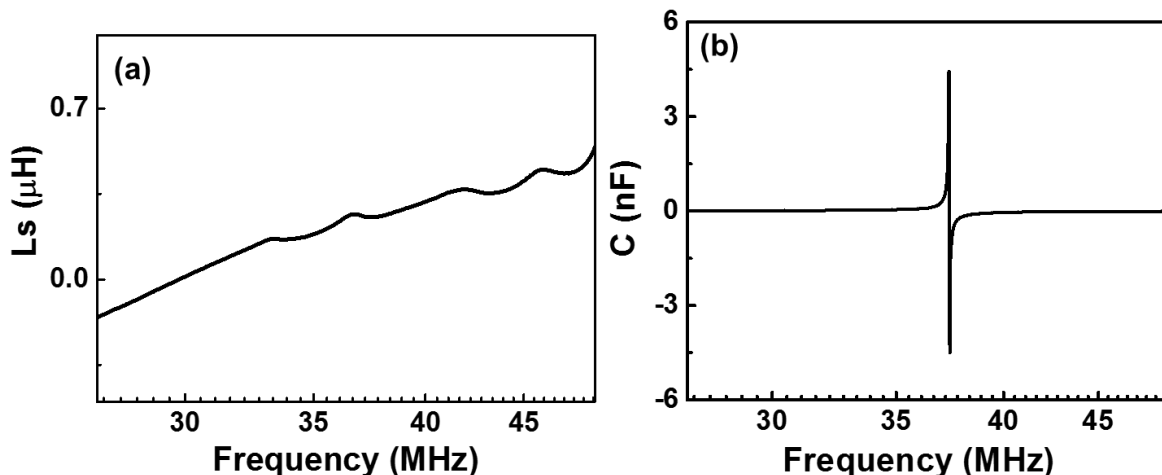


Figure 4.S1| Variation of electrical series inductance (a) and series capacitance (b) of the nanowire resonator as a function of frequency. Variation in inductance is insignificant at resonance whereas, a clear capacitance variation is seen at resonance.

S2. Electrical resonance of nanowire resonators

Electrical resonance measurements have been performed on nanowire resonators in a wide range of frequencies (ranging from 20-50 MHz). The resonances for different nanowire designs measured at room temperature are presented in Figure 4.S2a. The resonance frequencies of nanowire resonators exhibit a decreasing trend as a function of increasing nanowire length (electrode spacing) whereas the dissipation response is just the reverse. The variation of electrical resonance frequency and dissipation of nanowire resonators as a function of the nanowire length is presented in Figure 4.S2b. The observed variations can be attributed to the increasing capacitance (decreasing capacitive reactance (X_C)) as a function of decreasing electrode spacing which effectively is the length of the nanowire. In essence it is the predominant variation of electrical length at the nanoscale that governs the operational SRF.

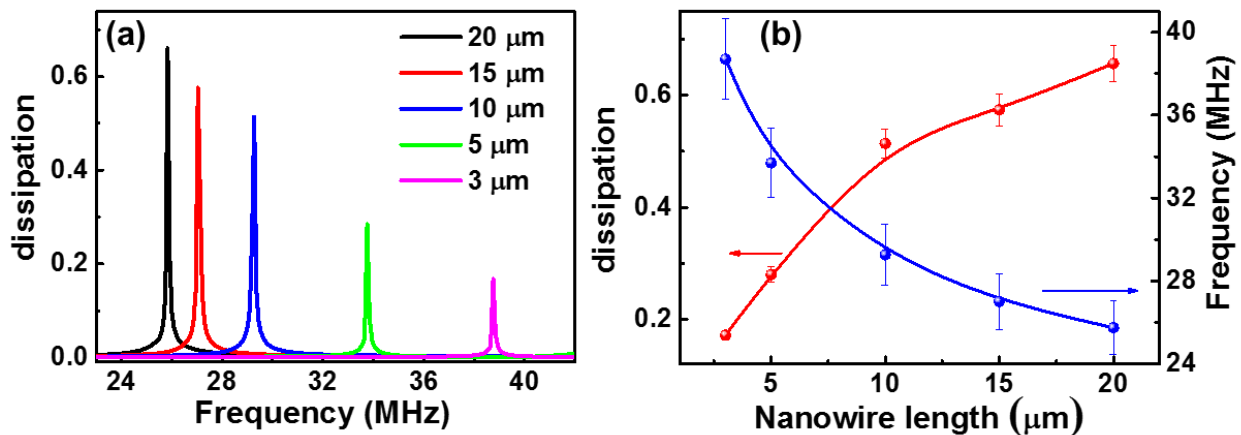


Figure 4.S2| (a) Electrical resonance response of nanowire resonators with various lengths of nanowires. (b) Dissipation and resonance frequency response of nanowire resonators obtained for various nanowire lengths.

S3. Dissipation response due to the adsorption of molecules

As discussed earlier, the effective dissipation (D) is the ratio of dissipated to stored energy per cycle

$$D = \frac{R_s}{X_c} = \frac{R_s}{T/C_s} = \frac{R_s C_s}{T} \quad (i)$$

$T \left[T = \frac{1}{\omega} \right]$, being the time period of a cycle.

$$\Rightarrow D_i = R_{S_i} C_{S_i} \omega_i \quad \Rightarrow \Delta C = C_{S_i} \left[\frac{D_2 \omega_1}{D_1 \omega_2} - 1 \right]$$

A quick analysis of the obtained data (Figure 4.S3) shows an increase in effective capacitance on adsorption of RDX molecules by a factor of 1.038 following equation (i). Increase in capacitance corresponds to an effective decrease in capacitive reactance, which leads to reduced storage of energy per cycle of response thus leading to a higher dissipation at its SRF as also clear from equation (i) above. The shift in SRF on adsorption may be attributed to the effective complex variation in resonator elements (dominant real part variation of complex permittivity), This observed response agrees to an earlier report where it was envisaged that the dissipation variations can be a useful indicator of the change in dipole-dipole interactions caused by the adsorption of a volatile chemical onto the polymer film employed in the study^{S1}. They related the higher dissipation at the device's SRF to the maximum efficient transfer of energy at the natural resonance frequency of molecules binding to the polymer. Such efficient energy transfer was conclusively associated to lower energy storage at SRF in their developed sensor system.

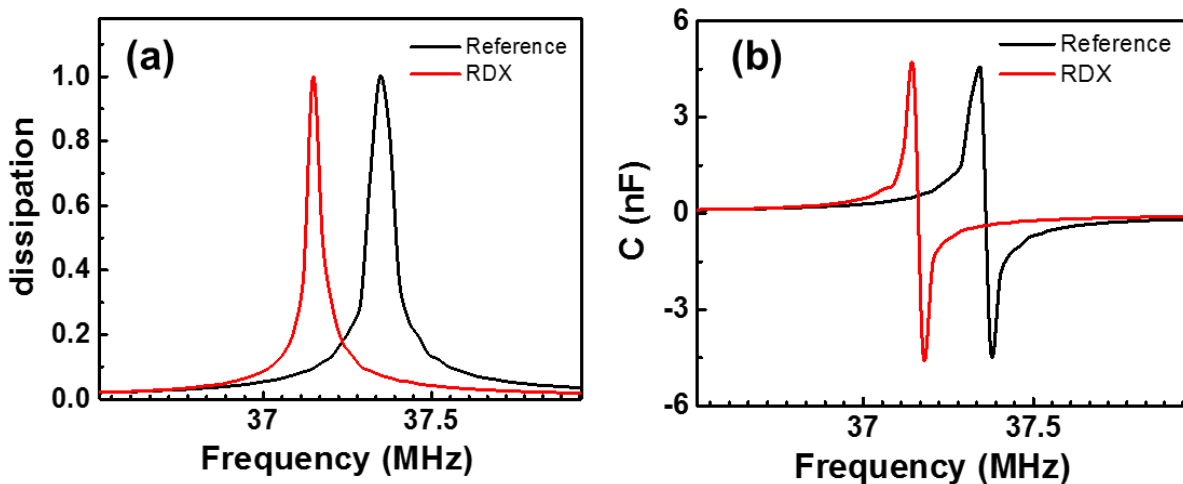


Figure 4.S3| Variation in dissipation (a) & capacitance (b) obtained for the nanowire resonator without and with RDX molecules. The order of shift is in KHz to even minute quantities of adsorbates of the order of fg.

S3.1 Adsorbed RDX mass calculation

a) From electrical resonance of the nanowire resonator

From the dynamic impedance parameter variations using equation (i),

$$\Delta C = 0.038 \times 4.48 nF$$

$$\Delta Q = \Delta C \times V = 8.512 \times 10^{-12} C$$

Now charge of an electron is $e^- = 1.602 \times 10^{-19} C$

$$\text{Therefore, Number of electrons } N_e = \frac{\Delta Q}{e^-} = 5.3134 \times 10^7$$

Now charge contribution per atom from individual sites of H₁ H₂ and N₂ in RDX = 0.84 e⁻.

There are 3 such sites in a RDX molecule^{S2}.

Hence the number of atoms taking part in charge change

$$N_{atoms,RDX} = \frac{N_e}{3 \times 0.84} = 2.1085 \times 10^7$$

Therefore, weight of RDX can be calculated as

$$\begin{aligned}
 w_{RDX} &= \frac{N_{atoms,RDX}}{AvagNo.} \times MW_{RDX} \\
 &= \frac{1.23 \times 10^9}{6.023 \times 10^{23}} \text{ moles} \times 222.12 \text{ gm/mole} \\
 &= 7.78 \times 10^{-15} \text{ gm} \cong 10 \text{ fg}
 \end{aligned}$$

b) From surface coverage

Typically, in monolayer coverage, it is considered that the total number of atoms in 1 cm² is about 10¹⁵ atoms/cm². However, for adsorbed mass calculations, authors consider that only fraction of RDX droplet is exposed to effectively half the nanowire surface. Therefore, the fraction of half the surface area of nanowire to the total area covered by 0.4 μl droplet on the substrate surface (as measured from the droplet stain) multiplied with concentration of RDX molecules in the solution used gives the estimated mass of adsorbed molecules.

Diameter of nanowire = 100 nm, Length of nanowire = 3 μm

Concentration of RDX molecules: 1000 μg/mL

Volume of droplet (RDX) = 0.4 μL

Hence effective mass of analyte in 0.4 μL = 0.4 μL × 1 μg / μL = 0.4 μg

Droplet diameter on surface = 2 mm (*measured*)

$$\text{Area of droplet on substrate: } \frac{\pi d^2}{4} = \frac{\pi \times (2 \times 10^{-3})^2}{4} = 3.14 \times 10^{-6} \text{ m}^2$$

$$\text{Area of nanowire: } \pi d_{NW} l = \pi \times 100 \times 10^{-9} \times 3 \times 10^{-6} \text{ m}^2$$

Assuming only top surface of nanowire is covered with droplet, area exposed

$$\frac{\pi d_{NW} l}{2} = \frac{\pi \times 100 \times 10^{-9} \times 3 \times 10^{-6}}{2} = 4.712 \times 10^{-13} \text{ m}^2$$

$$\text{Hence the estimated adsorbed mass is } \frac{4.712 \times 10^{-13}}{3.14 \times 10^{-6}} \times 0.4 \times 10^{-6} = 60 \text{ fg}$$

S4. The variation in dissipation due to IR absorption by molecules

The overall dissipation rise as a function of IR wavelengths (Figure 4.S4a), on absorption by the adsorbed analyte, predominantly becomes a function of the effective series capacitance change (higher capacitance and lower capacitive reactance – dominant imaginary part variation of complex permittivity reflecting more loss) (Figure 4.S4b). The capacitance variation is due to excited phonon relaxation induced carrier separation amplified by the higher density of surface states.

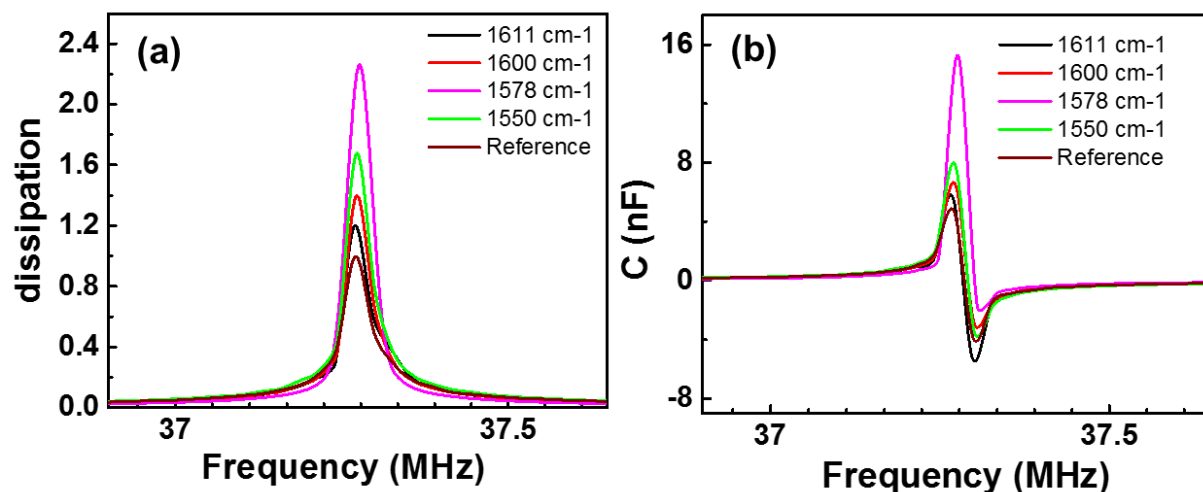


Figure 4.S4| Variation in dissipation (a), series capacitance (b) obtained for the nanowire resonator with RDX irradiated at different IR wavelengths.

References

- S1. Amrani, M. E. H., Persaud, K. C. & Payne, P. A. High-frequency measurements of conducting polymers: development of a new technique for sensing volatile chemicals. *Meas. Sci. Technol.* **6**, 1500–1507 (1999).
- S2. Ahuja, B. L., Jain, P., Sahariya, J., Heda, N. L., & Soni, P. Electronic properties of RDX and HMX: Compton scattering experiment and first-principles calculation. *J. Phys. Chem. A* **117** (27), 5685–5692 (2013).

V. Conclusions and Future prospects of the work

5.1 Conclusions

In conclusion, we draw attention to the fact that dissipation is crucial to resonance in light of the foregoing sections. Essentially, dissipation is present in all motion in general, originating from a time/phase lag between displacement and the cause of the displacement, i.e., an external action. In an electrical system, displacement takes the form of charge distribution while the external action is a voltage or potential. In either case, resonance is the particular condition of motion, where dissipation goes to a maximum under the influence of time dependent external forces and is thus inherently a variational problem concerning the system's dynamics. This stems from the path dependence of non-conservative dissipative forces. Resonance in essence, maximizes dissipation by the judicious selection of paths that minimizes the net time lag, each path corresponding to a certain time/phase lag between the displacement and the external action. The key to understanding the maximization process is that the dissipative forces originate from fluctuations or random interactions processes with a zero mean and delta-correlated in time. The zero mean of random Gaussian processes means that the information generated from such a random process is non-local in time domain. However, they add up in the frequency space maximizing the resonance width usually denoted by Γ . In most experiments, a measure of dissipation or the dissipation rate Γ is obtained as an inverse of time required for the oscillations to die down to $1/e$ times the maximum amplitude. Alternatively, in the frequency space response, it is obtained as the width of the resonance peak in units of frequency bandwidth Δf or t^{-1} .

All the discussions in the foregoing sections can be put to perspective, by invoking Kramer's rate law with relevance to Gibb's measure, in the most generalized way

$$\Gamma_r = \nu \exp\left(-\frac{\Delta\Psi}{\zeta}\right),$$

where, Γ_r describes the escape rate of an oscillating system from a metastable potential minima in units of t^{-1} or Δf , over a local barrier height $\Delta\Psi$, the pre-factor ν having the units of t^{-1} . Dynamics at the metastable minima represents the resonance condition (eigenstate) having different time rate of escape depending on the coordinate r of the minima with respect to the energy well minima 0 as shown below.

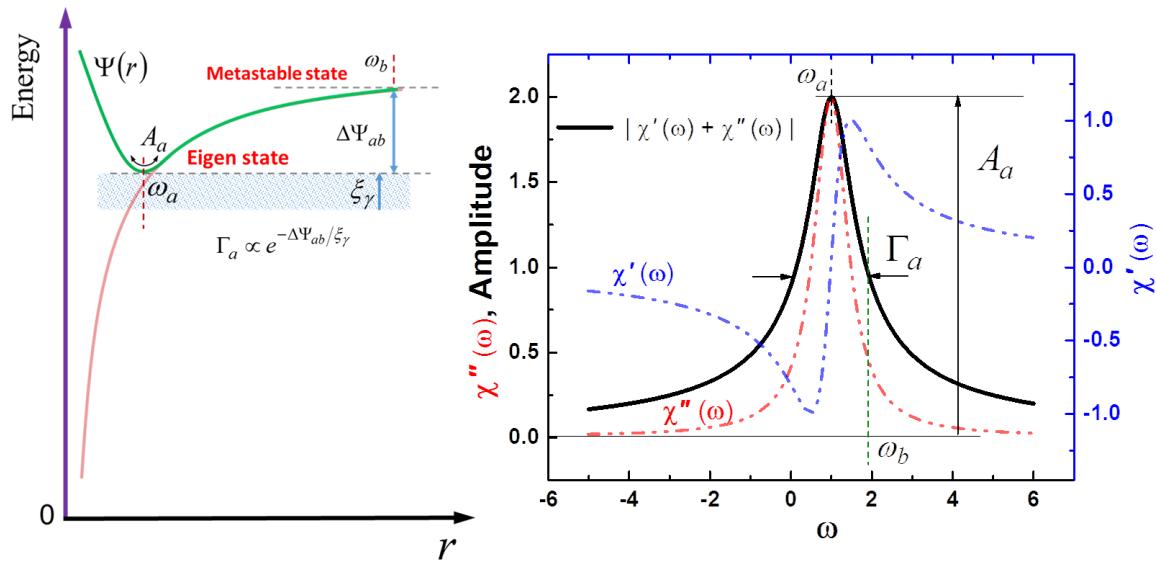


Fig 5.1| Eigenstate response at a shallow potential of an energy well.

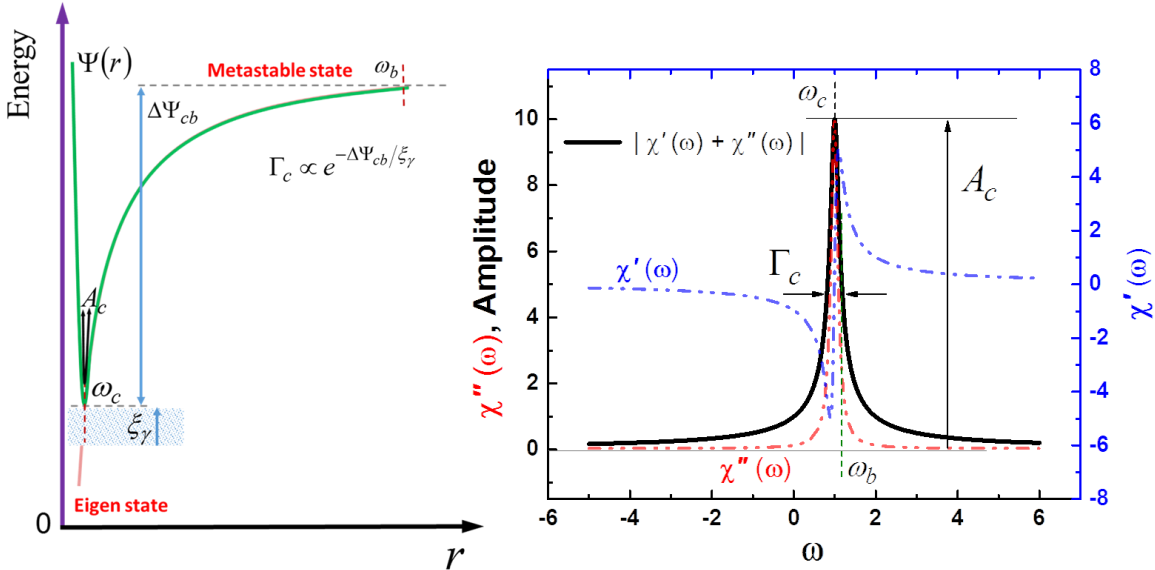


Fig 5.2| Eigenstate response at a deep potential of an energy well.

Apart from the external driving forces $F(t)$ and the harmonic forces $-\frac{d\Psi(r)}{dr}$ inside the potential well that drives the system to resonance, dissipative forces in the form of a linear damping force $-M\gamma\dot{r}$ and a fluctuation force $R(t)$ from random interactions with the media adds to the dynamical conditions. These forces gets introduced to Newton's equation of motion in the form of a Langevin equation,

$$\ddot{r} = v; \quad \ddot{v} = \dot{\nu} = -\frac{1}{M} \frac{d\Psi(r)}{dr} - \gamma\dot{r} + \frac{1}{M} F(t) + \frac{1}{M} R(t),$$

where the fluctuation force $R(t)$ would typically have a Gaussian probability distribution with zero mean - $\langle \xi_\gamma(t) \rangle = 0$. In the most generalized sense, the energy equivalence of the fluctuation forces on the system results in the energy barrier $\Delta\Psi$. The energy scale of the damping forces dependent on the media viscosity γ gives an inherent noise floor ξ_γ (in equation above) from the viscous interactions at every eigenstate.

The amplitude of resonance A_r is a function of the depth of the quadratic metastable potential minima Ψ_r , dependent on the curvature of the energy well at r . As represented in the figures above, at the transition state, the angular frequency of vibrations changes to ω_b with a much smaller amplitude. Here $\omega_{a,c}^2 = \frac{1}{M} \frac{d^2}{dr^2} \Psi(r_{a,c})$ is the squared angular frequency at the minima a and c , and $\omega_b^2 = \frac{1}{M} \left| \frac{d^2}{dr^2} \Psi(r_b) \right|$ denotes the squared angular frequency at the transition state, both dependent on the functional form of the potential energy function $\Psi(r)$, with M being the mass. The frequency or eigenvalue thus runs on the curvature of the potential function, with $\Psi(r_{a,c})$ in general representing a metastable energy level where a classical resonator undergoes resonant vibrations under the influence of the external action, when tuned to the Eigen state frequency $\omega_{a,c}$. Clearly, $\omega_c > \omega_a > \omega_b$. $\Delta\Psi$ in essence, represents the energy scale that originates from the random fluctuation interactions of the system with the media around, more profound at the nanoscale as revealed by results in *sections III and IV*. Escape rate from resonance, in essence, denotes the damping rate or the frequency bandwidth Γ with center at ω_r , outside which the system is driven to an off-resonance state or to a transition state of vibrations. Clearly, a shallower depth (small curvature) yields a higher dissipation rate Γ_a with respect to deeper eigenstate yielding a much smaller dissipation rate Γ_c . The energy scale $\Delta\Psi$ from random fluctuation effects imposed on the system determines the dissipation rate.

Considering all the above relations in perspective, we conclude that at resonance the dynamical coordinate of a system is forced to relax to one of the metastable minima or

eigenstate of a system by the external action $F(t)$. The system stays at the minima for a length of time until eventually the accumulated action of the random forces $R(t)$ proportional to a dissipated energy scale has a finite probability proportional to $e^{-\Delta\Psi/\xi_\gamma}$ driving it off the minima coordinate. In such a condition, when the accumulated action is equal or greater than $\Delta\Psi$ the system ceases to resonate any longer. The barrier height $\Delta\Psi$ thus allows the maintenance of the resonance condition, with Γ_r giving the frequency bandwidth of resonance. In the limit of $\Delta\Psi \rightarrow \xi_\gamma$, the exponential factor above reduces to 1 when $\Gamma_r \approx \nu$. Kramer's historic seminal result yields for the prefactor,

$$\nu = \left[\left[\frac{\gamma^2}{4} + \omega_b^2 \right]^{1/2} - \frac{\gamma}{2} \right] \frac{\omega_a}{2\pi\omega_b}$$

which, becomes relevant to resonance analysis with units of t^{-1} . Here γ is the damping coefficient giving rise to the viscous losses proportional to ξ_γ in the equation of motion. This result for the prefactor describes the spatial-diffusion-controlled dissipation rate of a particular Eigenstate at moderate to strong friction γ , as represented in the Figure above. For strong damping it further reduces to

$$\nu = \frac{\omega_a \omega_b}{2\pi\gamma},$$

which reduces to a relatively small Γ_r for $\gamma \gg \omega_b$. Further, it can be seen that ω_a/Γ_r yields a result that is widely used as the Q-factor of resonance.

Conventional approaches tries to minimize ξ_γ by controlling vacuum and or the temperature for reducing the damping effects as much as possible to achieve higher frequency sensitivity. However, it turns out that the effects that one has always attempted

to get rid of, has all the time dependent interaction information since the dissipation rate embodies the arrow of time. Our work shows the relevance and importance of the energy scales $\Delta\Psi$ with respect to ξ_γ in terms of information content, which can be exploited with better relevance to interpreting interactions with a media. The time rate of lag at resonance is inherently linked to the two energy scales in terms of phase, which evolves from the path of the dynamical coordinate change $r_{mimima} \rightarrow r_b$. A detailed discussion in *section I & II* highlights the relevance of the accumulated actions of the paths and energy transitions in terms of the phase ϕ and the Q i.e., amplification factor of resonance.

Sections III and IV discusses in length, the dissipation assisted transitions between closely coupled eigenstates relevant to design of novel dissipation based sensors. We have developed a new way of interpreting resonances for sensing using dynamic dissipation. Our approach opens up new avenues for the development of miniature nanoscale sensors. We believe that the introduced understanding of dynamical scale-separation will be extremely useful for future design of nano-scale resonators from a fundamental fluid-matter interaction viewpoint. The broad appeal of our method is its universality, as it is able to detect minute changes in the surrounding media. Nature may be using this paradigm (dissipation) as sensory signals for environmental perception in biological systems. The implications of induced multi-scale response dynamics through active nanoscale features is huge, especially reminiscent of cilia in biological systems at all scales. A possible mechanistic side to sensory perception by biological organisms, opened up by our analysis, would be a great breakthrough in biological and life sciences.

5.2 Future prospects

Dissipation inherently encodes path dependent process information. It stores the history of dynamic interactions in the resonance width Γ as an accumulated action of dissipative forces. Dissipation thus should not be neglected since it offers a wealth of information hitherto not utilized in dynamic analysis. Detailed studies on the closely coupled eigenstates can reveal the density of states of a system in question. Dissipation analysis at resonance conditions would pave the path for such determination. The fluctuation dependent energy scale $\Delta\Psi$ as revealed from this study can be exploited to design further novel dissipation based sensing and engineering applications, like resonant energy harvesting. In a generic perspective, a new field of dynamic resonant analysis can emerge in terms of measurement of phase at resonance that inherently encodes time interaction information. The information encoded in phase is huge and we envision the possibility of fundamental progress in understanding rate kinetics of chemical reactions from the phase information.

The fundamental result discussed in *section II* with consideration of non-isotropic space can be extended in the future in developing a resonance model of the universe. Our perception of the visible universe is dependent on the radiated component of the energy from events in the past. Radiation accounts for the dissipated component. A resonance model would allow the consideration of a stored energy in the vast cosmos, which may provide clues to unravelling the riddles of dark matter and dark energy in the future.

List of Publications

U.S. Patents (3 pending) and International PCT

1. **Arindam Phani**, Vakhtang Putkaradze, Prashanthi Kovur and Thomas Thundat, “Sensor including mechanical resonator with nano-structured surface”, US Patent App. 14/995,998, (2016).
2. Charles William Van Neste, Thomas George Thundat, John Errington Hawk, Richard Hull, Jonathan Backs, Nurichi Guseynov and **Arindam Phani**, “Electrical energy transfer”, US Patent App. 15/035,452, (2014).
3. Charles William Van Neste, Thomas George Thundat, John Errington Hawk, Tinu Mary Abraham, Jacob H Masliyah, Jonathan Backs, Richard Hull and **Arindam Phani**, “Resonant Dielectric Heating”, US Patent App. 14/537,825, (2014).
4. Kovur Prashanthi, **Arindam Phani** and Thomas Thundat, “Chemical Sensor”, International Patent Application Serial No. PCT/CA2015/050049 (2014).

Invention Disclosures:

1. “IR Enhanced dissipation spectroscopy”, **Arindam Phani**, Vakhtang Putkaradze, Thomas Thundat (In preparation).
2. “Droplet Sensor”, **Arindam Phani**, Allison Larocque, Rebecca Kostiuk, Malina Wu and Thomas Thundat, (In preparation).

PUBLICATIONS (in order of citations): Google Scholar – total citations: 29

1. “Single-contact transmission for the quasi-wireless delivery of power over large surfaces”, CW Van Neste, JE Hawk, A Phani, JAJ Backs, R Hull, T Abraham, ...Wireless Power Transfer 1 (02), 75-82 (2014). **Cited: 12**
2. “Photothermal electrical resonance spectroscopy of physisorbed molecules on a nanowire resonator”, K Prashanthi, A Phani, T Thundat, Nano letters 15 (8), 5658-5663 (2015). **Cited 6**
3. “Wireless single contact power delivery”, CW Van Neste, R Hull, T Abraham, JE Hawk, A Phani, T Thundat, Wireless Power Transfer Conference (WPTC), 2015 IEEE, 1-4 (2015). **Cited: 2**

4. “Clustering mechanism of ethanol-water mixtures investigated with photothermal microfluidic cantilever deflection spectroscopy”, MS Ghoraiishi, JE Hawk, A Phani, MF Khan, T Thundat, *Scientific reports* 6 (2016). **Cited: 1**
5. “Quasi-wireless surface power and control for battery-free robotics”, AK Pickering, R Hull, JE Hawk, A Phani, CW Van Neste, T Thundat, *Wireless Power Transfer* 2 (02), 134-142 (2015). **Cited: 1**
6. “A nanostructured surface increases friction exponentially at the solid-gas interface”, A Phani, V Putkaradze, JE Hawk, K Prashanthi, T Thundat, *Scientific Reports* 6 (32996), 1-11 (2016).
7. “Electrical excitation of the local earth for resonant, wireless energy transfer”, CW Van Neste, R Hull, JE Hawk, A Phani, MJ Unsworth, T Thundat, *Wireless Power Transfer* 3 (2), 117-125 (2016).
8. “Chemical Selectivity and Micro/Nano Sensors”, K Prashanthi, A Phani, TG Thundat, *ECS Transactions* 75 (17), 21-26 (2016).
9. “Quasi-wireless capacitive energy transfer for the dynamic charging of personal mobility vehicles”, CW Van Neste, A Phani, R Hull, JE Hawk, T Thundat, *Emerging Technologies: Wireless Power Transfer (WoW)*, 2016 IEEE PELS (2016).
10. “Quarter wavelength resonators for use in wireless capacitive power transfer”, CW Van Neste, Arindam Phani, Allison Larocque, J.E. Hawk, Radhika Kalra, M.J. Banaag, Malina Wu, Thomas Thundat, Conference: 2017 IEEE PELS Workshop on Emerging Technologies: Wireless Power Transfer (WoW)

Manuscripts Communicated or under Preparation:

11. “Standing Wave revisited: accumulated phase and resonance amplification”, Arindam Phani, Charles Van Neste, Thomas Thundat, (**communicated**).
12. “Dissipation IR enhanced spectroscopy for receptor free molecular recognition in ppm”, Arindam Phani, Rebecca Kostiuk, Allison Larocque, Vakhtang Putkaradze, Thomas Thundat, (**in preparation for Nat. Nanotechnology**).
13. “Resonance based minute concentration determination in the range of aM in uL droplets from surface tension variations”, Arindam Phani, Allison Larocque, Rebecca Kostiuk, Malina Wu, Thomas Thundat, (**in preparation for ACS Nano**).
14. “Resonance determination of local curvature along a solid-fluid interface contact line”, Arindam Phani, Malina Wu, Rebecca Kostiuk, Allison Larocque, Thomas Thundat, (**in preparation for APL**).

BIBLIOGRAPHY

1. Abbaspour, H., Trebaol, S., Morier-Genoud, F., Portella-Oberli, M. T. & Deveaud, B. Spinor stochastic resonance. *Phys. Rev. B - Condens. Matter Mater. Phys.* **91**, 1–7 (2015).
2. Ahuja, B. L., Jain, P., Sahariya, J., Heda, N. L. & Soni, P. Electronic properties of RDX and HMX: Compton scattering experiment and first-principles calculation. *J. Phys. Chem. A* **117**, 5685–5692 (2013).
3. Alben, S., Shelley, M. & Zhang, J. Drag reduction through self-similar bending of a flexible body. *Nature* **420**, 479–481 (2002).
4. Allison, A., Pearce, C. E. M. & Abbott, D. A variational approach to the analysis of dissipative electromechanical systems. *PLoS One* **9**, 1–20 (2014).
5. Anczykowski, B., Gotsmann, B., Fuchs, H., Cleveland, J. P. & Elings, V. B. How to measure energy dissipation in dynamic mode atomic force microscopy. *Appl. Surf. Sci.* **140**, 376–382 (1999).
6. Anderson, H., Jönsson, M., Vestling, L., Lindberg, U. & Aastrup, T. Quartz crystal microbalance sensor designl. Experimental study of sensor response and performance. *Sensors Actuators B Chem.* **123**, 27–34 (2007).
7. Ando, T., Fowler, A. B. & Stern, F. Electronic properties of two-dimensional systems. *Rev. Mod. Phys.* **54**, 437–672 (1982).
8. Armendáriz-Picón, C. Could dark energy be vector-like? *J. Cosmol. Astropart. Phys.* **2004**, 007–007 (2004).
9. Arnold, V. I. *Lectures on Partial Differential Equations*. (Springer Verlag, 2000). doi:10.1515/9783110200072
10. Aspelmeyer, M., Kippenberg, T. J. & Marquardt, F. Cavity optomechanics. *Rev. Mod. Phys.* **86**, 1391–1452 (2014).
11. Badzey, R. L. & Mohanty, P. Coherent signal amplification in a nanomechanical oscillator via stochastic resonance. *AIP Conf. Proc.* **850**, 1675–1676 (2006).
12. Bahar, L. Y. & Kwatny, H. G. Generalized Lagrangian and conservation law for the damped harmonic oscillator. *Am. J. Phys.* **49**, 1062–1065 (1981).
13. Balmert, A., Florian Bohn, H., Ditsche-Kuru, P. & Barthlott, W. Dry under water: Comparative morphology and functional aspects of air-retaining insect surfaces. *J. Morphol.* **272**, 442–451 (2011).
14. Barreca, D. et al. Urchin-like ZnO nanorod arrays for gas sensing applications. *CrystEngComm* **12**, 3419 (2010).
15. Basak, S. & Raman, A. Hydrodynamic coupling between micromechanical beams oscillating in viscous fluids. *Phys. Fluids* **19**, (2007).
16. Basak, S., Raman, A. & Garimella, S. V. Hydrodynamic loading of microcantilevers vibrating in viscous fluids. *J. Appl. Phys.* **99**, (2006).

17. Basset, A. B. *A treatise on Hydrodynamics*. (Deighton, Bell and Co., 1888).
18. Baumgart, J. & Friedrich, B. M. Fluid dynamics: Swimming across scales. *Nat. Phys.* **10**, 711–712 (2014).
19. Becker, N. B., Mugler, A. & Wolde, P. R. Prediction and Dissipation in Biochemical Sensing. *arXiv* **1312.5625v**, 1–9 (2013).
20. Bekenstein, J. D. Is a tabletop search for Planck scale signals feasible? *Phys. Rev. D - Part. Fields, Gravit. Cosmol.* **86**, 1–9 (2012).
21. Bell, A. & Fletcher, N. H. The cochlear amplifier as a standing wave: ‘Squirting’ waves between rows of outer hair cells? *J. Acoust. Soc. Am.* **116**, 1016–1024 (2004).
22. Bender, C. M. PT symmetry in quantum physics: From a mathematical curiosity to optical experiments. *Europhys. News* **47**, 17–20 (2016).
23. Bender, C. M., Gianfreda, M., Hassanpour, N. & Jones, H. F. Comment on ‘On the Lagrangian and Hamiltonian description of the damped linear harmonic oscillator’ [J. Math. Phys. 48, 032701 (2007)]. *J. Math. Phys.* **57**, (2016).
24. Bennett, A. L. *Modes of Vibration of piezoelectric quartz crystals*. (1961).
25. Berli, C. L. A. & Cardona, A. On the calculation of viscous damping of microbeam resonators in air. *J. Sound Vib.* **327**, 249–253 (2009).
26. Bhatnagar, P. L., Gross, E. P. & Krook, M. A model for collision processes in gases. I. Small amplitude processes in charged and neutral one-component systems. *Phys. Rev.* **94**, 511–525 (1954).
27. Bhattacharjee, S. *et al.* Trapping of electrons in troughs of self generated electromagnetic standing waves in a bounded plasma column. *Phys. Plasmas* **21**, (2014).
28. Bhiladvala, R. B. & Wang, Z. J. Effect of fluids on the Q factor and resonance frequency of oscillating micrometer and nanometer scale beams. *Phys. Rev. E* **69**, 36307 (2004).
29. Bian, X., Litvinov, S., Qian, R., Ellero, M. & Adams, N. A. Multiscale modeling of particle in suspension with smoothed dissipative particle dynamics. *Phys. Fluids* **24**, (2012).
30. Bid, A., Bora, A. & Raychaudhuri, A. K. Temperature dependence of the resistance of metallic nanowires of diameter ??15 nm: Applicability of Bloch-Gr??neisen theorem. *Phys. Rev. B - Condens. Matter Mater. Phys.* **74**, 1–8 (2006).
31. Binning, G. & Rohrer, H. Scanning tunneling microscopy - from birth to adolescence. *Rev. Mod. Phys.* **59**, 615–625 (1987).
32. Biroli, G. & Urbani, P. Breakdown of Elasticity in Amorphous Solids. *Nat. Phys.* **12**, 1130–1133 (2016).
33. Bleher, P. M., Dyson, F. & Lebowitz, L. Non-Gaussian Energy Level Statistics for Some Integrable Systems Pavel. *Phys. Rev. Lett.* **71**, 3047–3050 (1993).
34. Bloch, I. Ultracold quantum gases in optical lattices. *Nat. Phys.* **1**, 23–30 (2005).

35. Bodapati, A., Treacy, M. M. J., Falk, M., Kieffer, J. & Keblinski, P. Medium range order and the radial distribution function. *J. Non. Cryst. Solids* **352**, 116–122 (2006).
36. Bohm, D. A Suggested Interpretation of the Quantum Theory in Terms of "Hidden" Variables. *Phys. Rev.* **5**, 180 (1952).
37. Bohr, N. LXXIII On the constitution of atoms and molecules. *Philos. Mag. Ser. 6* **26**, 857–875 (1913).
38. Bohr, N. On the constitution of atoms and molecules. *Philos. Mag. Ser. 6* **26**, 476–502 (1913).
39. Boussaad, S. & Tao, N. J. Polymer wire chemical sensor using a microfabricated tuning fork. *Nano Lett.* **3**, 1173–1176 (2003).
40. Boyd, I. D. Predicting Breakdown of the Continuum Equations Under Rarefied Flow Conditions. *AIP Conf. Proc.* **663**, 899–906 (2003).
41. Brenner, H. & Leal, L. G. Conservation and constitutive equations for adsorbed species undergoing surface diffusion and convection at a fluid-fluid interface. *J. Colloid Interface Sci.* **88**, 136–184 (1982).
42. Bretherton, F. P. The motion of rigid particles in a shear flow at low Reynolds number. *J. Fluid Mech.* **14**, 284–304 (1962).
43. Brokaw, R. S. *NASA Technical Note: Viscosity of gas Mixtures*. (1968).
44. Brokaw, R. S. Approximate Formulas for the Viscosity and Thermal Conductivity of Gas Mixtures. *J. Chem. Phys.* **29**, 391–397 (1958).
45. Bronski, J. C., DeVille, L. & Park, M. J. Fully Synchronous Solutions and the Synchronization Phase Transition for the Finite N Kuramoto Model. *arXiv* **1111.5302v**, 1–25 (2012).
46. Buddenberg, J. W. & Wilke, C. R. Calculation of Gas Mixture Viscosities. *Ind. Eng. Chem.* **41**, 1345–1347 (1949).
47. Bullard, E. C. *et al.* Dynamic similarity of oscillatory flows induced by nanomechanical resonators. *Phys. Rev. Lett.* **112**, 1–6 (2014).
48. Burt, M. G. Electron capture by multiphonon emission at the B centre in gallium arsenide. *Journal of Physics C.(Solid.State.Physics)* **12**, 4827–4832 (1979).
49. Byeon, J. Semi-classical standing waves for nonlinear Schrödinger systems. *Calc. Var. Partial Differ. Equ.* **54**, 2287–2340 (2015).
50. Camerer, S. *et al.* Realization of an optomechanical interface between ultracold atoms and a membrane. *Phys. Rev. Lett.* **107**, 1–5 (2011).
51. Cao-Paz, A. M., Rodríguez-Pardo, L., Fariña, J. & Marcos-Acevedo, J. Resolution in QCM sensors for the viscosity and density of liquids: Application to lead acid batteries. *Sensors (Switzerland)* **12**, 10604–10620 (2012).

52. Carbo, R. M., Smith, R. W. M. & Poese, M. E. Stability of the parametrically excited damped inverted pendulum: Theory and experiment. *J. Acoust. Soc. Am.* **128**, 1623–1631 (2010).
53. Carr, S., Lawrence, W. & Wybourne, M. Accessibility of quantum effects in mesomechanical systems. *Phys. Rev. B* **64**, 1–4 (2001).
54. Cavalcanti, R. M. Wave function of a Brownian particle. *Phys. Rev. E* **58**, 6807–6809 (1998).
55. Chabalko, M. J., Shahmohammadi, M. & Sample, A. P. Quasistatic cavity resonance for ubiquitous Wireless power transfer. *PLoS One* **12**, 1–14 (2017).
56. Chandler, D. Fluctuation Theory and Critical Phenomena. *The Journal of Chemical Physics* **49**, 2121 (1968).
57. Chandrasekar, V. K., Senthilvelan, M. & Lakshmanan, M. On the Lagrangian and hamiltonian description of the damped linear harmonic oscillator. *J. Math. Phys.* **48**, (2007).
58. Chandrasekhar, S. Brownian Motion, Dynamical Friction and Stellar Dynamics. *Dialectica* **3**, 114–126 (1949).
59. Chen, C. *et al.* Nanoscale fluid-structure interaction: Flow resistance and energy transfer between water and carbon nanotubes. *Phys. Rev. E - Stat. Nonlinear, Soft Matter Phys.* **84**, 1–7 (2011).
60. Chen, H. *et al.* Extended-Boltzmann Kinetic Equation for Turbulent Flows. *Science (80-.).* **301**, 633–636 (2003).
61. CHEN, H., ORSZAG, S. A., STAROSELSKY, I. & SUCCI, S. Expanded analogy between Boltzmann kinetic theory of fluids and turbulence. *J. Fluid Mech.* **519**, 301–314 (2004).
62. Chen, Y., Zhang, C., Shi, M. & Peterson, G. P. Slip boundary for fluid flow at rough solid surfaces. *Appl. Phys. Lett.* **100**, 1–5 (2012).
63. Cho, N.-J. *et al.* Quartz resonator signatures under Newtonian liquid loading for initial instrument check. *J. Colloid Interface Sci.* **315**, 248–54 (2007).
64. Chon, J. W. M., Mulvaney, P. & Sader, J. E. Experimental validation of theoretical models for the frequency response of atomic force microscope cantilever beams immersed in fluids. *J. Appl. Phys.* **87**, 3978–3988 (2000).
65. Clarke, R. J., Cox, S. M., Williams, P. M. & Jensen, O. E. The drag on a microcantilever oscillating near a wall. *J. Fluid Mech.* **545**, 397 (2005).
66. Cleland, A. N. & Roukes, M. L. Noise processes in nanomechanical resonators. *J. Appl. Phys.* **92**, 2758–2769 (2002).
67. Coffey, T., Abdelmaksoud, M. & Krim, J. A scanning probe and quartz crystal microbalance study of the impact of C₆₀ on friction at solid-liquid interfaces. *J. Phys. Condens. Matter* **13**, 4991–4999 (2001).

-
68. Cole, G. D., Wilson-Rae, I., Werbach, K., Vanner, M. R. & Aspelmeyer, M. Minimization of phonon-tunneling dissipation in mechanical resonators. *Nat. Commun.* **2**, 231–238 (2010).
 69. Colquitt, D. J., Jones, I. S., Movchan, N. V. & Movchan, a. B. Dispersion and localization of elastic waves in materials with microstructure. *Proc. R. Soc. A Math. Phys. Eng. Sci.* **467**, 2874–2895 (2011).
 70. Cooke, J. C. Note on the principle of stationary phase. *IMA J. Appl. Math. (Institute Math. Its Appl.)* **22**, 297–303 (1978).
 71. Costache, M. V. & Valenzuela, S. O. Experimental Spin Ratchet. *Science (80-.)* **330**, 1645–1648 (2010).
 72. Cranch, G. A., Lane, J. E., Miller, G. A. & Lou, J. W. Low frequency driven oscillations of cantilevers in viscous fluids at very low Reynolds number. *J. Appl. Phys.* **113**, 194904 (2013).
 73. Crawford, J. D. Scaling and Singularities in the Entrainment of Globally Coupled Oscillators. *Phys. Rev. Lett.* **74**, 4341–4344 (1995).
 74. Daido, H. Order Function and Macroscopic Mutual Entrainment in Uniformly Coupled Limit-Cycle Oscillators. *Prog. Theor. Phys.* **88**, 1213–1218 (1992).
 75. Daikhin, L. & Michael Urbakh, and. Influence of surface roughness on the quartz crystal microbalance response in a solution New configuration for QCM studies. *Faraday Discuss.* **107**, 27–38 (1997).
 76. Dareing, D. W., Tian, F. & Thundat, T. Effective mass and flow patterns of fluids surrounding microcantilevers. *Ultramicroscopy* **106**, 789–794 (2006).
 77. Das, S. & Chakraborty, S. Augmented surface adsorption characteristics by employing patterned microfluidic substrates in conjunction with transverse electric fields. *Microfluid. Nanofluidics* **8**, 313–327 (2010).
 78. Davidson, T. A. *A Simple and Accurate Method for Calculating Viscosity of Gaseous Mixtures.* (1993).
 79. Davila, A. P. *et al.* Microresonator mass sensors for detection of Bacillus anthracis Sterne spores in air and water. *Biosens. Bioelectron.* **22**, 3028–35 (2007).
 80. Dayo, A., Alnasrallah, W. & Krim, J. Superconductivity-Dependent Sliding Friction. *Phys. Rev. Lett.* **80**, 1690–1693 (1998).
 81. De Gennes, P. G. Wetting: Statics and dynamics. *Rev. Mod. Phys.* **57**, 827–863 (1985).
 82. De Gennes, P. G. Coil-stretch transition of dilute flexible polymers under ultrahigh velocity gradients. *J. Chem. Phys.* **60**, 5030–5042 (1974).
 83. Dechant, A., Kessler, D. A. & Barkai, E. Deviations from Boltzmann-Gibbs statistics in confined optical lattices. *Phys. Rev. Lett.* **115**, 1–5 (2015).
 84. Derbes, D. Feynman's derivation of the Schrödinger equation. *American Journal of Physics* **64**, 881 (1996).
-

85. Derrick, E. C. and G. H. A Numerical Solution of wave equations for real and complex eigenvalues. *Aust. J. Phys.* **30**, 15–21 (1977).
86. Dirac, P. A. M. Forms of relativistic dynamics. *Rev. Mod. Phys.* **21**, 392–399 (1949).
87. Dixon, M. C. Quartz crystal microbalance with dissipation monitoring: Enabling real-time characterization of biological materials and their interactions. *J. Biomol. Tech.* **19**, 151–158 (2008).
88. Douglass, J. K., Wilkens, L., Pantazelou, E. & Moss, F. Noise enhancement of information transfer in crayfish mechanoreceptors by stochastic resonance. *Nature* **365**, 337–340 (1993).
89. Du, J., Harding, G. L., Ogilvy, J. A., Dencher, P. R. & Lake, M. A study of Love-wave acoustic sensors. *Sensors Actuators, A Phys.* **56**, 211–219 (1996).
90. Dufour, I., Heinrich, S. M. & Josse, F. Strong-axis Bending Mode Vibrations for Resonant Microcantilever (Bio)chemical Sensors in Gas or Liquid Phase. *Proc. 2004 IEEE Int. Freq. Control Symp. Expo.* **16**, 193–199 (2004).
91. Dybwad, G. L. A sensitive new method for the determination of adhesive bonding between a particle and a substrate. *J. Appl. Phys.* **58**, 2789–2790 (1985).
92. Dzyubenko, B., Lee, H.-C., Vilches, O. E. & Cobden, D. H. Surface electron perturbations and the collective behaviour of atoms adsorbed on a cylinder. *Nat. Phys.* **11**, 398–402 (2015).
93. E Wolf. Electromagnetic Diffraction in Optical Systems. I. An Integral Representation of the Image Field. *Proc. R. Soc. London A, Math. Phys. Sci.* **253**, 349–357 (1959).
94. Ekinci, K. L., Karabacak, D. M. & Yakhot, V. Universality in oscillating flows. *Phys. Rev. Lett.* **101**, 1–4 (2008).
95. Ekinci, K. L. & Roukes, M. L. Nanoelectromechanical systems. *Rev. Sci. Instrum.* **76**, 61101 (2005).
96. Elfring, G. J. & Lauga, E. Hydrodynamic phase locking of swimming microorganisms. *Phys. Rev. Lett.* **103**, 1–4 (2009).
97. Elfström, N., Karlström, A. E. & Linnros, J. Silicon nanoribbons for electrical detection of biomolecules. *Nano Lett.* **8**, 945–949 (2008).
98. Ellerby, H. M. Distribution of density Suctuations in a molecular theory of vapor-phase nucleation. *Phys. Rev. E - Stat. Nonlinear, Soft Matter Phys.* **49**, 4287–4297 (1994).
99. Eu, B. C. *Transport coefficients of fluids.* (2005).
100. Fauve, S. & Heslot, F. Stochastic resonances in a bistable system. *Phys. Lett.* **97A**, 5–7 (1983).
101. Fawcett, N. C., Craven, R. D., Zhang, P. & Evans, J. a. QCM response to solvated, tethered macromolecules. *Anal. Chem.* **70**, 2876–80 (1998).

102. Felts, J. R., Kjoller, K., Lo, M., Prater, C. B. & King, W. P. Nanometer-scale infrared spectroscopy of heterogeneous polymer nanostructures fabricated by tip-based nanofabrication. *ACS Nano* **6**, 8015–8021 (2012).
103. Ferreira, G. N. M., da-Silva, A.-C. & Tomé, B. Acoustic wave biosensors: physical models and biological applications of quartz crystal microbalance. *Trends Biotechnol.* **27**, 689–697 (2009).
104. Feynman, R. P. Forces in molecules. *Phys. Rev.* **56**, 340–343 (1939).
105. Feynman, R. P. & Hibbs, A. R. *Quantum mechanics and path integrals*. (McGraw-Hill, 1965).
106. Field, J. H. Derivation of the Schrodinger equation from the Hamilton-Jacobi equation in Feynman's path integral formulation of quantum mechanics. *Eur. J. Phys.* **32**, 63–87 (2011).
107. Filippo, S. De. A new PT -symmetric complex Hamiltonian with a real spectrum A new P T -symmetric complex Hamiltonian with a real spectrum. *J. Phys. A Math. Gen* **33**, L1–L3 (2000).
108. Finot, E., Passian, A. & Thundat, T. Measurement of mechanical properties of cantilever shaped materials. *Sensors* **8**, 3497–3541 (2008).
109. Flekkoy, E. G. & Rothman, D. H. Fluctuating fluid interfaces. *Phys. Rev. Lett.* **75**, 260–263 (1995).
110. French, A. P. *Vibrations and Waves: The M.I.T introductory physics series. Book* (W.W. Norton & Company Inc., 1971).
111. Fujisaka, H., Yamada, T., Kinoshita, G. & Kono, T. Chaotic phase synchronization and phase diffusion. *Phys. D Nonlinear Phenom.* **205**, 41–47 (2005).
112. G N Ord, J A Gualtieri & R B Mann. A Physical Basis for the phase in Feynman Path Integration. *arXiv quant-ph/0*, 1–4 (2004).
113. Gammaconi, L., Hanggi, P. & Jung, P. Stochastic resonance. *Rev. Mod. Phys.* **70**, 223–287 (1998).
114. Gangloff, D., Bylinskii, A., Counts, I., Jhe, W. & Vuletić, V. Velocity tuning of friction with two trapped atoms. *Nat. Phys.* **11**, 915–919 (2015).
115. Ganguli, G., Tejero, E., Crabtree, C., Amatucci, W. & Rudakov, L. Generation of electromagnetic waves in the very low frequency band by velocity gradient. *Phys. Plasmas* **21**, (2014).
116. Garcia, R. *et al.* Identification of nanoscale dissipation processes by dynamic atomic force microscopy. *Phys. Rev. Lett.* **97**, 1–4 (2006).
117. Garetto, D. *et al.* Modeling stressed MOS oxides using a multiphonon-assisted quantum approach-Part I: Impedance analysis. *IEEE Trans. Electron Devices* **59**, 610–620 (2012).

118. Gauthier, D. & Bienfang, J. Intermittent Loss of Synchronization in Coupled Chaotic Oscillators: Toward a New Criterion for High-Quality Synchronization. *Phys. Rev. Lett.* **77**, 1751–1754 (1996).
119. Gazzola, M., Argentina, M. & Mahadevan, L. Scaling macroscopic aquatic locomotion. *Nat. Phys.* **10**, 758–761 (2014).
120. Ghosh, A. & Ray, D. S. Born-Kothari condensation in an ideal Fermi gas. *Phys. Rev. A - At. Mol. Opt. Phys.* **95**, 6–11 (2017).
121. Ghosh, S., Choudhuri, A. & Talukdar, B. On the quantization of damped harmonic oscillator. *Acta Phys. Pol. B* **40**, 49–57 (2009).
122. Gieseler, J., Novotny, L. & Quidant, R. Thermal nonlinearities in a nanomechanical oscillator. *Nat. Phys.* **9**, 806–810 (2013).
123. Giessibl, F. J. Advances in atomic force microscopy. *Rev. Mod. Phys.* **75**, 949–983 (2003).
124. Gilmartin, H., Klein, A. & Li, C. Application of Hamilton? s principle to the study of the anharmonic oscillator in classical mechanics. *Am. J. Phys.* **47**, 636–639 (1979).
125. Gil-Santos, E. *et al.* Nanomechanical mass sensing and stiffness spectrometry based on two-dimensional vibrations of resonant nanowires. *Nat. Nanotechnol.* **5**, 641–5 (2010).
126. Gitterman, M. Classical harmonic oscillator with multiplicative noise. *Phys. A Stat. Mech. its Appl.* **352**, 309–334 (2005).
127. Gold, T. & Pumphrey, R. J. Hearing I. The cochlea as a frequency analyzer. *Proceeding R. Soc. B, Biol. Sci.* **135**, 462–491 (1948).
128. Goldstein, R. E., Polin, M. & Tuval, I. Noise and Synchronization in Pairs of Beating Eukaryotic Flagella. *Phys. Rev. Lett.* **103**, 1–4 (2009).
129. Golestanian, R., Yeomans, J. M. & Uchida, N. Hydrodynamic synchronization at low Reynolds number. *Soft Matter* **7**, 3074 (2011).
130. Goodrich, F. C. The Theory of Capillary Excess Viscosities. *Proc. R. Soc. Lond. A* **374**, 341–370 (1981).
131. Graham, R. & Tel, T. Existence of a potential for dissipative dynamical systems. *Phys. Rev. Lett.* **52**, 9–12 (1984).
132. Green, C. P. & Sader, J. E. Torsional frequency response of cantilever beams immersed in viscous fluids with applications to the atomic force microscope. *J. Appl. Phys.* **92**, 6262–6274 (2002).
133. Grimes, D. M. & Grimes, C. a. The complex Poynting theorem: reactive power, radiative Q, and \nlimitations on electrically small antennas. *Proc. Int. Symp. Electromagn. Compat.* 97–101 (1995). doi:10.1109/ISEMC.1995.523526
134. Gross, M. & Varnik, F. Interfacial roughening in nonideal fluids: Dynamic scaling in the weak- and strong-damping regime. *Phys. Rev. E - Stat. Nonlinear, Soft Matter Phys.* **87**, 1–11 (2013).

-
- 135. Gueron, S. & Levit-Gurevich, K. Energetic considerations of ciliary beating and the advantage of metachronal coordination. *Proc. Natl. Acad. Sci. U. S. A.* **96**, 12240–12245 (1999).
 - 136. Gupta, T. K. Application of Zinc Oxide Varistors. *J. Am. Ceram. Soc.* **73**, 1817–1840 (1990).
 - 137. Guralnik, G. S., Hagen, C. R. & Kibble, T. W. B. Global conservation laws and massless particles. *Phys. Rev. Lett.* **13**, 585–587 (1964).
 - 138. Hak, F., Rodahl, M., Kasemo, B. & Brzezinski, P. Structural changes in hemoglobin during adsorption to solid surfaces: Effects of pH, ionic strength, and ligand binding. *Proc. Natl. Acad. Sci. U. S. A.* **95**, 12271–12276 (1998).
 - 139. Hammerer, K. *et al.* Optical lattices with micromechanical mirrors. *Phys. Rev. A - At. Mol. Opt. Phys.* **82**, (2010).
 - 140. Hammerer, K. *et al.* Strong coupling of a mechanical oscillator and a single atom. *Phys. Rev. Lett.* **103**, 2–5 (2009).
 - 141. Hänggi, P., Talkner, P. & Borovec, M. Reaction rate theory - 50 years after Kramers. *Rev. Mod. Phys.* **62**, 251–341 (1990).
 - 142. Hanle, P. a. The Schrödinger-Einstein correspondence and the sources of wave mechanics. *Am. J. Phys.* **47**, 644 (1979).
 - 143. Happel, J. Slow Viscous Flow through a Mass of Particles. *Ind. Eng. Chem.* **46**, 1194–1195 (1951).
 - 144. Hartmann, H. J. & Laubereau, A. Coherent pulse propagation in the infrared on the picosecond time scale. *Opt. Commun.* **47**, 117–122 (1983).
 - 145. Havelock, T. H. Wavefronts considered as the characteristics of partial differential equations. *Proc. London Math. Soc.* **S2-2**, 297–315 (1905).
 - 146. Heaviside, O. A gravitational and electromagnetic analogy. *The Electrician* 281 (1893).
 - 147. Henry, C. H. & Lang, D. V. Nonradiative capture and recombination by multiphonon emission in GaAs and GaP. *Phys. Rev. B* **15**, 989–1016 (1977).
 - 148. Herman L F Helmholtz. *On the sensation of tone*. (Longmans Green and Co., 1885).
 - 149. Hernández-Mínguez, A. *et al.* High-frequency acoustic charge transport in GaAs nanowires. *Nanotechnology* **25**, 135204 (2014).
 - 150. Herrera, L., Nunez, L., Patino, A. & Rago, H. A variational principle and the classical and quantum mechanics of the damped harmonic oscillator. *Am. J. Phys* **54**, 273–277 (1986).
 - 151. Hertl, S., Wimmer, L. & Benes, E. Investigation of the amplitude distribution of AT-cut quartz crystals. *J. Acoust. Soc. Am.* **78**, 1337–1343 (1985).
 - 152. Hiebert, W. Mass sensing: Devices reach single-proton limit. *Nat. Nanotechnol.* **7**, 278–80 (2012).
 - 153. Holm, D. D. & Putkaradze, V. Aggregation of finite-Size particles with variable mobility. *Phys. Rev. Lett.* **95**, 1–4 (2005).
-

154. Hosaka, H., Itao, K. & Kuroda, S. Damping characteristics of beam-shaped micro-oscillators. *Sensors and Actuators A* **49**, 87–95 (1995).
155. Hu, H.-M. S., Watson, G. S., Cribb, B. W. & Watson, J. a. Non-wetting wings and legs of the cranefly aided by fine structures of the cuticle. *J. Exp. Biol.* **214**, 915–920 (2011).
156. Hunger, D. *et al.* Coupling ultracold atoms to mechanical oscillators. *Comptes Rendus Phys.* **12**, 871–887 (2011).
157. Huxley, M. N. Exponential sums and Lattice points. *Proc. London Math. Soc.* **60**, 471–502 (1990).
158. Imboden, M. & Mohanty, P. Dissipation in nanoelectromechanical systems. *Phys. Rep.* **534**, 89–146 (2014).
159. Isobe, M. Granular Turbulence in Two Dimensions: Microscale Reynolds Number and Final Condensed States. *Int. J. Mod. Phys. C* **23**, 1250032 (2012).
160. Iyer, S. S. & Candler, R. N. Mode- and Direction-Dependent Mechanical Energy Dissipation in Single-Crystal Resonators due to Anharmonic Phonon-Phonon Scattering. *Phys. Rev. Appl.* **5**, 1–9 (2016).
161. Jacobson, T. Thermodynamics of Spacetime: The Einstein Equation of State. *Phys. Rev. Lett.* **75**, 1260 (1995).
162. Jain, M. K. & Grimes, C. a. Effect of surface roughness on liquid property measurements using mechanically oscillating sensors. *Sensors Actuators, A Phys.* **100**, 63–69 (2002).
163. Jeffrey, D. J. & Onishi, Y. Calculation of the resistance and mobility functions for two unequal rigid spheres in low-Reynolds-number flow. *J. Fluid Mech.* **139**, 261 (1984).
164. Jensen, K., Kim, K. & Zettl, A. An atomic-resolution nanomechanical mass sensor. *Nat. Nanotechnol.* **3**, 533–7 (2008).
165. Jeong, I.-K., Heffner, R. H., Graf, M. J. & Billinge, S. J. L. Lattice dynamics and correlated atomic motion from the atomic pair distribution function. *Phys. Rev. B* **67**, 104301 (2003).
166. Jöckel, A. *et al.* Spectroscopy of mechanical dissipation in micro-mechanical membranes. *Appl. Phys. Lett.* **99**, 14–16 (2011).
167. Johannsmann, D. Viscoelastic, mechanical, and dielectric measurements on complex samples with the quartz crystal microbalance. *Phys. Chem. Chem. Phys.* **10**, 4516 (2008).
168. Johannsmann, D., Reviakine, I. & Richter, R. P. Dissipation in films of adsorbed nanospheres studied by quartz crystal microbalance (QCM). *Anal. Chem.* **81**, 8167–8176 (2009).
169. John Maddox. Heat conduction is a can of worms. *Nature* **338**, 373 (1989).
170. Jones, I. S., Movchan, A. B. & Gei, M. Waves and damage in structured solids with multi-scale resonators. *Proc. R. Soc. A Math. Phys. Eng. Sci.* **467**, 964–984 (2011).
171. Jones, J. R. & Walters, T. S. A vibrating-rod elastoviscometer. *Rheol. Acta* **7**, 360–363 (1968).

172. Joo, J., Lee, D., Yoo, M. & Jeon, S. ZnO nanorod-coated quartz crystals as self-cleaning thiol sensors for natural gas fuel cells. *Sensors Actuators B Chem.* **138**, 485–490 (2009).
173. Joseph, D. & Preziosi, L. Heat waves. *Rev. Mod. Phys.* **61**, 41–73 (1989).
174. Kadanoff, L. P. & Martin, P. C. Hydrodynamic equations and correlation functions. *Ann. Phys. (N. Y.)* **24**, 419–469 (1963).
175. Kanazawa, K. K. Mechanical behaviour of films on the quartz microbalance. *Faraday Discuss.* **107**, 77–90 (1997).
176. Karabacak, D. M., Yakhot, V. & Ekinci, K. L. High-Frequency Nanofluidics: An Experimental Study Using Nanomechanical Resonators. *Phys. Rev. Lett.* **98**, 254505 (2007).
177. Karl F Herzfeld. Nodal surfaces in molecular wave functions. *Rev. Mod. Phys.* **21**, 527–530 (1949).
178. Karniadakis, G., Beskok, A. & Aluru, N. *Microflows and Nanoflows Fundamentals and Simulation*. **29**, (Springer, 2005).
179. Kato, N. Fermat's Principle for Bloch Waves. *J. Phys. Soc. Japan* **18**, 1785 (1963).
180. Khaderbad, M. A. *et al.* Electrical actuation and readout in a nanoelectromechanical resonator based on a laterally suspended zinc oxide nanowire. *Nanotechnology* **23**, 25501 (2012).
181. Khamehchi, M. A. *et al.* Negative-Mass Hydrodynamics in a Spin-Orbit-Coupled Bose-Einstein Condensate. *Phys. Rev. Lett.* **118**, 1–6 (2017).
182. Kim, Y.-H., Cierpka, C. & Wereley, S. T. Flow field around a vibrating cantilever: coherent structure eduction by continuous wavelet transform and proper orthogonal decomposition. *J. Fluid Mech.* **669**, 584–606 (2011).
183. Kinikar, A. *et al.* Quantized edge modes in atomic-scale point contacts in graphene. *Nat. Nanotechnol.* 1–6 (2017). doi:10.1038/nnano.2017.24
184. Kinsler, P., Favaro, A. & McCall, M. W. Four Poynting theorems. *Eur. J. Phys.* **30**, 983–993 (2009).
185. Kipling, A. L. & Thompson, M. Network analysis method applied to liquid-phase acoustic wave sensors. *Anal. Chem.* **62**, 1514–1519 (1990).
186. Kitano, K., Inoue, Y., Matsuno, R., Takai, M. & Ishihara, K. Nanoscale evaluation of lubricity on well-defined polymer brush surfaces using QCM-D and AFM. *Colloids Surfaces B Biointerfaces* **74**, 350–357 (2009).
187. Kobayashi, K. Surface-state conduction of medium-sized nanowires. *Phys. Rev. B* **69**, 115338 (2004).
188. Kolkowitz, S. *et al.* Coherent Sensing of a Mechanical Resonator with a Single-Spin Qubit. *Science (80-.).* **335**, 1603–1606 (2012).
189. Korsch, H. J., Physik, F. & Kaiserslautern, U. Semiclassical description of resonances. in *Resonances : The unifying route towards the formulation of dynamical processes* 253–278 (Springer Verlag, 1987).

190. Kotar, J., Leoni, M., Bassetti, B., Lagomarsino, M. C. & Cicuta, P. Hydrodynamic synchronization of colloidal oscillators. *Proc. Natl. Acad. Sci.* **107**, 7669–7673 (2010).
191. Kozlov, A. S., Baumgart, J., Risler, T., Versteegh, C. P. C. & Hudspeth, a J. Forces between clustered stereocilia minimize friction in the ear on a subnanometre scale. *Nature* **474**, 376–9 (2011).
192. Kraft, M., Pendry, J. B., Maier, S. A. & Luo, Y. Transformation optics and hidden symmetries. *Phys. Rev. B - Condens. Matter Mater. Phys.* **89**, (2014).
193. Kramers, H. A. Brownian motion in a field of force and the diffusion model of chemical reactions. *Physica* **7**, 284–304 (1940).
194. Krim, J. Widom, A. Damping of a crystal oscillator by an adsorbed monolayer and its relation to interfacial viscosity. *Phys. Rev. B* **38**, 184–189 (1988).
195. Krishnamurthy, S., Ghosh, S., Chatterji, D., Ganapathy, R. & Sood, A. K. A micrometre-sized heat engine operating between bacterial reservoirs. *Nat. Phys.* **12**, 1134–1138 (2016).
196. Kubo, R. The fluctuation-dissipation theorem. *Reports Prog. Phys.* **29**, 255–284 (1966).
197. Kumar, N., Soni, H., Ramaswamy, S. & Sood, A. K. Flocking at a distance in active granular matter. *Nat. Commun.* **5**, 1–9 (2014).
198. Kunstatter, G. & Vincent, D. E. A boundary layer model for the Kaluza-Klein monopole. *Phys. Lett.* **163B**, 96–100 (1985).
199. Kuramoto, Y. Cooperative Dynamics of Oscillator Community. *Prog. Theor. Phys. Suppl.* **79**, 223–240 (1984).
200. Kwon, B., Rosenberger, M., Bhargava, R., Cahill, D. G. & King, W. P. Dynamic thermomechanical response of bimaterial microcantilevers to periodic heating by infrared radiation. *Rev. Sci. Instrum.* **83**, (2012).
201. Lagomarsino, M. C., Jona, P. & Bassetti, B. Metachronal waves for deterministic switching two-state oscillators with hydrodynamic interaction. *Phys. Rev. E* **68**, 21908 (2003).
202. Lamb Jr, W. E. Suppose Newton had invented wave mechanics. *Am. J. Phys.* **62**, 201–206 (1994).
203. Lamb, H. *Hydrodynamics*. (Cambridge University Press, 1895). doi:10.1007/s13398-014-0173-7.2
204. Lamb, W. E. Super classical quantum mechanics: The best interpretation of nonrelativistic quantum mechanics. *Am. J. Phys.* **69**, 413 (2001).
205. Landau, L. D. & Lifshitz, E. M. Course of Theoretical Physics Vol 5, Statistical Physics. *Pergamon Press* 544 (1980). doi:10.1115/1.3644010
206. Lau, J. H. Vibration Frequencies and Mode Shapes for a Constrained Cantilever. *Trans. ASME* **51**, 182–187 (1984).
207. Lauga, E. & Powers, T. R. The hydrodynamics of swimming microorganisms. *Rep. Prog. Phys.* **72**, 96601 (2009).

208. Lawrence, P. Gradients in the Insect Segment: the Orientation of Hairs in the Milkweed Bug *Oncopeltus Fasciatus*. *J. Exp. Biol.* **44**, 607–620 (1966).
209. Lax, M. Classical Nose. V. Noise in Self-Sustained Oscillators. *Phys. Rev.* **160**, 290–307 (1967).
210. Lee, J. *et al.* Support: Formation of a protected for conduction in Quantum Point Contacts Under Extreme Biasing in quantum point contacts under extreme biasing. *Nat. Nanotechnol.* 1–6 (2014).
211. Lei, M., De Graff, A. M. R., Thorpe, M. F., Wells, S. A. & Sartbaeva, A. Uncovering the intrinsic geometry from the atomic pair distribution function of nanomaterials. *Phys. Rev. B - Condens. Matter Mater. Phys.* **80**, 1–9 (2009).
212. Leichtberg, S., Weinbaum, S., Pfeffer, R. & Gluckman, M. J. J. A Study of Unsteady Forces at Low Reynolds Number: A Strong Interaction Theory for the Coaxial Settling of Three or More Spheres. *Philos. Trans. R. Soc. A Math. Phys. Eng. Sci.* **282**, 585–610 (1976).
213. Levashov, V. A., Billinge, S. J. L. & Thorpe, M. F. Density fluctuations and the pair distribution function. *Phys. Rev. B* **72**, 24111 (2005).
214. Levinson, B. C. P. A. M. T. Ordered Capillary-Wave States: Quasicrystals, Hexagons, and Radial Waves. *Phys. Rev. Lett.* **68**, 2157–2161 (1992).
215. Li, G., Ren, Z. & Zhang, X. Dissipation induced by phonon elastic scattering in crystals. *Sci. Rep.* **6**, 34148 (2016).
216. Li, M. *et al.* Nanoelectromechanical resonator arrays for ultrafast, gas-phase chromatographic chemical analysis. *Nano Lett.* **10**, 3899–3903 (2010).
217. Li, M., Tang, H. X. & Roukes, M. L. Ultra-sensitive NEMS-based cantilevers for sensing, scanned probe and very high-frequency applications. *Nat. Nanotechnol.* **2**, 114–20 (2007).
218. Li, N. *et al.* Colloquium: Phononics: Manipulating heat flow with electronic analogs and beyond. *Rev. Mod. Phys.* **84**, 1045–1066 (2012).
219. Lifshitz, R. Phonon-mediated dissipation in micro- and nano-mechanical systems. *Phys. B Condens. Matter* **316–317**, 397–399 (2002).
220. Linden, J., Thyssen, A. & Oesterschulze, E. Suspended plate microresonators with high quality factor for the operation in liquids. *Appl. Phys. Lett.* **104**, 3–6 (2014).
221. Liu, Y., Viens, M. & Cheeke, D. Behavior of extensional modes in a thin rod immersed in a viscous medium. *J. Acoust. Soc. Am.* **99**, 706–712 (1996).
222. Loewenberg, M. The unsteady Stokes resistance of arbitrarily oriented, finite-length cylinders. *Phys. Fluids A Fluid Dyn.* **5**, 3004–3006 (1993).
223. Lopez Arteaga, I., Busturia, J. M. & Nijmeijer, H. Energy dissipation of a friction damper. *J. Sound Vib.* **278**, 539–561 (2004).
224. Loui, A. *et al.* Detection and discrimination of pure gases and binary mixtures using a dual-modality microcantilever sensor. *Sensors Actuators A Phys.* **159**, 58–63 (2010).

225. Lu, J. *et al.* Observation of topological valley transport of sound in sonic crystals. *Nat. Phys.* **1**, (2016).
226. Lubomirsky, I. & Stafsudd, O. Invited review article: Practical guide for pyroelectric measurements. *Rev. Sci. Instrum.* **83**, (2012).
227. Lucklum, R. & Hauptmann, P. The quartz crystal microbalance: mass sensit. *Sensors Actuators B* **70**, 30–36 (2000).
228. M F Bishop and A A Maradudin. Energy flow in a semi-infinite spatially dispersive absorbing dielectric. *Phys. Rev.* **14**, 3384–3393 (1976).
229. Muhlethaler, J., Kolar, J. W. & Ecklebe, A. Loss modeling of inductive components employed in power electronic systems. *8th Int. Conf. Power Electron. - ECCE Asia* 945–952 (2011).
230. Macdonald, E. K., Wilson, H. N. & Konuş, U. Better customer insight-in real time. *Harv. Bus. Rev.* **90**, 1–7 (2012).
231. Magnard, J.-L. *et al.* Biosynthesis of monoterpane scent compounds in roses. *Science* **349**, 81–83 (2015).
232. Mahboob, I., Nishiguchi, K., Okamoto, H. & Yamaguchi, H. Phonon-cavity electromechanics. *Nat. Phys.* **8**, 387–392 (2012).
233. Mak, C. & Krim, J. Quartz-crystal microbalance studies of the velocity dependence of interfacial friction. *Phys. Rev. B* **58**, 5157–5159 (1998).
234. Mannelli, I., Minunni, M., Tombelli, S. & Mascini, M. Quartz crystal microbalance (QCM) affinity biosensor for genetically modified organisms (GMOs) detection. *Biosens. Bioelectron.* **18**, 129–140 (2002).
235. Márkus, F. & Gambár, K. Generalized Hamilton-Jacobi equation for simple dissipative processes. *Phys. Rev. E - Stat. Nonlinear, Soft Matter Phys.* **70**, 1–6 (2004).
236. Martin, M. J. & Houston, B. H. Gas damping of carbon nanotube oscillators. *Appl. Phys. Lett.* **91**, 103116 (2007).
237. Martin, S. J., Frye, G. C., Ricco, a. J. & Senturia, S. D. Effect of surface roughness on the response of thickness-shear mode resonators in liquids. *Anal. Chem.* **65**, 2910–2922 (1993).
238. Martin, S. J., Granstaff, V. E. & Frye, G. C. Characterization of a Quartz Crystal Microbalance with Simultaneous Mass and Liquid Loading. *Anal. Chem.* **2281**, 2272–2281 (1991).
239. Matatagui, D. *et al.* Love-wave sensor array to detect, discriminate and classify chemical warfare agent simulants. *Sensors Actuators, B Chem.* **175**, 173–178 (2012).
240. Matravers, D. R. & Triginer, J. Particle number density fluctuations and pressure. *Class. Quantum Grav.* **18**, 3917–3928 (2001).
241. Maxwell, J. C. On the Dynamical Theory of Gases. *Proc. R. Soc. London* 49–88 (1866).

242. Maxwell, J. C. On Stresses in Rarified Gases Arising from Inequalities of Temperature. *Philos. Trans. R. Soc. London* **170**, 231–256 (1879).
243. Mayer, B., Collins, C. C. & Walton, M. Transient analysis of carrier gas saturation in liquid source vapor generators. *J. Vac. Sci. Technol. A Vacuum, Surfaces, Film.* **19**, 329–344 (2001).
244. Mecea, V. M. Is quartz crystal microbalance really a mass sensor? *Sensors Actuators, A Phys.* **128**, 270–277 (2006).
245. Medeiros, E. S. D. E., Cardoso, J. A. & Es, M. Existence of standing waves for schrodinger equations involving the fractional laplacian. *Electron. J. Differ. Equations* **2017**, 1–10 (2017).
246. Merali, Z. Theoretical physics: The origins of space and time. *Nature* **500 (7464)**, 516–519 (2013).
247. Meziane, A., Norris, A. N. & Shuvalov, A. L. Nonlinear shear wave interaction at a frictional interface: Energy dissipation and generation of harmonics. *J. Acoust. Soc. Am.* **130**, 1820–1829 (2011).
248. Miljkovic, N., Preston, D. J., Enright, R. & Wang, E. N. Electrostatic charging of jumping droplets. *Nat. Commun.* **4**, 1–9 (2013).
249. Milyutin, E. & Muralt, P. Electro-mechanical coupling in shear-mode FBAR with piezoelectric modulated thin film. *IEEE Trans. Ultrason. Ferroelectr. Freq. Control* **58**, 685–688 (2011).
250. Min, Y., Akbulut, M., Kristiansen, K., Golan, Y. & Israelachvili, J. The role of interparticle and external forces in nanoparticle assembly. *Nat. Mater.* **7**, 527–538 (2008).
251. Mindlin, R. D. High frequency vibrations of piezoelectric crystal plates. *Int. J. Solids Struct.* **8**, 895–906 (1972).
252. Mindlin, R. D. On the equations of elastic materials with micro-structure. *Int. J. Solids Struct.* **1**, 73–78 (1965).
253. Miroollo, R. E. & Strogatz, S. H. The spectrum of the locked state for the Kuramoto model of coupled oscillators. *Phys. D Nonlinear Phenom.* **205**, 249–266 (2005).
254. Mo, Y., Turner, K. T. & Szlufarska, I. Friction laws at the nanoscale. *Nature* **457**, 1116–1119 (2009).
255. Montaldi, E. & Dodonov, V. V. A New Equation for Quantum Dissipative Systems. *Nuovo Cim.* **53**, 291–300 (1979).
256. Moser, J. *et al.* Ultrasensitive force detection with a nanotube mechanical resonator. *Nat. Nanotechnol.* **8**, 493–496 (2013).
257. N G Van Kampen. The Method of Stationary Phase. *Physica* **24**, 437–444 (1958).
258. Nelson, D. F. Generalizing the Poynting Vector. *Phys. Rev. Lett.* **76**, 4713–4716 (1996).
259. Neufeld, P. D. Empirical Equations to Calculate gas mixture viscosities as a function of the Transport Collision Integrals Ω . *J. Chem. Phys.* **57**, 1100 (1972).

260. Newell, W. E. Miniaturization of tuning forks. *Science (80-.)* **161**, 1320–1326 (1968).
261. Nicolás, J. A. & Vega, J. M. Three-dimensional streaming flows driven by oscillatory boundary layers. *Fluid Dyn. Res.* **32**, 119–139 (2003).
262. Nika, D. L. *et al.* Suppression of phonon heat conduction in cross-section-modulated nanowires. *Phys. Rev. B - Condens. Matter Mater. Phys.* **85**, 1–10 (2012).
263. Nishikawa, I., Iwayama, K., Tanaka, G., Horita, T. & Aihara, K. Finite-size scaling in globally coupled phase oscillators with a general coupling scheme. *Prog. Theor. Exp. Phys.* **2014**, 1–11 (2014).
264. Noever, D. A. Diffusive slip and surface transport properties. *J. Colloid Interface Sci.* **147**, 186–191 (1991).
265. Nouira, H., Foltête, E., Hirsinger, L. & Ballandras, S. Investigation of the effects of air on the dynamic behavior of a small cantilever beam. *J. Sound Vib.* **305**, 243–260 (2007).
266. Oden, P. I., Chen, G. Y., Steele, R. a., Warmack, R. J. & Thundat, T. Viscous drag measurements utilizing microfabricated cantilevers. *Appl. Phys. Lett.* **68**, 3814–3816 (1996).
267. Ortiz-Young, D., Chiu, H.-C., Kim, S., Voitchovsky, K. & Riedo, E. The interplay between apparent viscosity and wettability in nanoconfined water. *Nat. Commun.* **4**, 2482 (2013).
268. Palasantzas, G. Random surface roughness influence on gas damped nanoresonators. *Appl. Phys. Lett.* **90**, (2007).
269. Park, J. Y., Song, D. E. & Kim, S. S. An approach to fabricating chemical sensors based on ZnO nanorod arrays. *Nanotechnology* **19**, 105503 (2008).
270. Parker, D. F. *Fields, Flows and Waves*. (Springer-Verlag London Ltd., 2003).
271. Passian, A., Protopopescu, V. & Thundat, T. Fluctuation and dissipation of a stochastic micro-oscillator under delayed feedback. *J. Appl. Phys.* **100**, 10–14 (2006).
272. Passian, A., Wig, A., Meriaudeau, F., Ferrell, T. L. & Thundat, T. Knudsen forces on microcantilevers. *J. Appl. Phys.* **92**, 6326–6333 (2002).
273. Patan??, L., Hellbach, S., Krause, A. F., Arena, P. & D??rr, V. An insect-inspired bionic sensor for tactile localization and material classification with state-dependent modulation. *Front. Neurorobot.* **6**, 1–18 (2012).
274. Paul, M. R., Clark, M. T. & Cross, M. C. The stochastic dynamics of micron and nanoscale elastic cantilevers in fluid: fluctuations from dissipation. *Nanotechnology* **17**, 4502–4513 (2006).
275. Paul, M. R., Clark, M. T. & Cross, M. C. Coupled motion of microscale and nanoscale elastic objects in a viscous fluid. *Phys. Rev. E - Stat. Nonlinear, Soft Matter Phys.* **88**, 1–17 (2013).
276. Payne, L. E. & Pell, W. H. The Stokes flow problem for a class of axially symmetric bodies. *J. Fluid Mech. Digit. Arch.* **7**, 529–549 (1959).

277. Pelton, M. *et al.* Damping of Acoustic Vibrations in Gold Nanoparticles. *Nat. Nanotechnol.* **4**, 492–495 (2009).
278. Pendry, J. B., Luo, Y. & Zhao, R. Transforming the optical landscape. *Science (80-.)* **348**, 521–524 (2015).
279. Pendry, J. B., Schurig, D. & Smith, D. R. Controlling Electromagnetic Fields. *Science (80-.)* **312**, 1780–1782 (2006).
280. Pernstich, K. P., Rössner, B. & Batlogg, B. Field-effect-modulated Seebeck coefficient in organic semiconductors. *Nat. Mater.* **7**, 321–325 (2008).
281. Pikovski, I., Vanner, M. R., Aspelmeyer, M., Kim, M. & Brukner, C. Probing Planck-scale physics with quantum optics. *Nat. Phys.* **8**, 393–398 (2011).
282. Planck, M. *Eight Lectures on Theoretical Physics*. (Columbia University Press, 1915).
283. Plihal, M., Shambrook, A. & Maradudin, A. A. Two-dimensional photonic band structures. *Opt. Commun.* **80**, 199–204 (1991).
284. Polin, M., Tuval, I., Drescher, K., Gollub, J. P. & Goldstein, R. E. Chlamydomonas Swims with Two. *Science (80-.)* **325**, 487 (2009).
285. Pomorska, A. *et al.* Positive frequency shifts observed upon adsorbing micron-sized solid objects to a quartz crystal microbalance from the liquid phase. *Anal. Chem.* **82**, 2237–2242 (2010).
286. Pooley, C. M., Alexander, G. P. & Yeomans, J. M. Hydrodynamic interaction between two swimmers at low reynolds number. *Phys. Rev. Lett.* **99**, 1–4 (2007).
287. Potel, C. & Gatignol, P. A stationary phase argument for the modal wave beam deviation in the time – space domain for anisotropic multilayered media. *Ultrasonics* **40**, 549–553 (2002).
288. Poynting, J. H. On the Transfer of Energy in the Electromagnetic Field. *Philos. Trans. R. Soc. London* **175**, 343–361 (1884).
289. Prevenslik, T. Nanoscale Heat Transfer by Quantum Mechanics. in *5th International Conference on thermal Engineering: Theory and Application* 1–4 (2010).
290. Purcell, E. E. M. Life at low Reynolds number. *Am. J. Phys.* **45**, 3 (1977).
291. Putkaradze, V. & Weidman, P. Turbulent wake solutions of the Prandtl α equations. *Phys. Rev. E* **67**, 1–7 (2003).
292. Qian, Z. H., Jin, F., Lu, T. J. & Kishimoto, K. Transverse surface waves in a functionally graded piezoelectric substrate coated with a finite-thickness metal waveguide layer. *Appl. Phys. Lett.* **94**, 1–4 (2009).
293. Ray, R. & Sengupta, S. Stochastic resonance in underdamped, bistable systems. *Phys. Lett. Sect. A Gen. At. Solid State Phys.* **353**, 364–371 (2006).
294. Rayleigh, Lord. IX. Some general theorems concerning forced vibrations and resonance. *Philos. Mag. Ser. 6* **3**, 97–117 (1902).

295. Rayleigh, Lord. XXXVIII. On the flow of viscous liquids, especially in two dimensions. *Philos. Mag. Ser. 5* **36**, 354–372 (1893).
296. Rayleigh, Lord. LXXXII. On the motion of solid bodies through viscous liquid. *Philos. Mag. Ser. 6* **21**, 697–711 (1911).
297. Reddy, S. M., Jones, J. P. & Lewis, T. J. The coexistence of pressure waves in the operation of quartz-crystal shear-wave sensors. *J. Appl. Phys.* **83**, 2524–2532 (1998).
298. Reed, C. E., Kanazawa, K. K. & Kaufman, J. H. Physical description of a viscoelastically loaded AT-cut quartz resonator. *J. Appl. Phys.* **68**, 1993–2001 (1990).
299. Reid, R. C., Poling, B. E. & Prausnitz, J. M. *The Properties of Gases and Liquids*. (McGraw-Hill, 1987).
300. Reinisch, J. & Heuer, A. What is moving in silica at 1 K? A computer study of the low-temperature anomalies. *Phys. Rev. Lett.* **95**, 5–8 (2005).
301. Rescigno, T. N. & McCurdy, C. W. Numerical grid methods for quantum-mechanical scattering problems. *Phys. Rev. A* **62**, 32706 (2000).
302. Reyes, P. I., Duan, Z., Lu, Y., Khavulya, D. & Boustany, N. ZnO nanostructure-modified QCM for dynamic monitoring of cell adhesion and proliferation. *Biosens. Bioelectron.* **41**, 84–89 (2013).
303. Rey-Mermet, S., Lanz, R. & Muralt, P. Bulk acoustic wave resonator operating at 8 GHz for gravimetric sensing of organic films. *Sensors Actuators, B Chem.* **114**, 681–686 (2006).
304. Reynolds, O., Brightmore, A. & Moorby, W. The sub-mechanics of the universe. *University Press Cambridge* **3**, 12–14 (1903).
305. Reynolds, O. An Experimental Investigation of the Circumstances Which Determine Whether the Motion of Water Shall Be Direct or Sinuous, and of the Law of Resistance in Parallel Channels. *Philos. Transactions R. Soc. London* **174**, 935–982 (1883).
306. Richards B . and Wolf E . Electromagnetic Diffraction in Optical Systems . II . Structure of the Image Field in an Aplanatic System. *Proc. R. Soc. London A , Math. Phys.* **253**, 358–379 (1959).
307. Ridley, B. K. Multiphonon, non-radiative transition rate for electrons in semiconductors and insulators. *J. Phys. C Solid State Phys.* **11**, 2323–2341 (2001).
308. Rieger, J., Isacsson, A., Seitner, M. J., Kotthaus, J. P. & Weig, E. M. Energy losses of nanomechanical resonators induced by atomic force microscopy-controlled mechanical impedance mismatching. *Nat. Commun.* **5**, 3345 (2014).
309. Riewe, F. Nonconservative Lagrangian and Hamiltonian mechanics. *Phys. Rev. E* **53**, 1890–1899 (1996).
310. Rodahl, M. *et al.* Simultaneous frequency and dissipation factor QCM measurements of biomolecular adsorption and cell adhesion. *Faraday Discuss.* **107**, 229–246 (1997).

311. Rodahl, M., Höök, F., Krozer, A., Brzezinski, P. & Kasemo, B. Quartz crystal microbalance setup for frequency and Q-factor measurements in gaseous and liquid environments. *Rev. Sci. Instrum.* **66**, 3924–3930 (1995).
312. Rodahl, M. & Kasemo, B. A simple setup to simultaneously measure the resonant frequency and the absolute dissipation factor of a quartz crystal microbalance. *Rev. Sci. Instrum.* **67**, 3238–3241 (1996).
313. Rosas-Ortiz, O., Fernandez-Garcia, N. & Cruz, S. C. y. A Primer on Resonances in Quantum Mechanics. *AIP Conf. Proc.* **31**, 1077 (2008).
314. Rosenblum, M. G., Pikovsky, A. & Kurths, J. From Phase to Lag Synchronization in Coupled Chaotic Oscillators. *Phys. Rev. Lett.* **78**, 4193–4196 (1997).
315. Rouyer, F., Lhuillier, D., Martin, J. & Salin, D. Structure, density, and velocity fluctuations in quasi-two-dimensional non-Brownian suspensions of spheres. *Phys. Fluids* **12**, 958–963 (2000).
316. Rudd, R. Coarse-grained molecular dynamics and multiscale modeling of NEMS resonators. *Comput. Nanosci. Nanotechnol.* 173 (2002). at <<https://e-reports-ext.llnl.gov/pdf/240489.pdf>>
317. Sabine, E. Experiments to Determine the Difference in the Number of Vibrations Made by an Invariable Pendulum in the Royal Observatory at Greenwich, and in the House in London in Which Captain Kater's Experiments Were Made. *Philos. Transactions R. Soc. London* **119**, 83–102 (1829).
318. Sader, J. E. Frequency response of cantilever beams immersed in viscous fluids with applications to the atomic force microscope. *J. Appl. Phys.* **84**, 64 (1998).
319. Safavi-Naeini, A. H. *et al.* Observation of quantum motion of a nanomechanical resonator. *Phys. Rev. Lett.* **108**, 1–5 (2012).
320. Saito, N. & Inoue, Y. Different acoustic wave effects of thickness-extension and thickness-shear mode resonance oscillation on catalytic activity and selectivity of thin Pd and Ag films deposited on ferroelectric LiNbO₃ single crystals. *J. Chem. Phys.* **113**, 469–472 (2000).
321. Sakaguchi, H. Cooperative Phenomena in Coupled Oscillator Systems under External Fields. *Prog. Theor. Phys.* **79**, 39–46 (1988).
322. Sarpkaya, T. On the parameter $\beta = Re/KC = D_2/vT$. *J. Fluids Struct.* **21**, 435–440 (2005).
323. Saul T Epstein. The causal interpretation of Quantum Mechanics. *Phys. Rev.* **89**, 319 (1953).
324. Saviot, L., Netting, C. H. & Murray, D. B. Damping by bulk and shear viscosity of confined acoustic phonons for nanostructures in aqueous solution. *J. Phys. Chem. B* **111**, 7457–7461 (2007).
325. Scales, J. a & Snieder, R. What is a wave? *Nature* **401**, 739–740 (1999).
326. Schleich, W. P., Greenberger, D. M., Kobe, D. H. & Scully, M. O. Schrodinger equation revisited. *Proc. Natl. Acad. Sci.* **110**, 5374–5379 (2013).

327. Schmid, S., Kurek, M., Adolphsen, J. Q. & Boisen, A. Real-time single airborne nanoparticle detection with nanomechanical resonant filter-fiber. *Sci. Rep.* **3**, 3–7 (2013).
328. Schrodinger, E. *Collected papers on Wave Mechanics*. (Blackie & Son Ltd., 1928).
329. Schuil, A. E. LXIX. A note on the viscosity of gases and molecular mean free path. *London, Edinburgh, Dublin Philos. Mag. J. Sci.* **28**, 679–684 (1939).
330. Schütz, S. *et al.* Insect antenna as a smoke detector. *Nature* **398**, 298–299 (1999).
331. Sciama, D. W. On the origin of inertia. *Mon. Not. R. Astron. Soc.* **113**, 34–42 (1953).
332. Seelig, J. D. & Jayaraman, V. Neural dynamics for landmark orientation and angular path integration. *Nature* **521**, 186–191 (2015).
333. Seoánez, C., Guinea, F. & Castro Neto, A. H. Dissipation in graphene and nanotube resonators. *Phys. Rev. B - Condens. Matter Mater. Phys.* **76**, 1–8 (2007).
334. Sharipov, F. Rarefied gas dynamics and its applications to vacuum technology. *CAS 2006 - Cern Accel. Sch. Vac. Accel. Proc.* 1–13 (2007). at
<<http://www.scopus.com/inward/record.url?eid=2-s2.0-84882963591&partnerID=tZ0tx3y1%5Cnhttp://cds.cern.ch/record/1046845>>
335. Shen, B. Q. *et al.* Detection of Single Nanoparticles Using the Dissipative Interaction in a High- Q Microcavity. *Phys. Rev. Appl.* **5**, 1–8 (2016).
336. Singh, S. & Kaushal, R. S. Complex dynamical invariants for one-dimensional classical systems. *Phys. Scr.* **67**, 181–185 (2003).
337. Slater, J. Wave functions in a periodic potential. *Phys. Rev.* **51**, 846 (1937).
338. Slater, J. C. Physics and the wave equation. *Bull. Am. Math. Soc.* **52**, 392–401 (1946).
339. Smith, D. R. & Schurig, D. Electromagnetic Wave Propagation in Media with Indefinite Permittivity and Permeability Tensors. *Phys. Rev. Lett.* **90**, 77405 (2003).
340. Smoluchowski, M. On the Practical Applicability of Stokes' Law of Resistance, and the modifications of it required in certain cases. *Proc. Fifth Int. Congr. Math.* **2**, 193 (1912).
341. Sommerfeld, A. *Wave mechanics*. (Methuen & Co Ltd., 1930).
342. Spitzer, D. *et al.* Bio-inspired nanostructured sensor for the detection of ultralow concentrations of explosives. *Angew. Chemie - Int. Ed.* **51**, 5334–5338 (2012).
343. Spletzer, M., Raman, A., Wu, A. Q., Xu, X. & Reifenberger, R. Ultrasensitive mass sensing using mode localization in coupled microcantilevers. *Appl. Phys. Lett.* **88**, 254102 (2006).
344. Steensholt, G. ??ber die Stabilit??t der Ionengitter. *Zeitschrift f??r Phys.* **91**, 765–766 (1934).
345. Steinberger, A., Cottin-Bizonne, C., Kleimann, P. & Charlaix, E. High friction on a bubble mattress. *Nat. Mater.* **6**, 665–8 (2007).
346. Stern, E. *et al.* Importance of the debye screening length on nanowire field effect transistor sensors. *Nano Lett.* **7**, 3405–3409 (2007).

347. Stevens, K. W. H. The Wave Mechanical Damped Harmonic Oscillator. *Proc. Phys. Soc.* **72**, 1027–1036 (1958).
348. Stipe, B. C., Mamin, H. J., Stowe, T. D., Kenny, T. W. & Rugar, D. Noncontact friction and force fluctuations between closely spaced bodies. *Phys. Rev. Lett.* **87**, 96801 (2001).
349. Stokes, G. G. On the effect of the Internal friction of fluids on the motion of pendulums - Section III. *Trans. Cambridge Philos. Soc.* **IX**, 8 (1850).
350. Strogatz, S. H. From Kuramoto to Crawford: exploring the onset of synchronization in populations of coupled oscillators. *Phys. D Nonlinear Phenom.* **143**, 1–20 (2000).
351. Sun, X., Wang, M. Q. & Zhang, G. Ultrastructural observations on antennal sensilla of *Cnaphalocrocis medinalis* (Lepidoptera: Pyralidae). *Microsc. Res. Tech.* **74**, 113–121 (2011).
352. Sutherland, W. LII. *The viscosity of gases and molecular force*. *Philos. Mag. Ser. 5* **36**, 507–531 (1893).
353. Tabor, M. & Gennes, P. G. De. A Cascade Theory of Drag Reduction. *Europhys. Lett.* **2**, 519–522 (1986).
354. Takagi, S. Space-Time of Constant Acceleration. *Prog. Theor. Phys.* **82**, 471 (1989).
355. Tam, C. K. W. The drag on a cloud of spherical particles in low Reynolds number flow. *J. Fluid Mech.* **38**, 537 (1969).
356. Tamada, K. & Fujikawa, H. The steady two-dimensional flow of viscous fluid at low reynolds numbers passing through an infinite row of equal parallel circular cylinders. *Q. J. Mech. Appl. Math.* **10**, 425–432 (1957).
357. Tamayo, J., Ruz, J. J., Pini, V., Kosaka, P. & Calleja, M. Quantification of the surface stress in microcantilever biosensors: revisiting Stoney's equation. *Nanotechnology* **23**, 475702 (2012).
358. Tanaka, H. Universality of Viscoelastic Phase Separation in Dynamically Asymmetric Fluid Mixtures. *Phys. Rev. Lett.* **76**, 787–790 (1996).
359. Tao, J. & Yu, X. (Bill). Hair flow sensors: from bio-inspiration to bio-mimicking—a review. *Smart Mater. Struct.* **21**, 113001 (2012).
360. Taylor, G. An experimental study of Standing waves. *Proc. R. Soc. London A, Math. Phys. Sci.* **218**, 44–59 (1953).
361. Taylor, G. Analysis of the Swimming of Microscopic Organisms. *Proc. R. Soc. A Math. Phys. Eng. Sci.* **209**, 447–461 (1951).
362. Tellechea, E., Johannsmann, D., Steinmetz, N. F., Richter, R. P. & Reviakine, I. Model-independent analysis of QCM data on colloidal particle adsorption. *Langmuir* **25**, 5177–5184 (2009).
363. Terman, F. E. Resonant Lines in Radio Circuits. *Trans. IEEE* **53**, 21–24 (1934).
364. Ternes, M., Lutz, C. P., Hirjibehedin, C. F., Giessibl, F. J. & Heinrich, A. J. The Force Needed to Move an Atom on a Surface. *Science (80-.)* **319**, 1066–1069 (2008).

365. Thompson, P. a. & Troian, S. M. A general boundary condition for liquid flow at solid surfaces. *Nature* **389**, 360–362 (1997).
366. Thomson, W. On stationary waves in flowing water. *Philos. Mag. Ser. 5* **XXIII**, 52 (1887).
367. Toland, C. J. A. and J. F. The semi-analytic theory of standing waves. *Proc. R. Soc. London A, Math. Phys. Sci.* **411**, 123–137 (1987).
368. Topaj, D. & Pikovsky, A. Reversibility vs. synchronization in oscillator lattices. *Phys. D Nonlinear Phenom.* **170**, 118–130 (2002).
369. Toscano, G. *et al.* Resonance shifts and spill-out effects in self-consistent hydrodynamic nanoplasmatics. *Nat. Commun.* **6**, 1–11 (2014).
370. Treutlein, P. A Single Spin Feels the Vibrations. *Science (80-.)* **335**, 1584–1585 (2012).
371. Troesch, A. W. & Kim, S. K. Hydrodynamic forces acting on cylinders oscillating at small amplitudes. *J. Fluid Struct.* **5**, 113–126 (1991).
372. Tropea, C. D. & Gackstatter, R. The flow over two-dimensional surface-mounted obstacles at low Reynolds numbers. *J. Fluid Eng.* **107**, 489–494 (1985).
373. Truskett, T., Torquato, S. & Debenedetti, P. Density fluctuations in many-body systems. *Phys. Rev. E* **58**, 7369–7380 (1998).
374. Tuck, E. O. Calculation of unsteady flows due to small motions of cylinders in a viscous fluid. *J. Eng. Math.* **3**, 29–44 (1969).
375. Tuoc, V. N., Huan, T. D., Thao, N. T. & Tuan, L. M. Theoretical prediction of low-density hexagonal ZnO hollow structures. *J. Appl. Phys.* **120**, (2016).
376. Tuwankotta, J. M. & Verhulst, F. SYMMETRY AND RESONANCE IN HAMILTONIAN SYSTEMS. *SIAM J. Appl. Math.* **61**, 1369–1385 (2000).
377. Uchida, N. Many-body theory of synchronization by long-range interactions. *Phys. Rev. Lett.* **106**, 1–4 (2011).
378. Urbakh, M. & Daikhin, L. Roughness effect on the frequency of a quartz-crystal resonator in contact with a liquid. *Phys. Rev. B* **49**, 4866–4870 (1994).
379. Van Eysden, C. a. & Sader, J. E. Frequency response of cantilever beams immersed in viscous fluids with applications to the atomic force microscope: Arbitrary mode order. *J. Appl. Phys.* **101**, (2007).
380. Van Neste, C. W., Senesac, L. R. & Thundat, T. Standoff spectroscopy of surface adsorbed chemicals. *Anal. Chem.* **81**, 1952–1956 (2009).
381. Van Netten, S. M. Hydrodynamic detection by cupulae in a lateral line canal: Functional relations between physics and physiology. *Biol. Cybern.* **94**, 67–85 (2006).
382. Varghese, B. *et al.* Electrical and photoresponse properties of Co₃O₄ nanowires. *J. Appl. Phys.* **111**, (2012).
383. Venkateshvaran, D. *et al.* Approaching disorder-free transport in high-mobility conjugated polymers. *Nature* **515**, 384–388 (2014).

384. Verbridge, S. S., Ilic, R., Craighead, H. G. & Parpia, J. M. Size and frequency dependent gas damping of nanomechanical resonators. *Appl. Phys. Lett.* **93**, 20–23 (2008).
385. Verbridge, S. S., Shapiro, D. F., Craighead, H. G. & Parpia, J. M. Macroscopic tuning of nanomechanics: Substrate bending for Reversible control of frequency and quality factor of nanostring resonators. *Nano Lett.* **7**, 1728–1735 (2007).
386. Vilfan, A. & J??licher, F. Hydrodynamic flow patterns and synchronization of beating cilia. *Phys. Rev. Lett.* **96**, 1–4 (2006).
387. Villanueva, L. G. *et al.* Surpassing fundamental limits of oscillators using nonlinear resonators. *Phys. Rev. Lett.* **110**, 1–5 (2013).
388. Vissers, M. R., Weides, M. P., Kline, J. S., Sandberg, M. & Pappas, D. P. Identifying capacitive and inductive loss in lumped element superconducting hybrid titanium nitride/aluminum resonators. *Appl. Phys. Lett.* **101**, (2012).
389. Voinova, M. V., Jonson, M. & Kasemo, B. ‘Missing mass’ effect in biosensor’s QCM applications. *Biosens. Bioelectron.* **17**, 835–841 (2002).
390. Voisin, C., Christofilos, D., Del Fatti, N. & Vallée, F. Environment effect on the acoustic vibration of metal nanoparticles. *Phys. B Condens. Matter* **316–317**, 89–94 (2002).
391. Voke, P. R. & Collins, M. W. Forms of the generalised Navier_Stokes equations. *J. Eng. Math.* **18**, 219–233 (1984).
392. Vujanovic, B. & Strauss, A. M. Application of the Hamilton?Jacobi method to linear nonconservative vibration theory. *J. Math. Phys.* **29**, 1604–1609 (1988).
393. W. F. Edwards, C. S. Kenyon, and D. K. L. Continuing investigation into possible electric fields arising from steady conduction currents. *Phys. Rev. D - Part. Fields, Gravit. Cosmol.* **14**, 922–938 (1976).
394. Wang, R. C., Liu, C. P., Huang, J. L. & Chen, S.-J. ZnO hexagonal arrays of nanowires grown on nanorods. *Appl. Phys. Lett.* **86**, 251104 (2005).
395. Wang, Z. J. The role of drag in insect hovering. *J. Exp. Biol* **207**, 4147–4155 (2004).
396. Ward, A. J. & Pendry, J. B. Refraction and geometry in Maxwell’s equations. *J. Mod. Opt.* **43**, 773–793 (1996).
397. Ward, M. D. & Buttry, D. a. In situ interfacial mass detection with piezoelectric transducers. *Science (80-.)* **249**, 1000–1007 (1990).
398. Wayne, R. Charged particles are prevented from going faster than the speed of light by light itself: A biophysical cell biologist’s contribution to physics. *Acta Phys. Pol. B* **41**, 2297–2323 (2010).
399. Wheeler, J. A. & Feynman, R. P. Classical electrodynamics in terms of direct interparticle action. *Rev. Mod. Phys.* **21**, 425–433 (1949).
400. Wheeler, J. A. & Feynman, R. P. Interaction with the absorber as the mechanism of radiation. *Rev. Mod. Phys.* **17**, 157–181 (1945).

401. Widom, A. Krim, J. Q factors of quartz oscillator modes as a probe of submonolayer-film dynamics. *Phys. Rev. B* **34**, 1403 (1986).
402. Wilson-Rae, I. Intrinsic dissipation in nanomechanical resonators due to phonon tunneling. *Phys. Rev. B - Condens. Matter Mater. Phys.* **77**, 1–31 (2008).
403. Wimmer, L., Hertl, S., Hemetsberger, J. & Benes, E. New method of measuring vibration amplitudes of quartz crystals. *Rev. Sci. Instrum.* **55**, 605–609 (1984).
404. Winfree, A. T. Biological rhythms and the behavior of populations of coupled oscillators. *J. Theor. Biol.* **16**, 15–42 (1967).
405. Wu, T. Y. T. Cavity and Wake Flows. *Annu. Rev. Fluid Mech.* **4**, 243–284 (1972).
406. Wu, Y.-T. *et al.* Quartz crystal microbalance (QCM) in high-pressure carbon dioxide (CO₂): experimental aspects of QCM theory and CO₂ adsorption. *Langmuir* **20**, 3665–73 (2004).
407. Xu, Y., Lin, J.-T., Alphenaar, B. W. & Keynton, R. S. Viscous damping of microresonators for gas composition analysis. *Appl. Phys. Lett.* **88**, 143513 (2006).
408. Yakhot, V. & Colosqui, C. Stokes' Second Problem in High Frequency Limit: Application to Nanomechanical resonators. *J. Fluid Mech.* **586**, 249–258 (2007).
409. Yamamoto, K. & Sera, K. Flow of a rarefied gas past a circular cylinder. *Phys. Fluids* **28**, 1286 (1985).
410. Yang, N., Zhang, G. & Li, B. Violation of Fourier's law and anomalous heat diffusion in silicon nanowires. *Nano Today* **5**, 85–90 (2010).
411. Yang, Y. T., Callegari, C., Feng, X. L., Ekinci, K. L. & Roukes, M. L. Zepogram-scale nanomechanical mass sensing. *Nano Lett.* **6**, 583–586 (2006).
412. Yao, N. Y. *et al.* Many-body localization in dipolar systems. *Phys. Rev. Lett.* **113**, 1–5 (2014).
413. Yarom, E. & Sharon, E. Experimental observation of steady inertial wave turbulence in deep rotating flows. *Nat. Phys.* **10**, 510–514 (2014).
414. Yasumura, K. Y. *et al.* Quality factors in micron- and submicron-thick cantilevers. *J. Microelectromechanical Syst.* **9**, 117–125 (2000).
415. Yeom, J., Agonafer, D. D., Han, J.-H. & Shannon, M. A. Low Reynolds number flow across an array of cylindrical microposts in a microchannel and figure-of-merit analysis of micropost-filled microreactors. *J. Micromechanics Microengineering* **19**, 65025 (2009).
416. Yi, D., Passian, A., Lereu, A. L. & Thundat, T. An experimental investigation of analog delay generation for dynamic control of microsensors and atomic force microscopy. *Ultramicroscopy* **107**, 1020–1026 (2007).
417. Yiotis, A. G., Psihogios, J., Kainourgiakis, M. E., Papaioannou, A. & Stubos, A. K. A lattice Boltzmann study of viscous coupling effects in immiscible two-phase flow in porous media. *Colloids Surfaces A Physicochem. Eng. Asp.* **300**, 35–49 (2007).

418. Yukawa, Y., Saito, N., Nishiyama, H. & Inoue, Y. Different acoustic wave effects of thickness extension and thickness shear mode resonance oscillation on ethanol decomposition over Pd catalysts deposited on poled ferroelectric LiNbO₃ single crystals. *Surf. Sci.* **532–535**, 359–363 (2003).
419. Yum, K., Wang, Z., Suryavanshi, A. P. & Yu, M. F. Experimental measurement and model analysis of damping effect in nanoscale mechanical beam resonators in air. *J. Appl. Phys.* **96**, 3933–3938 (2004).
420. Zhang, C. & Feng, G. Contributions of amplitude measurement in qcm sensors. *IEEE Trans. Ultrason. Ferroelectr. Freq. Control* **43**, 942–947 (1996).
421. Zhang, H. P., Be'er, A., Florin, E.-L. & Swinney, H. L. Collective motion and density fluctuations in bacterial colonies. *Proc. Natl. Acad. Sci.* **107**, 13626–13630 (2010).
422. Zhang, X. C. C., Myers, E. B. B., Sader, J. E. E. & Roukes, M. L. L. Nanomechanical torsional resonators for frequency-shift infrared thermal sensing. *Nano Lett.* **13**, 1528–1534 (2013).
423. Zhang, Y., Du, B., Chen, X. & Ma, H. Convergence of dissipation and impedance analysis of quartz crystal microbalance studies. *Anal. Chem.* **81**, 642–648 (2009).
424. Zheng, J. H., Tan, H. S. & Ng, S. C. Theory of non-radiative capture of carriers by multiphonon processes for deep centres in semiconductors. *J. Phys. Condens. Matter* **6**, 1695–1706 (1994).
425. Zheng, Z. *et al.* Phase Slips and Phase Synchronization of Coupled Oscillators. *Phys. Rev. Lett.* **81**, 3–6 (1998).
426. Zhu, Y. & Granick, S. Rate-Dependent Slip of Newtonian Liquid at Smooth Surfaces. *Phys. Rev. Lett.* **87**, 96105 (2001).
427. Zhu, Y. & Granick, S. Limits of the Hydrodynamic No-Slip Boundary Condition. *Phys. Rev. Lett.* **88**, 106102 (2002).
428. Zwanzig, R. & Bixon, M. Hydrodynamic Theory of the Velocity Correlation Function. *Phys. Rev. A* **2**, 2005–2012 (1970).

Appendix I: MATLAB code for estimation of viscosity of gas mixtures

```
% The dependence of the diffusion coefficient on temperature for gases
can be expressed using Chapman-Enskog theory (predictions accurate on
average to about 8%
%
% D=\frac{1.858 \cdot 10^{-3} T^{3/2} \sqrt{1/M_1+1/M_2}}{p \sigma_{12}^2 \Omega}
% where
%
% 1 and 2 index the two kinds of molecules present in the gaseous
mixture
% T is the absolute temperature (K)
% M is the molar mass (g/mol)
% p is the pressure (atm)
% \sigma_{12}=\frac{1}{2}(\sigma_1+\sigma_2) is the average collision
diameter (the values are tabulated[4]) (\AA)
% ? is a temperature-dependent collision integral (the values are
tabulated[4] but usually of order 1) (dimensionless).
% D is the diffusion coefficient (which is expressed in cm2/s when the
other magnitudes are expressed in the units as given above[3][5])..
e=2.718
T=23; %degree Celcius
RH=46;
pws = e*( 77.3450 + 0.0057*(273.15 + T) - 7235 / (273.15 + T) ) /
(273.15 + T)^8.2;
pw=(RH/100)*pws; % ambient air partial pressure at room temparature
with 46% RH
pt=1; % total pressure 1 atm;

M1= 28.965; %gm/mole -- Dry Air
M2= 18.015; %gm/mole -- Water Vapor
M3= 46.07; %gm/mole -- Ethanol
M4= 215; %gm/mole -- Petroleum Ether
M5 = 29.099; %gm/mole -- 46% RH ambient air
M6 = 84.16; %gm/mole -- Cyclohexane
M7 = 60.10; %gm/mole -- 2-Propanol
M8 = 58.08; %gm/mole -- Acetone
M9 = 32.04; %gm/mole -- methanol
M10 = 124.08; %gm/mole -- DMMP

rho1= 1.19312;
rho2= 0.9899*rho1; %100% RH
rho3= 1.59*rho1; %ethanol
rho4= 2.5* rho1; %Petro Ether
rho5= 0.99958*rho1; %Ambient air - 46% RH
rho6= 2.9*rho1; %cyclohexane
rho7= 2.1*rho1; %2-Propanol
rho8= 2*rho1; %Acetone
rho9= 1.11*rho1; %Methanol
rho10= 2.72*rho1; %DMMP
```

```

T = 296;          %kelvin
P = 1;            %atm

sigma1 = 32.8947;      % Dry Air Angstrom collision diameter
sigma2 = 32.872;       % Water Vapor Angstrom collision diameter
sigma3 = 33.85;        % Ethanol Angstrom collision diameter 32.8985
sigma4 = 47.2789;      % Petroleum Ether Angstrom collision diameter
sigma5 = 33.872;       % Ambient air 46% RH
sigma6 = 33.87;        % cyclohexane
sigma7 = 33.65;        % 2-Propanol
sigma8 = 33.877;       % Acetone
sigma9 = 33.809;       % methanol
sigma10= 39.38;        % DMMP

Ome=1;                %assuming no interaction

sigma12=1/2*(sigma1 + sigma2);
sigma13=1/2*(sigma1 + sigma3);
sigma14=1/2*(sigma1 + sigma4);
sigma15=1/2*(sigma1 + sigma5);
sigma16=1/2*(sigma1 + sigma6);
sigma17=1/2*(sigma1 + sigma7);
sigma18=1/2*(sigma1 + sigma8);
sigma19=1/2*(sigma1 + sigma9);
sigma110=1/2*(sigma1 +sigma10);

D12= ((1.858*10^-3*T^(3/2))*sqrt((1/M1) + (1/M2)))/(p*(sigma12^2)*Ome);
D13= ((1.858*10^-3*T^(3/2))*sqrt((1/M1) + (1/M3)))/(p*(sigma13^2)*Ome);
D14= ((1.858*10^-3*T^(3/2))*sqrt((1/M1) + (1/M4)))/(p*(sigma14^2)*Ome);
D15= ((1.858*10^-3*T^(3/2))*sqrt((1/M1) + (1/M5)))/(p*(sigma15^2)*Ome);
D16= ((1.858*10^-3*T^(3/2))*sqrt((1/M1) + (1/M6)))/(p*(sigma16^2)*Ome);
D17= ((1.858*10^-3*T^(3/2))*sqrt((1/M1) + (1/M7)))/(p*(sigma17^2)*Ome);
D18= ((1.858*10^-3*T^(3/2))*sqrt((1/M1) + (1/M8)))/(p*(sigma18^2)*Ome);
D19= ((1.858*10^-3*T^(3/2))*sqrt((1/M1) + (1/M9)))/(p*(sigma19^2)*Ome);
D110= ((1.858*10^-3*T^(3/2))*sqrt((1/M1) +
(1/M10)))/(p*(sigma110^2)*Ome);

mu1 = 184.6*10^-6;    %Dry Air at 23C
mu2 = 120*10^-6;      %Water Vapor at 23C
mu3 = 138.255*10^-6;  %Ethanol at 23C 83.5
mu4 = 174.6*10^-6;    %Petro Ether at 23C
mu5 = 184.4*10^-6;    %Ambient air at 23C
mu6 = 102.385*10^-6;  %Cyclohexane at 23C
mu7 = 120.99*10^-6;   %2-Propanol at 23C
mu8 = 123.23*10^-6;   %Acetone
mu9 = 165.579*10^-6;  %Methanol
mu10= 98.011*10^-6;   %DMMP 0.5309*dry air

n21= 0.003;           %water vapor
n31= 0.007;           %ethanol - dry air
n41= 0.0309;          %Petro Ether - dry air
n51= 0.0028;          %ambient air 46% RH - dry air
n61= 0.0129;          %cyclohexane - dry air
n71= 0.006;           %2-Propanol
n81= 0.023;           %Acetone
n91= 0.0132;          %methanol

```

```

n101=0.0000133;           %DMMP

n12=1/n21; n13=1/n31; n14=1/n41; n15=1/n51; n16=1/n61; n17=1/n71;
n18=1/n81; n19=1/n91; n110=1/n101;

k=1;

mu12= (mu1/(1+(n21*((1.385*mu1)/(D12*rho1))))) +
(mu2/(1+(n12*((1.385*mu2)/(D12*rho2))))) +
(mu5/(1+(n15*((1.385*mu5)/(D15*rho5))))) ;
delmu2=k*(mu12-mu1)/mu1

mu13= (mu1/(1+(n31*((1.385*mu1)/(D13*rho1))))) +
(mu3/(1+(n13*((1.385*mu3)/(D13*rho3))))) +
(mu5/(1+(n15*((1.385*mu5)/(D15*rho5))))) ;
delmu3=k*(mu13-mu1)/mu1

mu14= (mu1/(1+(n41*((1.385*mu1)/(D14*rho1))))) +
(mu4/(1+(n14*((1.385*mu4)/(D14*rho4))))) +
(mu5/(1+(n15*((1.385*mu5)/(D15*rho5))))) ;
delmu4=k*(mu14-mu1)/mu1

mu15= (mu1/(1+(n51*((1.385*mu1)/(D15*rho1))))) +
(mu5/(1+(n15*((1.385*mu5)/(D15*rho5))))) ;
delmu5=k*(mu15-mu1)/mu1

mu16= (mu1/(1+(n61*((1.385*mu1)/(D16*rho1))))) +
(mu6/(1+(n16*((1.385*mu6)/(D16*rho6))))) +
(mu5/(1+(n15*((1.385*mu5)/(D15*rho5))))) ;
delmu6=k*(mu16-mu1)/mu1

mu17= (mu1/(1+(n71*((1.385*mu1)/(D17*rho1))))) +
(mu7/(1+(n17*((1.385*mu7)/(D17*rho7))))) +
(mu5/(1+(n15*((1.385*mu5)/(D15*rho5))))) ;
delmu7=k*(mu17-mu1)/mu1

mu18= (mu1/(1+(n81*((1.385*mu1)/(D18*rho1))))) +
(mu8/(1+(n18*((1.385*mu8)/(D18*rho8))))) +
(mu5/(1+(n15*((1.385*mu5)/(D15*rho5))))) ;
delmu8=k*(mu18-mu1)/mu1

mu19= (mu1/(1+(n91*((1.385*mu1)/(D19*rho1))))) +
(mu9/(1+(n19*((1.385*mu9)/(D19*rho9))))) +
(mu5/(1+(n15*((1.385*mu5)/(D15*rho5))))) ;
delmu9=k*(mu19-mu1)/mu1

mu110= (mu1/(1+(n101*((1.385*mu1)/(D110*rho1))))) +
(mu10/(1+(n110*((1.385*mu10)/(D110*rho10))))) +
(mu5/(1+(n15*((1.385*mu5)/(D15*rho5))))) ;
delmu10=k*(mu110-mu1)/mu1

sigma35=1/2*(sigma3+sigma5);
sigma53=1/sigma35;
n35=n31/n51;
n53=1/n35;

```

```

D35= ((1.858*10^-3*T^(3/2))*sqrt((1/M3) + (1/M5)))/(p*(sigma35^2)*Ome);
D53= ((1.858*10^-3*T^(3/2))*sqrt((1/M5) + (1/M3)))/(p*(sigma53^2)*Ome);
mu35= (mu3/(1+(n53*((1.385*mu3)/(D35*rho3)))) + 
(mu5/(1+(n35*((1.385*mu5)/(D35*rho5))))));
D51= ((1.858*10^-3*T^(3/2))*sqrt((1/M5) + (1/M1)))/(p*(sigma15^2)*Ome);
D31= ((1.858*10^-3*T^(3/2))*sqrt((1/M3) + (1/M1)))/(p*(sigma13^2)*Ome);

% mixture with water vapor (3 component mixture)
mulm=mu1/(1+((1.385*mu1)/(1*rho1)*((n31/D13)+(n51/D15))) + 
0.7*mu3/(1+((1.385*mu3)/(n31*rho3)*((n31/D31)+(n35/D35))) + 
0.23*mu5/(1+((1.385*mu5)/(n51*rho5)*((n31/D51)+(n35/D53)))));
delmum1=(mulm-mu1)/mu1

```

Appendix II: MATLAB code for simulating oscillating Standing Wave patterns with accumulated phase

```

close all;
clear all;
radian=pi/180;
Phif=90*radian;
Phi0=0*radian;
delphi=(Phif-Phi0);
Phi=linspace(0.1,90,101);
f=2.750542*10^6;
% x=linspace(0,0.0012,101);
% ff=(1+x)*f;
w=2*pi*f; V0=0.341; alpha0=cos(delphi);

c=2.998*10^8;
mu=4*pi*10^-7;

R=V0/0.009;
I0=0.009;
E0=V0/0.6;

d=0.1524; % physical dimension of coil
N=210;
r=0.060325; % diameter of coil
C=pi*r;
l=sqrt((d/N)^2+C^2);
Len=(N*l);
qlambda=c/(4*f);
frac=qlambda/Len;

dlen=1/Len;
dtheta=(delphi)*radian*dlen;
theta=linspace(dtheta,0,101);

alpha=(cos(theta));
beta=sqrt(w).*[cosh(theta)+sinh(theta)];
v=sqrt(w).*[cosh(theta)-sinh(theta)];

```

```

zeta=sqrt(beta.^2+alpha.^2);

lambda=(v)./(f);
Q1=2*(cumsum(exp((2./lambda.*theta))));

%/////////// propagating wave generator///////////
t=linspace(0,60e-8,260);
a1=linspace(0,qlambda,101);
[x1,y]=meshgrid(a1,-1:0.1:1);
k1=2*pi/qlambda;
z1=(exp(i*k1*x1));

%//////////quarter wave generation///////////
k=0.25*(2*pi./(lambda));
a=linspace(0,lambda,101);
[x,y]=meshgrid(a,-1:0.1:1);
z=imag((Q1).*exp(-i*(k.*x)));

transwave = VideoWriter('C:\PHANI\Work\Standing Wave\Science
paper\Simul\propwave.avi');
open(transwave);

%////////// prop wave figure ///////////
figure
for n=1:length(t)
surf(x1,y,real(z1.*exp(-i*w.*t(n))), 'FaceAlpha', 0.75);
view(3)
zlim([-1.5 1.5])
xlim([min(min(x1)) max(max(x1))]);
ylim([min(min(y)) max(max(y))])
shading interp
currframe=getframe(gcf);
writeVideo(transwave,currframe);
close(transwave);

standwave = VideoWriter('C:\PHANI\Work\Standing Wave\Science
paper\Simul\standwavequarter.avi');
open(standwave);

% ////////// quarter standing wave figure ///////////
figure

for n=1:length(t)
surf(x,y,real(z.*exp(-i*beta.*v.*t(n))), 'FaceAlpha', 0.75);
view(3)
zlim([-220 220])
xlim([min(min(x)) max(max(x))]);
ylim([min(min(y)) max(max(y))])
shading interp
currframe=getframe(gcf);
writeVideo(standwave,currframe);
end
close(standwave);

```